THE RESPONSE OF THE GENERAL CIRCULATION

TO IMPOSED FORCINGS

by

Paul W. Staten

A dissertation submitted to the faculty of
The University of Utah
in partial fulfillment of the requirements for the degree of

Doctor of Philosophy

Department of Atmospheric Sciences

The University of Utah

May 2013

The University of Utah Graduate School

STATEMENT OF THESIS APPROVAL

The thesis of **Paul W. Staten**

has been approved by the following supervisory committee members:

Thomas Reichler	, Chair	**12/11/2012** Date Approved
John Horel	, Member	**12/11/2012** Date Approved
Jian Lu	, Member	**12/11/2012** Date Approved
Jim Steenburgh	, Member	**12/11/2012** Date Approved
Courtenay Strong	, Member	**12/11/2012** Date Approved

and by **Kevin Perry**, Chair of

the Department of **Atmospheric Sciences**

and by Charles A. Wight, Dean of The Graduate School.

ABSTRACT

Among the most societally important trends in observations and models are poleward shifts in global circulation features. In order to investigate the magnitude and mechanisms of such circulation shifts, we explore the general circulation response to imposed forcings, using the Geophysical Fluid Dynamics Laboratories Atmospheric Model version 2.1.

Present-day simulations exhibit robust poleward shifts in zonal mean circulation features, compared to a preindustrial control, as do future simulations compared to present-day. These responses vary by season, and the response to combined forcings is well-approximated by the sum of the individual responses. Results suggest that warming sea surface temperatures are the main driver of circulation change over both hemispheres. This work also projects that the southern hemisphere jet will continue to shift poleward, albeit more slowly during the summer due to expected ozone recovery in the stratosphere.

The relationship between shifts in the position of the eddy-driven jet and of the Hadley cell edge are examined. From year to year, the eddy-driven jet shifts more than the Hadley cell edge, with a ratio of approximately 1.5:1 between the two depending on season, hemisphere, and simulation. Furthermore, the mean position of the Hadley cell edge explains a substantial portion of the variability of this ratio. The author attributes this to the varying susceptibility of the Hadley cell to the influence of midlatitude eddies.

Finally, the transient response to suddenly imposed forcings is examined. For both direct radiative forcings and sea surface warming, broad tropospheric and stratospheric temperature changes can be seen almost immediately. Once zonal winds near the tropopause accelerate a few days later, zonal winds and eddies respond throughout the rest of the troposphere, shifting the surface circulation. The transient changes in the Ferrel cell center and the Hadley cell edge appear simultaneous, illustrating the need for consideration of both tropical and extratropical processes in the theory for the latitude of either the Hadley cell edge or the eddy-driven jet.

TABLE OF CONTENTS

LIST OF FIGURES

LIST OF TABLES

ACKNOWLEDGEMENTS

I would like to express my appreciation to Thomas Reichler, for serving as my advisor and mentor. Thomas has always watched out for me, and provided everything I need to succeed. His patience, honesty, enthusiasm, and his genuine concern have been a consistent source of motivation for me during my time at the University of Utah.

I am grateful for the service of my graduate committee members, John Horel, Jian Lu, Jim Steenburgh, and Courtenay Strong, for their pragmatism, encouragement, and insight. I would also like to recognize Holly Godsey and Cristine Lewis for the opportunities they each opened for me, both in teaching and research.

I thank my wife Clerie, who made my dreams her own and believed in me before I did. She and I have in turn been constantly supported by our extended family, making the pursuit of this degree while parenting not only feasible, but enjoyable.

CHAPTER 1

INTRODUCTION

1.1 The general circulation of the atmosphere

Key points in this section include:

- The structure of the global atmospheric circulation is changing.
- A changing circulation may adversely affect society.
- Modeling studies such as this help us better understand, predict, and adapt to climate change.

The observed global mean temperature increase during the last century is a symptom of a more fundamental change in the earth climate system, namely the changing distribution of radiative heating and cooling, and the resulting shifts in the general circulation of the atmosphere. These shifts are among the most robust climate projections described in the IPCC assessments (Solomon et al., 2007). Observations and model simulations reveal an expanding Hadley cell – which dominates tropical climate – and a broadening of the dry subsidence regions along its poleward flanks. Rainfall over the Mediterranean, for example, is expected to decrease as the Hadley cell edge encroaches on the region. The Ferrel cell – which dominates midlatitude climate – is also shifting poleward. This shift

is often characterized as a falling pressure tendency over the poles, and a corresponding poleward shift in the midlatitude jet (Thompson et al., 2000).

The need and the ability to understand the changing zonal mean circulation of the earth have never been greater than they are today. As much of the world population resides in the subtropics and midlatitudes, Hadley cell and Ferrel cell shifts, as well as the resulting changes in surface climate and hydrology, are likely to strongly impact society on a global scale. Notwithstanding, the mechanisms behind such shifts are poorly understood (Schneider et al., 2010). One reason is that the observational records capable of recording large scale circulation change are fragmented, and short compared to relevant climate change timescales. Another difficulty arises from the possibility that shifts in a given feature are due to a combination of often competing mechanisms. Finally, although the Hadley and Ferrel cells – representing the tropical and the extratropical circulation regimes – behave quite differently, and are often considered as distinct components, they are intrinsically connected, and the interactions between the two involve various degrees of tropical and extratropical dynamics.

Fortunately, the tools needed to study large scale circulation increases have been maturing over recent decades. Satellites have complimented the global network of in situ observation systems, international organizations have recognized the importance of producing consistent, calibrated climate measurements, and numerical models has allowed us to reproduce and understand climate processes. The present dissertation is focused on using such modeled general circulation change to replicate, project, and diagnose past and

future changes in the general circulation.

1.2 Observing general circulation shifts

Key points in this section include:

- Different indicators of the tropical width reveal different rates of widening.
- Extratropical circulation features, such as the jet stream, are also shifting poleward.

Although there is no universal standard for the width of the tropics, several related features stand out that allow measures of circulation widening to be taken. Recent estimates of tropical widening may be considered to have begun with Rosenlof (2002), who estimated a widening of the upwelling branch of the Brewer-Dobson circulation, at a rate of 0.3° latitude per decade. As the tropopause is much higher in the tropics, Reichler and Held (2005) examine the width of the tropopause in reanalyses and radiosonde data, and find that the tropics are widening between 0.4–0.7° latitude per decade. They also note that the widening seems to be strongest over the southern hemisphere, and during the summer (for each hemisphere).

Since the sea surface temperature changes related to climate change bear some semblance to the El Niño warm pool, Fu et al. (2006) reasoned that the global atmospheric response likely has some commonality to that observed following El Niño events. Using microwave sounding unit (MSU) data, they highlight tropospheric warming and stratospheric cooling, supporting their hypothesis. Lu et al. (2008) show that, although tropical sea surface temperatures (SSTs) do exhibit a local warming maxima in the ENSO region,

strong changes near the poles, including changes due to sea ice melt, produce a warming pattern that contrasts strongly with El Niño events. Specifically, they show that El Niño events are associated with a strengthening and contracting of the Hadley cell circulation, while global climate change is associated with a weakening and broadening of the Hadley cell. Their study also suggests that the midlatitude jet shifts poleward due to a change in baroclinicity.

Seidel and Randel (2007) examine tropopause heights using radiosonde measurements and reanalysis data and calculate a much stronger tropical expansion rate, at 5–8° latitude over 1979–2005, which is on the high end of observational estimates. Hudson et al. (2006) examine an altogether different dataset – total column ozone – and based on latitudinal stratospheric ozone regimes, calculate a more moderate poleward shift of the boundaries between the regimes of roughly 1.1° latitude per decade, or a widening rate of 2.2° latitude per decade.

Hu and Fu (2007) analyze yet another dataset, outgoing longwave radiation, as well as the mass meridional stream functions in reanalyses. An important result from their work, aside from their estimate of the tropical expansion rate to be 0.7–1.5° latitude per decade, is their detailed analysis of seasonality. They find that, in reanalyses, the Hadley cells shift poleward most strongly during their respective Summer and Fall seasons; the outgoing longwave radiation thresholds do not show such a seasonality. (Their results, and the others just discussed, were compiled by Seidel et al. (2008), who provide a concise graphical summary of the same in Figure 2 of their study.) Hu et al. (2011) reaffirm and expand their

earlier results, examining several metrics of Hadley cell expansion, including outgoing longwave radiation and precipitation, finding similar trends to those described above. They also produce similar trends in a climate model, and find that some of the observed shifts can be reproduced in a simulation coupled to observed sea surface temperatures.

Focusing beyond the tropics, Archer and Caldeira (2008) calculate jet shifts, based on mass and mass-flux weighted average winds in reanalyses, and find that the jet streams have been rising as well as shifting poleward. Strong and Davis (2007), examining maximum wind surface, likewise find poleward shifts in the jet over many longitudes. Over the southern hemisphere, they found that the subtropical jet weakened (consistent with a weakening and expansion of the Hadley cell, as described above), and that the eddy-driven jet intensified. The general poleward shift in extratropical circulation features is broadly consistent with a shift towards more positive annular modes (hereafter AMs), as shown by Thompson and Solomon (2002), Thompson and Wallace (2000), and Thompson et al. (2000). These studies also suggest a link between stratospheric ozone depletion and changes in tropospheric climate, even extending down to the surface (Thompson and Solomon, 2002; Thompson et al., 2000).

1.3 Peering deeper using general circulation models

Key points in this section include:

- Model studies show the troposphere to be sensitive to changes in the thermal structure of the lower stratosphere.

- Ozone depletion and greenhouse gas increases have produced a strong poleward southern hemisphere jet shift.
- Ozone recovery and greenhouse gas increases will have competing effects on the jet during coming decades.
- Circulation changes may be the dominant driver behind precipitation changes in mid- and high latitudes.

In contrast to observational studies, modeling studies have the advantages of reproducibility, the choice of forcings and boundary conditions, and the ability to reduce the complexity of the experiment. Models range from the highly idealized back-of-the-envlope one-dimensional models, to the fully complex. The former aid understanding climate processes, and the latter aid in diagnosing, replicating, and projecting climate change (Held, 2005).

Kushner et al. (2001) used a general circulation model (GCM) to reproduce the pattern of extratropical circulation widening seen during recent decades, including the shift in tropospheric westerlies, over the southern hemisphere. Models quite accurately reproduce observed changes in the southern annular mode (SAM), with widening being attributed to ozone depletion (Gillett and Thompson, 2003) and, to a lesser degree, to greenhouse gas concentration increases (Fyfe et al., 1999; Arblaster and Meehl, 2006). On the other hand, general circulation models seem to underestimate the observed change in the northern annular mode (NAM) index (Miller et al., 2006). The reasons are not known, but they may be related to modeled troposphere-stratosphere connections.

To better understand the relationship between changes in the annular mode in the stratosphere and in the troposphere, Polvani and Kushner (2002) perform a relatively simple simulation, integrating the full primitive equations in a dry model with zonally uniform forcings and boundary conditions. They find that applying a cooling to the upper winter-hemisphere stratosphere could produce poleward shifts in the wintertime midlatitude jet, and a drop in surface pressure at high latitudes in that hemisphere. They also find that the shifts cannot be adequately explained by downward control theory (Haynes et al., 1991). Their choice of forcing is deliberately reminiscent of the effect of ozone depletion, and they do find some commonality between their modeled response, and that in observations. Simpson et al. (2009) argue that stratospheric temperature anomalies affect the troposphere through wavedriving. By holding eddy forcing constant, Simpson et al. (2009) preempt the usual tropospheric response to stratospheric temperature anomalies. Song and Robinson (2004), Kushner and Polvani (2004), Williams (2006), and Gerber and Polvani (2009) all perform work along these lines, showing an influence of the stratosphere on the troposphere via wavedriving. Gerber and Polvani (2009) explain that topographically forced planetary eddies have a significant impact in the stratosphere, illustrating a connection operating in the reverse direction.

Shindell and Schmidt (2004) compare the modeled and observed SAM-like pressure and temperature changes in the antarctic, and noted that the observed patterns of both can be approximated in a general circulation model coupled to a mixed-layer ocean, when forced by greenhouse gas increases and stratospheric ozone depletion. They also note that

the weak surface temperature trends over Antarctica are a result of contrasting influence of ozone depletion and greenhouse gases, and that while ozone recovery is expected to moderate the continued trend towards a positive annular mode aloft, it may exacerbate arctic surface warming beneath. This competition between ozone recovery and continued greenhouse gas increases is also seen in a model study by Arblaster and Meehl (2006), who examine not just greenhouse gases and ozone depletion, but different types of aerosols as well. Their results agree well with Shindell and Schmidt (2004), and suggest that stratospheric ozone depletion strengthens the antarctic polar vortex, and that continued greenhouse gas increases will continue to strengthen the polar vortex, even as ozone concentrations rebound.

The climate models used in these studies may underestimate the role that the stratosphere plays in deepening both of the polar vortices, or in strengthening the annular modes. Miller et al. (2006) examine annular mode trends in the IPCC AR4 models, using the annular mode response to aerosol forcings following volcanic eruptions as a test case, and find that the multi-model average annular mode response to stratospheric temperature changes is smaller than that in the real atmosphere. Perlwitz et al. (2008) compare a chemistry climate model with the models used for the Fourth Assessment Report, and find a near-cancellation of circulation changes due to ozone recovery, but the trend is not quite reversed.

Comparing coupled chemistry climate models (CCMs) with simulations from the third phase of the Coupled Model Intercomparison Project (CMIP3), Son et al. (2008), Son

et al. (2009b), and Son et al. (2009a) find that future ozone recovery may cancel out or even reverse the poleward tendency of the midlatitude jet due to greenhouse gas increases and sea surface temperature (SST) warming. These studies include many different models of varying quality, which may make it difficult to cleanly separate the effects of individual forcings from the effects of model differences. Their results generally show that models from the Chemistry-Climate Model Validation Activity (CCMVal) project a stronger deceleration of winds on the poleward flanks of the jet than the AR4 models with prescribed ozone recovery. Son et al. (2010), however, find that the CCMVal-2 show a response more similar to the same subset of AR4 models. They look at the fluxes of wave activity, and relate the sensitivity of the circulation to O_3 recovery to the SAM timescale.

The importance of the tropospheric response to ozone depletion and recovery extends past the extratropics. Previdi and Liepert (2007) describe a statistical connection between the modeled circulation changes in the extratropics, and in the Hadley cell, finding that about half of the expansion of the simulated Hadley cell edge and subtropical dry zones can be explained by changes in the annular modes. Kang and Polvani (2010) find that the eddy-driven jet and the Hadley cell edge tend to shift together from year to year, with about a 2-to-1 ratio between them. This relationship between the two features suggests that tropical climate may respond to stratospheric ozone depletion. Indeed, models do show a widening Hadley cell in response to greenhouse gas increases (Johanson and Fu, 2009) and stratospheric ozone depletion, although simulation studies also vary substantially in the magnitude of Hadley cell widening (Reichler, 2009). Understanding the cause of these

changes has proven difficult, as model simulations seem to underestimate observed tropical widening trends. The cause of this discrepancy is an outstanding issue (Johanson and Fu, 2009).

Another challenge to general circulation modeling is the interaction between the atmosphere and the ocean. Deser and Phillips (2009) address this issue by examining ten-member ensembles of 1950–2000 transient climate simulations using the National Center for Atmospheric Research (NCAR) Community Atmosphere Model version 3 (CAM3) to compare the direct effects of radiative forcings and the indirect effect of changing SSTs on the general circulation. Their study emphasized the role that direct radiative forcings played in shifting extratropical precipitation patterns, but did not distinguish between the effects of greenhouse gases or ozone depletion. In addition, Deser and Phillips (2009) apply prescribed observed SSTs, introducing inconsistencies and sensitivity to natural slow oscillations in SSTs (e.g., the Pacific decadal oscillation and El Niño Southern Oscillation). Polvani et al. (2011b) perform ensemble projections of the next several decades with ozone and other forcings, and with ozone in isolation, using prescribed SSTs. They show that ozone alone ought to shift the jet equatorward, but that ozone depletion and greenhouse gas increases together produce mostly statistically insignificant trends over the coming decades.

Model studies have also shown ozone depletion to be responsible for significant precipitation shifts. Kang et al. (2011) show that the poleward shift of the southern hemisphere jet due to ozone depletion has been accompanied by a precipitation shift, and that this shift in

precipitation resembles observed precipitation changes. Scheff and Frierson (2012) compare the precipitation shifts associated with a widening of the subtropical dry regions and a poleward shift of the jet, to the expected intensification of precipitation and evaporation due to the thermodynamical "rich get richer" mechanism (Held and Soden, 2006). They find that the precipitation changes due to a changing general circulation explain most of the major precipitation shifts due to climate change.

1.4 Constraints on the width of the Hadley cell

Key points in this section include:

- Most Hadley cell width scalings consider eddy generation due to baroclinicity to be a primary factor in terminating the Hadley cell.
- Eddy dissipation likely serves to widen the cell, by removing angular momentum, thereby reducing shear and increasing stability.
- The seasonal cycle, El Niño, and climate change modify the Hadley cell through the previous two means.
- The importance of eddy dissipation may explain how changes in the extratropics affect the Hadley cell width.

An attractive approach – and a necessary step – to understanding the reasons for a widening Hadley cell is to ask the question: what is required in order to have a Hadley cell in the first place? Held and Hou (1980) describe what is commonly considered a "simplest" model of the Hadley cell, showing analytically that, even in an atmosphere

without baroclinic waves and their associated fluxes of energy and momentum, a Hadley cell circulation would exist and would terminate before the poles, assuming (1) angular momentum conservation in the upper branch of the Hadley cell, and (2) energy conservation, so that diabatic heating is balanced by radiative cooling. Under these assumptions, they arrive at a Hadley cell edge scaling of

$$\phi_H \approx \left(\frac{5}{3} \frac{g H_t}{\Omega^2 a^2} \frac{\Delta_h}{T_0} \right)^{\frac{1}{2}}, \tag{1}$$

where H_t is the height of the tropical tropopause (or scale height of the Hadley cell, not necessarily the altitude of the cold-point or lapse-rate tropopause), Δ_h is the equilibrium equator-to-pole surface potential temperature difference, T_0 is the global mean reference temperature, and Ω, g, and a are as conventionally defined.

Plugging in parameters relevant to the present-day climate of the earth ($H_t \approx 15$ km, $\Delta_h \approx 80$ K, and $T_0 \approx 295$ K), Schneider et al. (2010) calculate the Hadley cell limit by this scaling to be at 29° (32° if a small angle approximation is used). While this is certainly in the ballpark (Hadley cell edge estimations from coupled data in this study range from 27° to 36°, depending on the hemisphere and season), modeled Hadley cell shifts do not scale in the way this theory predicts, as illustrated in Walker and Schneider (2006). This scaling, however, lacks the effect of waves.

Held (2000) addresses this deficiency, and derives an alternative scaling for the edge of the Hadley cell—one that includes the effect of baroclinic instability. Nearly angular momentum-conserving poleward flow in the upper branch of the Hadley cell, above a layer of weak zonal winds, produces a vertical shear in the zonal winds. At some point, this shear

becomes unstable, and becomes favorable for the growth of initially small disturbances. Korty and Schneider (2008) describe the edge of the Hadley cell as the latitude at which baroclinic eddies become deep enough to reach the upper troposphere. Held (2000), still assuming angular momentum conservation in the upper branch of the Hadley cell, and applying a two-layer model criterion for the unstable shear (Phillips, 1954), achieve the scaling

$$\phi_H \propto \left(\frac{NH_t}{\Omega a}\right)^{\frac{1}{2}}, \tag{2}$$

where N is the vertically averaged Brunt Väisälä frequency. Using the more general Eady growth rate (Lindzen and Farrell, 1980) yields

$$\phi_H \propto \left(\frac{NH_t}{\Omega^2 a}\right)^{\frac{1}{3}}. \tag{3}$$

Both of these scalings capture the behavior of the Hadley cell more realistically. While Lu et al. (2007) find very little correlation between the Hadley cell width and tropical tropopause height in IPCC AR4 models (finding them to be anti-correlated, from year to year, within each model), they note a strong correlation between ϕ_H and the extratropical tropopause height, which is itself strongly related to tropospheric stability.

Going further, Lu et al. (2008) examine AR4 model output, breaking down the contributions to the Phillips criticality measure from lower tropospheric vertical wind shear (or meridional temperature gradient), and lower tropospheric stability. While they do find correlations between both of the components of Phillips criticality and the modeled Hadley cell response, the contribution of vertical wind shear seems less robust.

One drawback to these studies is that, although they account for the *generation* of waves in the baroclinically unstable environment on the flanks of the Hadley cell, they do not account for the *dissipation* of waves within the Hadley cell. The atmosphere is assumed to be nearly inviscid, but in reality, waves propagating from the midlatitudes create a sort of macro-scale diffusion. Thus, the above assumption of angular momentum conserving flow is often broken (at times quite severely). A useful metric of the validity of the angular momentum conservation assumption is the local Rossby number (Walker and Schneider, 2006). The local Rossby number can be understood by examining a simplified tropical upper-tropospheric momentum balance. Above the Hadley cell centers, friction can be ignored, as can the vertical advection of momentum by the mean flow. The former assumption is generally understood for the free atmosphere, and the latter is quite accurate for the Tropics. The horizontal momentum budget then becomes

$$(f+\overline{\zeta})\overline{v} = f(1-Ro)\overline{(v)} \approx S, \tag{4}$$

where overbars denote the zonal mean, v is the meridional velocity, ζ is the relative vorticity, f is the Coriolis parameter, $Ro = -\overline{\zeta}/f$ is the local Rossby number, and S is the eddy momentum flux. The Held and Hou (1980) theory described above assumes high local Rossby number flow $Ro \to 1$, where S and $\overline{v}$ are no longer related. Other theories examine the lim $Ro \to 0$, where mass flux ($\propto \overline{v}$) is completely determined by eddy momentum flux S. Walker and Schneider (2006) demonstrate that both the nonlinear momentum flux by the zonal mean flow (nonlinear, because the wind is both the 'advector' and the 'advectee'), and by the baroclinic eddies are important, using a range of simulations

with an idealized, dry general circulation model (GCM).

An important point, brought up in both Walker and Schneider (2006) and Lu et al. (2008), is that the mechanisms which determine the strength and width of the Tropics may vary by season. Specifically, the wintertime Hadley cell is considerably stronger than the summertime cell. As an equinox is passed, the intertropical convergence zone (ITCZ) crosses into the summer hemisphere (Schneider and Bordoni, 2008; Bordoni and Schneider, 2009). The advection of cooler air from the winter hemisphere, in consequence of the approximate gradient momentum balance in the tropical upper troposphere, pushes the ITCZ further into the summer hemisphere than the latitude of maximum radiative heating. Thus, the moist deep convection generally associated with the ITCZ occurs predominantly on the equatorward side, mainly fueling the wintertime Hadley cell. Easterlies in the upper equatorial troposphere prevent midlatitude eddies from propagating into the heart of this wintertime Hadley cell. The strong mean flow, driven by radiative heating, and the shielding of the tropics by the upper level easterlies from wave activity, produce relatively high Rossby number flow in the wintertime cell; the idealized work by Walker and Schneider (2006) suggests $Ro \approx 0.5$, over the wintertime cell. In contrast, the driving of the summertime cell is very weak; thus, midlatitude waves that propagate into the summertime cell have a strong effect on its strength and structure (Schneider and Bordoni, 2008; Bordoni and Schneider, 2009). This susceptibility to waves is succinctly expressed in Walker and Schneider (2006) as $Ro \leq 0.2$. The summertime Hadley cell (especially over the northern hemisphere) tends to be relatively indistinct, and the roles played by various

mechanisms are likewise murky.

The equinoctial seasons are, interestingly, not necessarily characterized by what one would consider equinoctial cells; that is, by a hemispherically symmetric circulation. It turns out that a small displacement of the zone of maximum radiative heating produces very sharply hemispherically asymmetric cells (Lindzen and Hou, 1988). The transition from one solstitial pattern to the other is somewhat less than gradual; in fact, due to a number of feedbacks involving both nonlinear mean-flow interactions, and eddy-mean flow interactions (Schneider and Bordoni, 2008; Bordoni and Schneider, 2009), it can be quite rapid. Thus, mechanistic studies describing the poleward shift in the seasonal mean Hadley cell boundary during Spring or Fall, should perhaps consider the mechanisms of change during solstitial seasons, and the factors that affect the timing of the transition between the two.

Recent work by Kang and Lu (2012) attempts to account for the seasonal effect of eddies on the width of the Hadley cell, by re-deriving the Held (2000) scaling, incorporating the local Rossby number, and variations in the latitude of the ITCZ, ϕ_i. For $\phi_i = 0$ and Ro$= 1$, their scalings reduce precisely to those above. Using AR4 model data, they fit a local Rossby number to their scaling for each season using the first 20 years of data. Then they compare trends in Hadley cell limits to predicted values using their scaling, and find very good agreement, suggesting that subtropical tropospheric stability is a major factor in changes in the Hadley cell width, even when eddy generation and dissipation are taken into account.

The El Niño-Southern Oscillation (ENSO) also strongly affects the width of the Hadley cell. During El Niño years, intensified tropical convection creates a more intense overturning Hadley circulation, which in turn produces stronger westerlies. This intensified vertical wind shear implies a reduction in baroclinic stability, and the cell terminates more quickly (Seager et al., 2003)—hence the narrowing of Hadley cell during El Niño years, noted in Lu et al. (2008). On the other hand, the stronger westerlies also may make the tropics more susceptible to the action of midlatitude eddies. The dissipation of these eddies removes angular momentum from the tropics, and acts to widen the cell, in opposition to the contracting effect of El Niño (Chang, 1995, 1998; Robinson, 2002; Seager et al., 2003).

Another possible effect of eddies on the Hadley cell, related to El Niño, is described by Orlanski (2003) and Orlanski (2005). He finds that increased baroclinicity in the Pacific affects the intensity of cyclonic and anticyclonic wave breaking events, which affects the distrubition of eddy momentum flux divergence on the flanks of the jet, and thus may also modulate the Hadley cell edge latitude. Abatzoglou and Magnusdottir (2006) find that anticyclonic wavebreaking events are much more common during La Niña years than during ENSO neutral or El Niño years.

Many of the studies described above include the effect of dissipating midlatitude eddies, but they do not consider how midlatitude eddies may be changing, independent of the tropics. From a Lagrangian standpoint, the thermally direct Hadley cell extends well into midlatitudes. Figure 1 from Walker and Schneider (2006) illustrates this nicely, using the isentropic meridional mass stream function. Viewed in this manner, the notion that

changes in the extratropics may affect the tropics seems more obvious.

But even in the Eulerian viewpoint, changes in midlatitude eddy generation, propagation, and eventual dissapation, and the resulting changes in eddy momentum flux divergence in the Hadley regime, understandably affect the Hadley circulation. Inasmuch as eddies sap the Hadley cell of its angular momentum, the Hadley cell can propagate further poleward before the resulting vertical shear in zonal wind becomes baroclinically unstable; this is a restatement of some of the ideas above (Schneider and Bordoni, 2008; Bordoni and Schneider, 2009; Kang and Lu, 2012; Levine and Schneider, 2010). Here, however, the focus is on the possibility that the changing local Rossby number in the Hadley cell is a result of a change in the eddy activity from the extratropics, rather than a change in the susceptibility of the Hadley cell to such activity. The particulars of these changes in the extratropics are discussed below, but it should be kept in mind (and variations in the local Rossby number provide a helpful reminder) that changes in extratropical wave activity and in the Hadley cell cannot be considered purely in isolation.

There is one other way in which changing climate at high latitudes may affect the Hadley cell, and this is alluded to by Kang and Lu (2012), and requires some additional explanation. The Kang and Lu (2012) paper makes explicit the effect of the latitude of the ITCZ on the predicted latitude of the Hadley cell; generally, the further the ITCZ is away from the equator (in either direction), the further the Hadley cell may extend. Applying the angular momentum conservation argument, the further the ITCZ is from the equator, the less angular momentum there is for the either Hadley cell to conserve. The

location of the ITCZ, in turn, is dependent on the temperature and moisture fluxes across the tropics (Mantsis and Clement, 2009; Kang et al., 2008, 2009). Frierson and Hwang (2012) demonstrates that the ITCZ position is even sensitive to globally homegenous forcings, such as the radiative forcing due to increasing greenhouse gas concentrations, due to inhomogenous boundary conditions (e.g., land cover) beneath. As the strong seasonal cycle in the Hadley cell is dependent on the position of the ITCZ, it seems likely that this effect is likely to be seen in changes of the timing of the seasonal cycle, and indeed, studies suggest this to be the case (Chiang and Bitz, 2005; Biasutti and Sobel, 2009).

1.5 On the extratropical circulation

Key points in this section include:

- The influence of eddies on the extratropical zonal mean flow is ubiquitous.
- Explanations for zonal mean jet shifts have been proposed, which often fall into two groups:
    1. linear wave arguments, involving the notion of a critical latitude, and
    2. nonlinear arguments, involving changes in the eddy life cycle.

The notion that eddies may exert a control on the zonal mean circulation has been put forward since the early part of the 20th century (Jeffreys, 1926), but the numerical modeling techniques needed to study this relationship have only been commonplace for a few decades. The proposed dynamical mechanisms which define the character and extent of the extratropical circulation are, understandably, quite varied.

The extratropical zonal mean circulation is strongly tied to the behavior of large-scale eddies. Eddy-mean flow interactions are complex and inherently nonlinear, but some understanding can be gained through a linear treatment, considering how waves of a given wavenumber and phase speed propagate meridionally, given a prescribed background flow.

Midlatitude eddies, which travel westward relative to the midlatitude background wind, propagate meridionally at a speed that decreases as they approach the speed of the background flow. Thus, as waves propagate equatorward, which the majority of synoptic scale waves do (Held, 2000) away from the jet, they approach some critical latitude, at which point their phase speed matches the background zonal wind, and their meridional propagation speed approaches zero. Even in the presence of slight dampening, these waves, then, must dissipate some time before reaching this critical latitude.

Inasmuch as tropical wind speeds increase or decrease, the critical latitude should shift equatorward or poleward, respectively. This idea has been used by Robinson (2002) to explain some of the zonally symmetric circulation impacts of the El Niño Southern Oscillation (ENSO), and is closely linked to seasonal changes in the local Rossby number. Robinson (2002) notes that El Niño events are associated with an intensification of tropical overturning in the Hadley cell. The Coriolis force then acts on this intensified poleward flow, producing anomalously strong westerlies aloft. These anomalous westerlies are argued to permit the propagation of eddies further equatorward. During an ENSO-neutral year, eddy dissipation near the eddy-driven jet acts to reduce baroclinicity on its equatorward flanks, keeping the midlatitude jet some distance from the tropics. During an El

Niño year, the relative lack of dissipation near the equatorward flank of the eddy-driven jet increases baroclinicity on its equatorward flank, shifting the jet equatorward.

Even if tropical winds remain constant, however, the critical latitude may still shift, depending on the phase speed of the midlatitude waves. The mechanism proposed by Chen and Held (2007) suggests that increasing eddy phase speeds (in response to zonal westerly acceleration in the UTLS region) are responsible for an increase in the critical latitude of wave absorption, and a poleward shift of dissipation and of the zone of maximum baroclinicity. This mechanism is generally cited to explain shifts on the equatorward side of the eddy-driven jet, as zonal winds on the poleward flanks of the jet generally increase with climate change, and the flow-relative phase speed of midlatitude eddies changes less compared to the zonal winds on the equatorward side of the jet. (If zonal winds remained unchanged on the poleward flank of the jet, this mechanism would result in a narrowing of the jet, rather than, or in addition to, a poleward shift.)

Kidston et al. (2010) focus on the flow-relative phase speed of the jets, noting that the observed and modeled increase in eddy length scale should be accompanied by a decrease in the flow-relative phase speed of midlatitude waves, since Rossby waves propagate westward relative to the background flow, depending on their wavenumber. This flow-relative phase speed decrease should allow waves to propagate further from the jet core before dissipating. Although most midlatitude waves propagate equatorward from the jet, some do propagate poleward. The poleward flanks of the jet are also sites of significant eddy generation. If eddy dissipation is displaced further poleward from the jet,

the net convergence in these regions will increase, and the jet is likely to shift poleward. In contrast, Barnes and Hartmann (2011) suggest that the eddy length scale should increase as a *result* of a poleward shift of the jet.

Other studies suggest that linear wave theory (as we have cited it above) is of limited importance. They argue, rather, that stratospheric perturbations impact the troposphere by modifying waves during their nonlinear stages (Wittman et al., 2004, 2007; Kunz et al., 2009; Rivire, 2009, 2011). In other words, they suggest that it is a change in how eddies form and break that matters, not so much as a change in the critical latitude. They describe two eddy lifecycles, dubbed LC1 and LC2. The two types of eddies propagate and break differently, and react differently to a changing zonal mean temperature and wind structure.

Williams (2006) and Lorenz and DeWeaver (2007) examine the relationship between the extratropical circulation and the height of the extratropical tropopause. But by modifying the tropopause, they alter stratospheric temperatures, which are implicated in other mechanisms here. While we do not discount the possibility that tropopause height may alter the behavior of midlatitude waves, the tropopause itself is a manifestation of the temperature structure in the stratosphere above and the troposphere beneath, and we see no simple way to delineate the altitude of the tropopause from these other variables.

The reader may notice that this discussion of extratropical circulation change mechanisms is decidedly more qualitative than the above discussion of Hadley circulation change. Again, this goes back to the complexity of eddy-mean flow interactions; no scaling has been put forward to the author's knowledge that describes the latitude of the eddy-driven

jet, as has been put forward for the Hadley cell edge shift. Of course, there is no complete theory for circulation widening (Schneider et al., 2010). Any mechanism that describes changes in one cell is ultimately incomplete without including the effect of the other.

1.6 Our work, in context

Key points in this section include:

- This dissertation is built of three related studies.
- This work is unique in its consistent framework, the number and length of simulations, and in some of our analyses.

The previous sections outlines a substantial body of research into the widening general circulation. Work by the author includes three related studies regarding the general circulation. The first study is a documentation of the equilibrium circulation response to various prescribed external forcings. This work involves investigation of the relationships between shifts of different circulation features. The second focuses on the relationship between two such indicators. Although this second paper examine the relationship between these features in the equilibrium responses, its primary concern is understanding their relationship from year to year. Substantial differences between the year-to-year response and the equilibrium response exist, and to better understand the chain of events in the long-term response, the third study examines large ensembles of three-month simulations with prescribed forcings switched on instantaneously.

From this description, it can be seen that this work is not intended to be completely realistic. It employs an idealized model framework with equilibrium or switched-on forcings, and even these forcings are idealized. This work falls somewhere in the middle of the spectrum of investigations described by Held (2005), in which idealized models improve understanding, and comprehensive models aim for prediction. Some of the forcings in this work are chosen to represent observed or predicted changes in forcings during the preindustrial era, the present day, or 50 or 100 years from now. Other forcings are chosen to emphasize one aspect of such change. The two-times ozone depletion projection, for example, will likely never be realized, and the ozone super-recovery experiment is likewise unlikely to occur, but the linearity of the circulation response to different forcings, at least in the neighborhood of the present day climate, makes these types of forcings useful for amplifying the signals expected in the real world. While this work is too complicated to be done analytically, it is idealized enough to allow at least the attribution of modeled changes to a given forcing, or to whether ocean temperatures are held fixed or allowed to respond. All three of the studies in this work employ nearly the same model framework.

The following relates each of this dissertation's chapters to several pertinent recent studies. Most of these studies are mentioned in previous sections, and the reader may refer to them to see other works which compare with my studies.

The first study, documented in Chapter 3, involves a careful examination of shifts in the circulation features due to greenhouse gases and ozone depletion. It employs a suite of experiments performed with a fully complex atmosphere-only model, each at least 500

years long, with individually prescribed greenhouse gas concentrations, stratosheric ozone levels, sea surface temperatures, and sea ice coverage. This work has similarities with Polvani et al. (2011b), although it includes over a dozen different simulations, each much longer, and the work examines the effects of sea surface temperatures separately. The author performs some analysis of phase speed spectra for different experiments, as with Lu et al. (2008). The author also examines the effects of forcings on global precipitation as in Kang et al. (2011). Furthermore, work is performed, investigating the role of sea ice coverage on the latitude of the northern hemisphere jet, which is related to Deser et al. (2010).

The second study, described in Chapter 4, is a targeted investigation of the ratio between shifts in the eddy-driven jet and the Hadley cell edge. Staten et al. (2011) find that poleward circulation features seem to shift more strongly in response to external forcings than equatorward circulation features do, with something resembling a two-to-one ratio. Kang and Polvani (2010) report a two-to-one ratio in interannual shifts between the jet and the Hadley cell edge, but also argue that the same ratio did not apply for circulation trends. With this possible discrepancy between these studies, this chapter took a closer look. This investigation finds some strong contrasts between the ratios for interannual shifts and of trends and forced shifts, and the author investigates possible reasons for the two-to-one ratio. A new scaling, developed by Kang and Lu (2012), is employed to aid our understanding. In the end it is found that the two-to-one ratio is mostly related to unforced internal atmospheric variability, which is precisely what investigations of climate trends

and forced shifts try to remove.

The third study, detailed in Chapter 5, attempts to bridge this divide between fast processes and the equilibrium response, by performing large ensembles of forced experiments with switched-on forcings. This study examines several experiments, each with one modified, exaggerated forcing. Wu et al. (2011) examine greenhouse gas increases in a similar framework, although they perform their simulations using a coupled model, which delays components of their circulation response. Chen et al. (2012) use an uncoupled model framework more similar to the present framework, to understand the effect of instant, uniform warming of the global ocean. However, they use an aquaplanet model with solstitial conditions, while this dissertation examines shifts in a model with realistic land and topography, and prescribe projected sea surface temperatures from coupled model output. The author attempts to diagnose changes, similar to these other studies, and examines the effect of eddies as in Wu et al. (2012), although Wu et al. (2012) go deeper into the changing propagation of eddies in the latitude-height plane, while the present treatment is more broad, covering the transient response in six ensemble experiments.

This work emphasis the importance of sea surface temperatures, which is somewhat unique. Most similar recent studies like focus on the importance of the direct radiative forcings, even when sea surface temperatures are held constant. Possible reasons for this discrepancy are discussed in Chapter 3. The present examination of the ratios of shifts in the jet and the Hadley cell edge is the most detailed of its kind, and the relationship found between the mean Hadley cell position and the year-to-year ratio is a novel result. Others

have examined the ratios, but did not pursue them further when they found that the ratios were not constant (Schneider, 2012). Results from this work, using the equilibrium and spinup simulations together, help to show evidence for, and limitations of, the mechanisms of extratropical circulation change based on linear wave dynamics. The spinup ozone simulation suggests a generally overlooked connection between ozone depletion over the arctic, and tropospheric surface climate over high latitudes.

CHAPTER 2

DATA

This chapter describes the data products analyzed in this dissertation. Several simulations were performed specifically for the work contained herein, while many were performed previously. As the work described in this dissertation makes heavy use of model data generated using the Geophysical Fluid Dynamics Laboratory (GFDL) Atmosphere Model version 2.1 (AM2.1), Section 2.1 describes this model setup in some detal. The simulation types performed before and during this study, including the prescribed forcings (e.g., greenhouse gas concentrations), are described in Section 2.2. In addition to the GFDL model, however, this work also involves analyzing ensembles of simulations performed with the Community Atmosphere Model version 4 (CAM4), produced at the National Center for Atmospheric Research (NCAR), as well as output from other models, namely the Community Atmosphere Model version 3 (CAM3), and the Community Climate Module versions 3 and 4 (CCSM3 and CCSM4, respectively). These data from other models are documented in Section 2.3. This work also draws data from reanalyses, as outlined in Section 2.4. As much of the work described in the various components of this dissertation utilize some common core calculations, this chapter concludes with a summary of some of

the most basic indices used in Section 2.5.

2.1 The GFDL AM2 model framework

Key points in this section include:

- We examine and perform simulations using recent versions of the GFDL climate and atmosphere models, which have been shown to produce a realistic climate mean state and variability, including El Niño-Southern Oscillation.
- We use data from an atmosphere-ocean coupled simulation, as well as data from uncoupled simulations.

2.1.1 The flexible modeling system

The simulation work performed for this and other studies by the Climate Research Group at the University of Utah is aided by the Flexible Modeling System (FMS). FMS is a software framework, built in Fortran 90, designed to support the construction and use of earth system models (Geophysical Fluid Dynamics Laboratory). It insulates developers and scientists from the 'dirty work' of running complex earth system models on distributed computing architectures. FMS handles exchanges of information between model components through standardized interfaces, and manages model output, creating common data format (CDF) files for easy analysis. Together, these functions allow users to focus on science, rather than on technical details.

FMS is updated periodically by GFDL. Thomas ported the version used in this study in 2007, and has been performing simulations since, using the high performance computing clusters at the Center for High Performance Computing (CHPC). This study makes extensive use of the simulations performed by Thomas Reichler, as well as simulations performed by the author as part of this work. The model setup is described in the following section.

2.1.2 The AM2.1 atmosphere model

Our simulations have been performed with the GFDL AM2.1, as mentioned above. AM2 and AM2.1 are quite similar models, and this dissertation will often refer to either as 'AM2', using'AM2.1' for descriptions specific to the updated model version. This section describes the specifics of the AM2 models, as well as the respective coupled models CM2 and CM2.1, inasmuch as it is pertinent to this study. In addition, this section summarize some evaluation and comparison work involving AM2.1 and other World Climate Research Programme (WCRP) Coupled Model Intercomparison Project phase 3 (CMIP3) models.

AM2.1 includes a hydrostatic, finite-volume dynamical core (Anderson et al., 2004; Delworth et al., 2006). Horizontal grid resolution in both versions is approximately 2° latitude by 2.5° longitude. A hybrid sigma-pressure grid is used, with 24 levels from about 30 m above the surface, to about 3 hPa. To put these resolutions in context, the Community Atmosphere Model version 3, a comparable model from the same generation, has 26 vertical levels, and can be run with a spectral dynamical core at up to a T85 resolution

(truncation at wavenumber 85, which corresponds to 1.41° longitude at the equator), or as a gridpoint dynamical core with 2° by 2.5° resolution (Collins et al., 2006). The Canadian Middle Atmosphere Model (CMAM), a more recent model used for the Chemistry-Climate Model Validation (CCMVal) project, has 71 levels in the vertical, a specral resolution of T37, which corresponds to about 3.75° longitude at the equator (Scinocca et al., 2008). The emphasis on the vertical resolution for CMAM is understandable considering the purpose of the model—to accurately simulate a coupled-chemistry stratosphere. Generally, though, the resolution of the various models in this and similar studies is comparable; the resolution of the AM2 model used in this study is neither outstanding, nor is it detrimental. The fact that the standard version of AM2 is the poorest vertically-resolved model of the three described is not a concern for this dissertation, as a modified formulation of the model, with 48 levels in the vertical, is also utilized. For further details concerning the dynamical core, including a justification for the choice of the gridpoint dynamical core (versus a spectral dynamical core), the reader is referred to Anderson et al. (2004). Anderson et al. (2004) discuss most of the model physics, including the land component (LM2), in further detail, but a few of the more relevant points are described here.

AM2 keeps track of the three-dimensional distribution of several species of aerosols, including sulfate, hydrophilic carbon, hydrophobic carbon, dust, and sea salt. AM2 includes the so-called "aerosol direct effect," or the effect of aerosols on the shortwave albedo of the atmosphere, scattering visible light away from the earth. However, it does not include the less-understood "aerosol indirect effect," or the effect of aerosols on cloud

properties, and the resulting change in cloud albedo. The aerosol indirect effect can act either to cool or to warm the atmosphere, and represents one of the more important sources of uncertainty in climate projections. The absence of the indirect effect in this model means that aerosols in AM2 act mainly to cool the ocean surface (Ming and Ramaswamy 2009). This has important ramifications for the choice of simulations performed for this study, as well as their interpretation, as described in Section 2.2.

While gravity wave parameterization is beyond the scope of this study, it is also worth mentioning here. Gravity wave breaking can cause significant drag on lower stratospheric flow, which in turn has a strong effect on tropospheric flow (Alexander et al., 2010). The choice of gravity wave parameterization scheme has a substantial effect on the midlatitude circulation, and on the strength of the jet. The scheme used in AM2 is that after Pierrehumbert (1986); Stern and Pierrehumbert (1988). It may also be worth noting that, as the AM2 model does not resolve gravity waves resulting from tropical deep convection, its simulated climates exhibit no quasi-biennial oscillation (QBO).

The differences between AM2 and AM2.1 are described in Delworth et al. (2006), and a few are summarized here. AM2.1 contains a finite *volume* dynamical core, rather than a finite *difference* dynamical core. The finite volume core has an improved representation of midlatitude winds, and a lower SST bias in the coupled model (CM2.1). This is pertinent because, as described in Section 2.2, the sea surface temperatures used in this study's uncoupled simulations are derived from coupled simulations with CM2.1. Other model modifications in AM2.1, relative to AM2, include the grid used by the dynamical core, a

retuning of the cloud parameterization scheme, a change in how the land model handles evaporation over frozen soil, and a change in the viscocity in the ocean in the extratropics. The latter modification impacts the sea ice work in Section 2.2, as it reduces sea ice coverage and a cold bias in the North Atlantic.

Following Fletcher et al. (2009), this work uses an enhanced version of AM2.1, with 48 levels in the vertical, rather than the standard 24. This is the same model as that used in Austin et al. (2007), but without interactive chemistry. Most of the additional layers are above 100 hPa, producing a well-resolved upper troposphere and lower stratosphere. In this work, the 48-level formulation is referred to as L48, or as the "high-top" version, and the 24-level formulation as L24, or as the "low-top" version.

2.1.3 The ocean component

The oceanic components of the CM2.0 and CM2.1 models have a horizontal resolution of 1°, becoming finer in the tropics, approaching $1/3^\circ$ at the equator, with poles over North America and Eurasia. Each has 50 vertical levels, with 22 levels in the top 220 m (Delworth et al., 2006).

The coupled models maintain a stable climate, even without flux adjustments. The CM2.1 model has particularly small drift, and realistic exchange between the deep ocean and upper levels. Although the simulated mean climate over multiple centuries appears realistic, CM2.0 does exhibit temperature and SST biases relative and CM2.1, due to improvements in surface wind stress calculations, tuning of the cloud and the land models,

and a reduction in the lateral viscocity in the extratropics (Delworth et al., 2006). Both models show a cold SST bias along the equator, and warm SST biases along the coast of South America (Wittenberg et al., 2006).

Each model has a realistic ENSO, returning roughly every 2–5 years, although the SST anomalies are too strong, and are not phase locked to the end of the year as tightly as in observations. ENSO-related anomalies are displaced 20°–30° westward of their observed locations (Wittenberg et al., 2006). For more on the coupled model formulation and realism, the reader is referred to Delworth et al. (2006), Gnanadesikan et al. (2006), Wittenberg et al. (2006), and Stouffer et al. (2006).

2.2 In-house simulations examined

Key points in this section include:

- This study draws data from dozens of $\geq$ 500-year atmosphere-only simulations, each with different constant, prescribed forcings.
- Ensembles of 90-day switch-on forcing experiments are also performed with the uncoupled model.

The GFDL model simulations examined and performed for this study can be divided into three classes, (1) a very long CM2.1 coupled time-slice simulation, (2) dozens of long AM2 uncoupled time-slice simulations, with various prescribed forcings, and (3) ensembles of short switch-on forcing experiments. Each of these groups is discussed in turn below.

2.2.1 Coupled time-slice simulations

The first simulation discussed is the very long (about 4000 years), coupled time-slice simulation. In these simulations, external forcings are held constant during the entire run time. Internal variability is still present in these time-slice simulations, but when performed long enough, this variability can be accounted for (and studied for its own sake, as in Chapter 4 of this dissertation), allowing the mean climate state to be desribed with some certainty. Using multiple time-slice simulations, each with different prescribed forcings, one can begin to attribute the differences between the simulated climates to the differences in forcing.

This simulation serves (1) to establish a benchmark climate state for the model, and (2) to calculate the sea surface temperatures for uncoupled control simulations. It is forced with radiative forcings (including those due to CO_2, at concentrations of 286 ppm) at their year-1870 conditions, and aerosols at their preindustrial levels. This simulation, then, is called the preindustrial control simulation, or the coupled control run.

Two other CM2.1 simulations from the CMIP3 dataset were used to produce year-2000, year-2050, and year-2100 SSTs for the uncoupled simulations: a 20c3m simulation, which includes a realistic, quite complete set of time-dependent forcings, intended to accurately resemble the climate forcing history of the earth, and an A1B run, or a 'middle of the road' scenario, including time-dependent forcings from a conservative to moderate estimation of what future greenhouse gas emissions (and other anthropogenic forcings) would be. Year-2050 and year-2100 SSTs are also derived from the A1B simulation.

2.2.2 Uncoupled time-slice simulations

In addition to the coupled simulation, this work makes use of several uncoupled time-slice simulations, each with one or more forcings applied (see Table 1). This work treats sea surface temperature changes as 'external' forcings, because in the uncoupled framework they are external to the modeled system. While the levels of prescribed forcings are often chosen to represent a given time period (e.g., well-mixed globally averaged greenhouse gas concentrations of 380 ppm), others are chosen in a more idealized manner, to produce a strong, clear signal (e.g., twice the observed depletion of stratospheric ozone).

Zonal mean ozone data comes from the Randel and Wu tropospheric and stratospheric ozone dataset (Randel and Wu, 2007), with monthly mean values taken from pre-1980 years (with no ozone label in Table 1) for the preindustrial states and future recovered states, and from the year 2000 (labeled O_3) for the present-day, depleted ozone state (see Figure 1). The Randel and Wu dataset draws from similar data as the SPARC ozone database (Cionni et al., 2011), which is used in several other recent studies mentioned in Chapter 1. The -0.4$\times O_3$ and 2$\times O_3$ ozone levels were performed specifically for this study, and did not draw data directly from the Randel and Wu dataset. Rather, their values were extrapolated, based on the experienced (1$\times$) ozone depletion.

The ozone depletion prescribed in this study is dominated by the southern hemisphere (SH) ozone hole (see Figure 1a), with the strongest depletion in September-October-November. The northern hemisphere (NH) also experiences spring-time depletion, although it is much weaker than that experienced over the antarctic. In the tropics some year-round increase is

Table 1: AM2.1 time-slice experiments.

Name	CO_2 (ppm)	O_3 ($\times$dep)	SST (year)
$0.5\times CO_2SST_{1870}$	143	0	1870
CO_2SST_{1870}	380	0	1870
$2\times CO_2SST_{1870}$	720	0	1870
$4\times CO_2SST_{1870}$	1320	0	1870
O_3SST_{1870}	286	1	1870
$CO_2O_3SST_{1870}$	380	1	1870
O_3SST_{2000}	286	1	2000
$CO_2O_3SST_{2000}$	380	1	2000
SST_{2050}	286	0	2050
$CO_{2,2050}SST_{2050}$	520	0	2050
SST_{2100}	286	0	2100
$SST_{2100}Ice_{1870}$	286	0	2100
$2\times CO_2SST_{2100}$	720	0	2100
CO_2SST_{2000}	380	0	2000
$-0.4\times O_3SST_{1870}$	286	-0.4	1870
$2\times O_3SST_{1870}$	286	2	1870
SST_{1870}	286	0	1870
SST_{2000}	286	0	2000
$CO_2O_3SST_{2050}$	380	1	2050

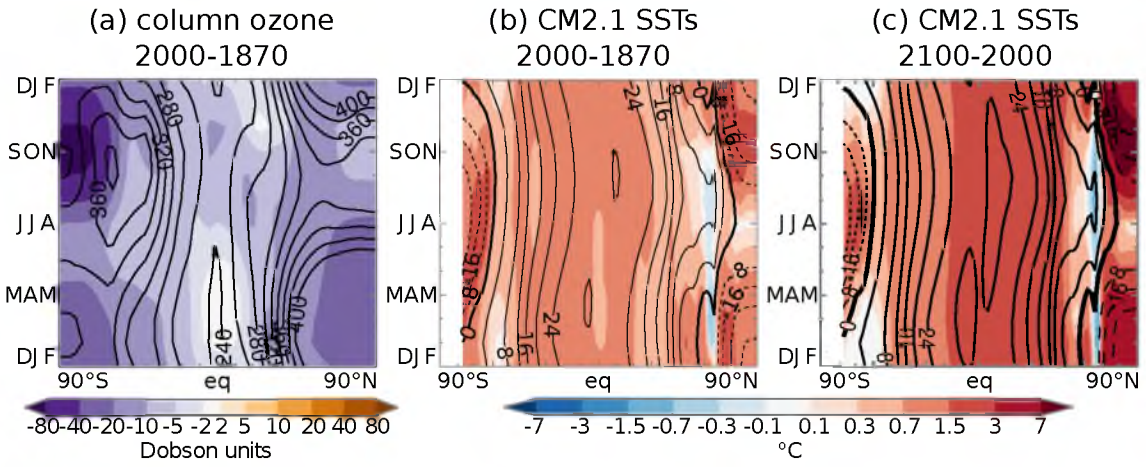

Fig. 1: Zonal mean (a) column-integrated ozone (in Dobson units) and (b, c) representative sea surface temperature forcings (in C; negative contours dashed) used in this study, by season and latitude. Black solid and dashed contours show control climatology, while shading shows the change between the time periods shown.

evident. The reader is referred to Randel and Wu (2007) for a more complete description of the changes seen in this dataset.

Well-mixed greenhouse gases are prescribed at their historical, present-day, and projected levels, with projected levels of CO_2, CH_4, and N_2O taken from the Intergovernmental Panel on Climate Change (IPCC) A1B scenario. This study uses CO_2 concentrations as a sort of shorthand to represent the levels of all these greenhouse gases, together. Specifically, in the experiment database (see Table 1), $0.5\times CO_2$, CO_2, $2\times CO_2$, $CO_{2,2050}$, and $4\times CO_2$ refer not only to a specified carbon dioxide concentration, but to corresponding CH_4, and N_2O concentrations as well. It is also worth mentioning here that in this study, the CO_2 response denotes the direct radiative effect, in the absence of a warming ocean.

Sea surface temperatures and sea ice coverage (together termed SSTs) come from the fully coupled Climate Model v2.1 coupled simulation, as described above. Prescribing

SSTs from the coupled model, rather than from observations, ensures that SSTs are mostly consistent with the dynamics in the atmosphere model. In order to reduce the effects of natural SST variability, such as the El Niõ Southern Oscillation, multiyear average SSTs are calculated for each month. Preindustrial SSTs are taken from 10 years of data from the preindustrial control run (PIcntrl) prepared for the IPCC fourth assessment report (AR4). Present-day and future SSTs are derived from the 20th century (20C3M) and A1B future scenarios, both also performed for the IPCC AR4, with present-day SSTs being averaged over 1997-2006, year-2050 SSTs being averaged over 2045-2055, and year-2100 SSTs being averaged over 2081-2100.

The changes in SSTs shown in Figure 1 include the temperature of regions formerly covered with sea ice. From 1870 to 2000 (Figure 1b), and from 2000 to 2050 (Figure 1c), much of this sea ice melts, increasing the temperature in the associated grid cells, and creating the impression of strong SST increases. This impression is valid, as this melting leads to strong, anomalous surface heat flux, and may play an important part in the well known poleward amplification of warming. Differences exist in the structure and seasonality of present day and future SST changes, and these differences in turn affect our projections of future climate. The SST changes from 2000 to 2050, shown in Staten et al. (2011), closely resemble the changes from 2000 to 2100, only not as strong.

Treating prescribed SSTs as an external forcing has the important benefit of allowing one to distinguish between the direct effect of radiative forcing due to greenhouse gas increases and ozone depletion, and the indirect effect (not to be confused with the indirect

aerosol effect) of the SST response to the combined forcings (see Deser and Phillips (2009)). This may be considered a decoupling of the enhanced greenhouse effect from the immediate radiative effect. Here the direct effect denotes the atmospheric temperature and circulation response to radiative forcings within the atmosphere itself, without allowing SSTs to respond. The indirect effect is the response of the atmosphere just to the changing SSTs, which are themselves a response to all the known forcings in the fully coupled simulation. This approach is useful for studying the mechanisms behind circulation shifts, as a given radiative forcing may cause a circulation shift via one set of mechanisms, while the SST response to that forcing may alter the general circulation via some other mechanisms. Thus the circulation change produced when both the radiative forcings and SST responses are included will be formed through a combination of mechanisms.

This work examines the effect of melting sea ice by analyzing the output from an additional time-slice simulation, created for this study, called $SST_{2100}Ice_{1870}$, where sea surface temperatures are increased from their preindustrial values to their year-2100 values, except where there is sea ice coverage in the preindustrial simulation. In this latter case, the sea ice is retained. There is one localized region where sea ice concentrations increase from 1870 to 2100 in the coupled simulation; this ice is left at its year-2100 value, as the its effects on the hemispheric circulation are small. The $SST_{2100}Ice_{1870}$ experiment has dual utility. By comparing it with SST_{1870} (which implicitly is prescribed with year-1870 sea ice coverage), one can (assuming a linear response by the atmosphere to sea ice and to sea surface temperature changes) isolate the effect of SST warming. By comparing it

with SST_{2100}, one can isolate the effect of sea ice depletion on the atmosphere. Sea ice concentrations in the AM2 model, are prescribed in a binary fashion; either a given grid point is covered with sea ice, or it is not. The sea ice fraction cannot be prescribed in this model.

While the prescribed SST warming in this study, along with the coupled SST changes from which it is derived, include the effect of increasing greenhouse gas concentrations, as well as the depletion and eventual recovery of stratospheric ozone, they also reflect changes in the atmosphere *not* explicitly examined in this study, namely anthropogenic aerosols. While the sea surface temperature averaging times do not come soon after any major volcanic eruptions, there has been a changing concentration of anthropogenic aerosols over the past several decades, and additional changes are prescribed in the A1B scenario, with which our SST-generating coupled model is driven. These changes in anthropogenic aerosols are not among the perturbed prescribed forcings in this study. Thus, it is certainly plausible that there exists some persistent temperature imbalance between the SSTs and the atmosphere, due not just to the lack of coupling, and passing warm and cold air masses, but simply due to the missing cooling from aerosols above. The general circulation response to anthropogenic aerosol emissions is a subject all its own (see, for example, Allen and Sherwood (2011)).

2.2.3 Uncoupled switch-on forcing simulations

The work in Chapter 5 utilizes ensembles of simulated responses to switched-on climate forcings. These experiments use the same modeling framework, beginning each ensemble with conditions from the preindustrial control experiment, and integrating for three months with constant, prescribed, switched-on forcings. As these experiments are used only in Chapter 5, they are documented in that chapter.

2.3 CAM4 and other models

Key points in this section include:

- This work utilizes some data from NCAR models, and from an earlier GFDL model.
- The work in Chapter 5 utilizes CAM4 switch-on forcing simulations in Chapter 5.

One advantage of our extensive use of time-slice simulations from the GFDL model is that it allows one to study the response of the atmosphere due only to given forcings. While this ideally yields some insight into mechanisms involved, it also means one cannot rule out the possibility that the mechanisms studied here are at least to some degree model-specific. While this does not devalue the meaningfulness of studying those mechanisms, it does mean that a second opinion is needed.

The GFDL models underpin much of this work. To validate the results from the GFDL model, this study make use of data from the National Center for Atmospheric Research (NCAR) Community Climate System Model version 3 (CCSM3) (Collins et al., 2006), along with the atmosphere only Atmosphere Model version 3 (CAM3), the Community

Climate System Model version 4 (CCSM4, now part of the Community Earth System Model framework) (Gent et al., 2011), and the corresponding atmosphere-only component, CAM4 (Neale et al., 2011). CCSM3 is a fellow CMIP3 model, used in several related studies, while CCSM4 is part of the CMIP5 dataset, which represents the state-of-the art of general circulation models. The other CCSM3 models generate somewhat different responses in the tropics than the GFDL model.

This work also examines output from an earlier version of the GFDL model (CM2.0), coupled to a mixed layer slab ocean, using an archived simulation from the CMIP3 multi-model dataset (Meehl et al., 2007).

We use the coarse resolution formulation of the CAM4 model in our switch-on experiments, with a $2.5^\circ \times 1.8^\circ$ grid, and 26-levels in the vertical. Like AM2.1, CAM4 uses a finite volume core. Ozone data in the CAM4 simulations in this study include zonally varying ozone levels at their year-2000 levels from the MOZART model (Horowitz et al., 2003), as well as the zonally symmetric ozone data used in the AM2 models in this study.

2.4 Reanalyses

To verify model results, many of the analyses in this work are repeated on data from the following four reanalysis datasets: the National Centers for Environmental Prediction-National Center for Atmospheric Research (NCEP/NCAR) 40 year Reanalysis Project (NNR) (Kalnay et al., 1996), the European Centre for Medium-Range Weather Forecasts (ECMWF) Interim Reanalysis (ERA Interim) (Dee and Uppala, 2009), the ECMWF 40

year Reanalysis (ERA40) (Uppala et al., 2005), and the National Oceanic and Atmospheric Administration-Cooperative Institute for Research in Environmental Sciences 20th Century Reanalysis version 2 (20CR) (Compo et al., 2011).

2.5 Common Indices

Many of the indices we describe here are sensitive to small changes in structure. Chapter 3 uses indices calculated from interpolated latitudinal profiles. During the research described in Chapter 4, it was found that this can often be avoided by calculating seasonal averages directly from the model-output fields themselves, rather than performing our index calculations, and then performing the seasonal averaging. Thus, the results in this dissertation present a mix of both methods. The choice of when to average can be nontrivial, even for large datasets; seasonal mean Hadley cell edges, for example, can differ by roughly a degree, depending on how averages are calculated. Calculating averages beforehand allows one to compare indices calculated from model data provided at different timescales.

Zonal mean temperature, zonal wind, sea level pressure, precipitation, surface evaporation, and the mass meridional stream function (Ψ) data are analyzed. This work denotes a clockwise (northward above, southward below, as with the northern Hadley cell) circulation as positive, and a counter-clockwise circulation as negative. The oleward Hadley cell boundaries, or edges (referred to in Chapter 4 as HC), are calculated as the first zero crossings of Ψ_{500} hPa poleward of the intertropical convergence zone (hereafter ITCZ),

after Lu et al. (2007). Poleward of the Hadley cell edges, the Ferrel cell center (FCC) is defined using several different metrics. The local surface wind maxima (or Ψ_{500} hPa extrema) were found to be sensitive to the structure of the jet. This complication in jet structure is noted by Schneider et al. (2010), and manifests itself by the crescent-shaped scatter plots, as in Figure 8 of Lu et al. (2008) and Figure 2 of Kang and Polvani (2010). Note that both of these studies plot the latitude of maximum near-surface westerlies; these are associated with the eddy momentum flux convergence in the upper troposphere, and thus with the resulting stream function extrema we analyze.) This work also analyzes a Ferrel cell center of mass, or, more correctly, a latitudinal cosine-weighted center of positive circulation (over the SH, or negative over the NH), finding this to be substantially more robust to changes in jet structure, as

$$FC = \int_{-90^\circ}^{\phi_{HC}} \phi \Psi_{500} \mathrm{d}\phi \Big/ \int_{-90^\circ}^{\phi_{HC}} \Psi_{500} \mathrm{d}\phi \text{ for } \phi < 0, \Psi_{500} > 0,$$

or

$$FC = \int_{\phi_{HC}}^{90^\circ} \phi \Psi_{500} \mathrm{d}\phi \Big/ \int_{\phi_{HC}}^{90^\circ} \Psi_{500} \mathrm{d}\phi \text{ for } \phi > 0, \Psi_{500} < 0. \quad (5)$$

The zero crossing of the stream function poleward of the Ferrel cell center in either hemisphere is denoted the Ferrel cell edge. At times the streamfunction never crosses zero poleward of the Ferrel cell center, in which case the Ferrel cell edge is set to 90°.

Indices are calculated based on the zonal wind, such as the zero crossings associated with the subsiding branch of the Hadley cell, and the low-level wind maxima associated with the maxima of eddy momentum flux convergence aloft. Indices are also calculated based on precipitation and/or evaporation fields. The precipitation – evaporation (P – E)

zero crossing ($P-E=0$) is defined as the first zero crossing of the $P-E$ field poleward of the latitude of minimum $P-E$, after Kang et al. (2011). The latitude of maximum precipitation is calculated over $\pm 30^{\circ}$–70° latitude.

Annular modes are calculated as the first empirical orthogonal function of zonal mean sea level pressure data poleward of $\pm 20^{\circ}$ latitude (Baldwin and Thompson, 2009). For consistency, the present-day time-slice simulation is used to produce a loading pattern. The pressure anomaly for each dataset with respect to the control time-slice simulation is then projected onto this pattern to produce an AM time series for each dataset.

2.5.1 Eddy cospectra calculations

Chapters 3 and 5 present results based on eddy cospectra, calculated after Chen and Held (2007) and Lu et al. (2008). As with these other studies, wind and temperature covariances are calculated, Hanning smoothing is applied (at least for the shorter time periods in Chapter 5), and data are transformed onto spectral coordinates. From here, either (1) coordinates are transformed once more and summed over wavenumber to calculate covariances as a function of phase speed and latitude, or (2) data are summed by frequency to calculate covariances as a function of wavenumber and latitude. This allows us to examine several eddy mechanisms described in Chapter 1.

CHAPTER 3

THE CLIMATOLOGICAL MEAN RESPONSE TO FORCINGS

3.1 Motivation for documenting the equilibrium response

Key points in this section include:

- This chapter documents the circulation response to individual forcings as a first step to understanding mechanisms.
- This chapter greatly expands upon the work performed in Rutz (2010)
- Many of the results in this chapter are published in Staten et al. (2011)

As this dissertation attempts to delineate some of the dynamical mechanisms of behind the general circulation response to different external forcings, it is necessary as a first step to examine the forced climate response itself. Thus, this section will focus on documenting the forced climate response to individual forcings over the 20th and 21st centuries. Hopefully, this work will aid in better understanding the mechanisms behind such change by isolating interfering, and at times competing, effects. It may also help to shed light on why models often underestimate tropical and northern hemisphere (NH) circulation shifts, as quantifying the response to individual forcings is also step towards understanding the

overall response. Finally, this work is valuable in its own right, as part of the broader discussion of modeled past and projected climate change. As part of this discussion – and for the sake of comparison – the forced hydrological response is examined, in addition to the general circulation response.

The work in this chapter is related to and expands the work of Rutz (2010). Rutz (2010) documents zonal mean circulation shifts occurring over the 20th century *only* using the standard formulation of AM2.1. This work documents not only forced circulation shifts during the 20th century, but also during the next 50 and 100 years. This work uses both the standard and stratosphere-resolving versions of AM2.1, and includes an examination of the effect of sea ice changes on the general circulation. This study examines changes in zonally varying precipitation, in addition to the zonal mean response. Finally, while the work of Rutz (2010) was almost completely descriptive, here an analysis of the co-spectra of mid-latitude eddies is performed, after Randel and Held (1991), in an attempt to understand better the reasons for the shifts seen in this model study. Most of the results of this section have already been published in Staten et al. (2011).

3.2 Time-slice experiments and our statistical approach

Of the studies described in Section 1.3, only Perlwitz et al. (2008) compare ozone depletion, greenhouse gas increases, and SST warming each in isolation, as in this study. Also in contrast to most of the studies described – Kang et al. (2011) being the only exception – this study takes decadally averaged SSTs from a companion coupled model,

rather than from observations, in order to filter out interannual SST variability and to apply model-consistent SST patterns. Combinations of past, present and future prescribed forcings are chosen to perform three sets of time-slice simulations in this study. Our '2000' simulations examine the individual and combined effects of year-2000 forcings, compared to a year-1870 preindustrial control. Simulations labeled '2050' and '2100' examine the effects of year-2050 and year-2100 forcings, respectively, compared to a year-2000 control (see Table 2). Simulations in which only greenhouse gases are perturbed from their control levels are labeled, simply, 'CO_2.' Perturbed ozone simulations are labeled 'O_3,' and perturbed SST simulations are labeled 'SST.' Simulations with all three forcings perturbed simultaneously are labeled 'all.' The simulations from which we present results in this chapter represent a subset of the simulations examined for this dissertation, and even these are just a subset of those performed at the University of Utah using the AM2.1 model.

The '2000' and '2050' simulations are performed precisely as described—with forcings held at their respective control levels except for those labeled. However, the author has not yet performed mixed present-day and year-2100 simulations. To reduce computational cost, these differences are approximated using an existing set of simulations, with specific forcings prescribed at present-day and year-2100 levels, and the other forcings held at their preindustrial values. For example, the '2100 SST' simulations are examined by using year-2000 SSTs for the control and year-2100 SSTs for the experiment, but 'CO_2' and 'O_3' forcings are held at their 1870 levels in both simulations. This approach is valid inasmuch

as the response to external forcings is linear; this assumption turns out to be reasonable in the neighborhood of present-day climate, as we will illustrate using the '2000' and '2050' simulations. The 2050–2000 simulations are detailed in Staten et al. (2011), while 2100–2000 results are documented here. The reader is referred to Staten et al. (2011) for more detail on the 2050–2000 response.

Changes in zonal mean quantities presented in this study, including temperature, wind, and the indicators described above are presented with measures of significance. The author calculates the significance from decadally averaged raw data, using a students t-test with unequal sample sizes and unequal variances. It should be kept in mind, however, that the zonal mean indicators described above and their associated confidence intervals are calculated from the latitudinally smoothed fields. The calculations based on unsmoothed fields occasionally produce extreme values for a given month and forcing, with accompa-

Table 2: Experiment pairs for respective centuries

group	forcing	control	experiment
2000–1870	O_3	SST_{1870}	O_3SST_{1870}
	CO_2	SST_{1870}	CO_2SST_{1870}
	SST	SST_{1870}	SST_{2000}
	All	SST_{1870}	$CO_2O_3SST_{2000}$
2050–2000	O_3	$CO_2O_3SST_{2000}$	CO_2SST_{2000}
	CO_2	$CO_2O_3SST_{2000}$	$CO_{2,2050}O_3SST_{2000}$
	SST	$CO_2O_3SST_{2000}$	$CO_2O_3SST_{2050}$
	All	$CO_2O_3SST_{2000}$	$CO_{2,2050}SST_{2050}$
2100–2000	O_3	$CO_2O_3SST_{2000}$	CO_2SST_{2000}
	CO_2	CO_2SST_{1870}	$2\times CO_2SST_{1870}$
	SST	SST_{2000}	SST_{2100}
	All	$CO_2O_3SST_{2000}$	$2\times CO_2SST_{2100}$

nying low confidences in those cases (although we have since improved our calculations, and much of this trouble can be preempted by averaging before the indicator calculations, as described previously). In general, however, the magnitudes and seasonalities of the different indicators are fairly insensitive to the degree of latitudinal smoothing.

3.3 The zonal mean temperature and wind response

Key points in this section include:

- Ozone depletion cools the SH stratosphere during SON, shifting the tropospheric jet poleward during DJF.
- Ozone depletion weakens the NH polar vortex during DJF.
- Ozone recovery is expected to have the opposite effects as depletion.
- Greenhouse gases cool the stratosphere and shift jets poleward over both hemispheres during most seasons.
- SST warming likewise shifts the jets, and is key to the tropospheric temperature and wind response.
- The responses to combined forcings are very similar to the linear sums of the individual responses.
- We expect the SH jet to continue shifting poleward, even during the next 50 years, due to the combined effects of CO_2 and SSTs.

3.3.1 The 20th century temperature and wind response

Before examining the specific changes in the overturning circulation, this section documents the zonal mean temperature and wind responses, taking a holistic view of zonal mean temperature and zonal wind changes during the 20th and 21st centuries, by season. Figure 2 shows the forced zonal mean temperature changes, by forcing, for the '2000' set of experiments, as well as the corresponding zonal mean zonal wind response, for December–February. The 20th century figures also include a panel showing the reanalysis trend over the past decades, to put our data in context, and to provide a reality check.

Ozone depletion ('O_3'), as expected, acts mainly to cool the stratosphere, particularly over the summer hemisphere lower stratosphere (Figure 2a), where the depletion is strongest, due to the particular isolation of antarctic polar stratospheric air during the polar night. This effect is strongest over the SH, with peak cooling of over 2 °C at 100 hPa, poleward of 80 °S. The effect of ozone depletion on tropospheric temperatures is small and mostly insignificant at the 5% level, even with the resulting changes in general circulation taken into account (these figures are, after all, equilibrium responses). However, cooling extends near the surface over Antarctica, consistent with (Gillett et al., 2002).

The zonal mean wind response (see Figure 2b)to stratospheric response can be characterized to a first order as being in thermal wind balance with the stratospheric temperature response (not shown). Ozone depletion alone strengthens SH stratospheric westerlies by as much as about 2 ms^{-1} over the SH, while it weakens NH stratospheric westerlies by about 1 ms^{-1} during DJF. In contrast to the stratospheric response, the tropospheric response

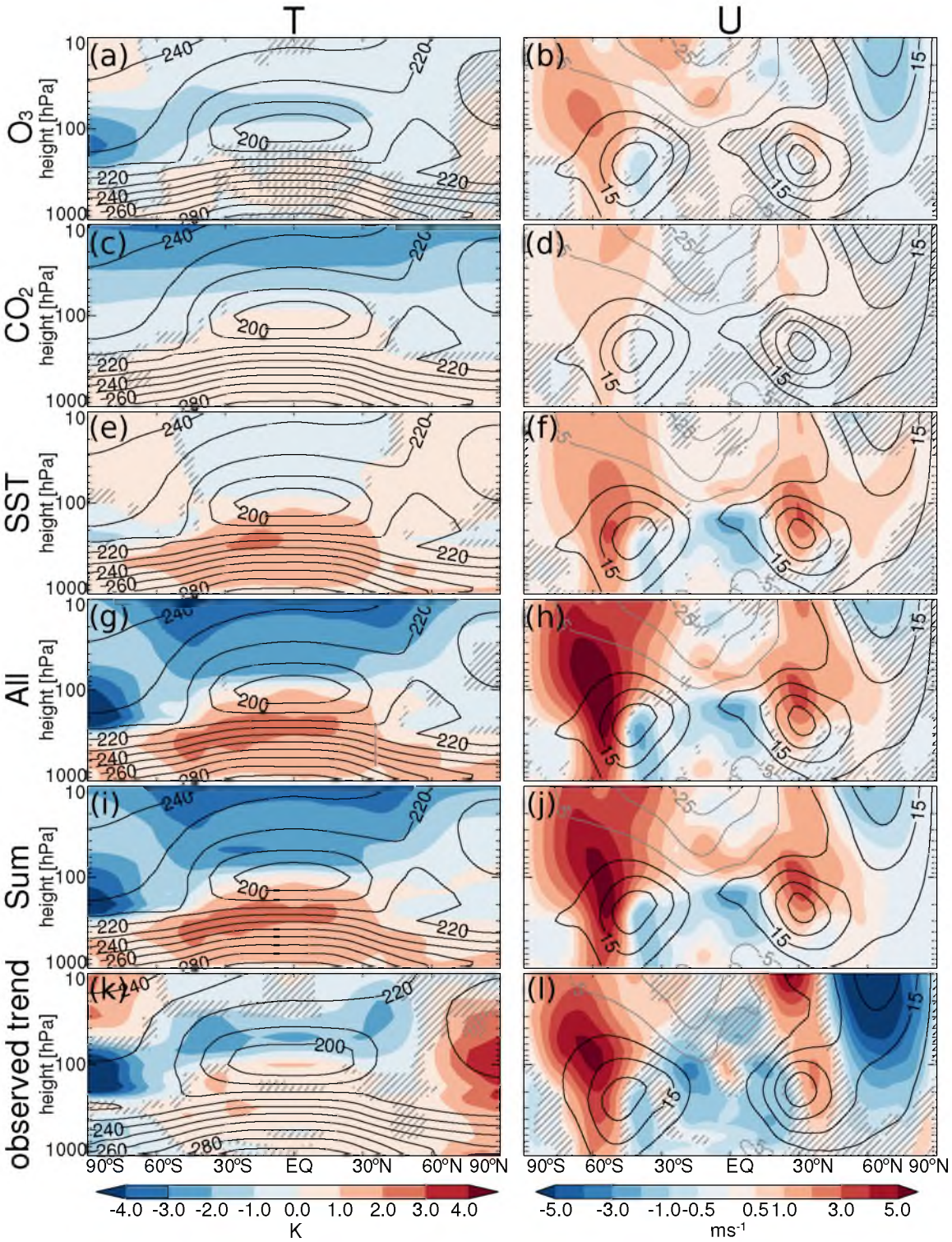

Fig. 2: December-January-February 1870–2000 temperature and zonal wind, by column, for the experiments and observations labeled, by row. Control climatologies are contoured every 10 K or 10 ms^{-1}, with negative contours in gray. Anomalies are shaded as shown. Gray hatching represents lack of significance at the 5% level.

to ozone is small except for a meridional dipole near the SH jet, with winds along the poleward flank of the SH jet increasing or decreasing by about 1 ms^{-1} at the surface, with larger changes aloft. Ozone recovery again has the opposite effect. The dipole about the tropospheric jet suggests a dynamical downward influence of the stratosphere on the troposphere, reminiscent of the results of Polvani and Kushner (2002).

Increasing greenhouse gas concentrations ('CO_2') contribute to stratospheric cooling of at least 1 °S above 60 hPa, intensifying with height at least up to 10 hPa (Figure 2c). The tropospheric temperature response is small, but still significant despite using fixed control SSTs. Greenhouse gas increases induce year-round easterly anomalies in the tropics (less than 0.5 ms^{-1}; Figure 2d), and westerly anomalies in southern high latitudes (up to 1 ms^{-1}), with a similar dipole structure about the SH tropospheric midlatitude jet as from ozone depletion during DJF, again extending down to the surface. Over the NH one can see a weak, but at times significant, deceleration along the poleward flank of the midlatitude jet.

In contrast to changing ozone and greenhouse gas concentrations, SST increases ('SST') significantly warm the troposphere (Figure 2e), with warming often exceeding 1 K in '2000' and 2 K in the future scenarios. The stratosphere cools in the vicinity of the tropopause and over the tropics. This pattern of warming and cooling is likely associated with a rise in tropopause heights, and is an expected consequence of SST warming Lu et al. (2010).

SSTs exhibit a strong control over tropospheric circulation (Figure 2f), as they largely

dictate the temperature and humidity structure of the entire troposphere. SST warming produces stronger dipole wind anomalies about the midlatitude jet than that produced by either greenhouse gas increases or ozone changes alone, and these are strongest over the SH, likely because the large percentage of the SH that is covered by ocean.

The combined forcings ('all') act constructively over the past century (Figure 2g), strongly resembling the linear sum of the individual forcings (Figure 2i), cooling the SH lower stratosphere over 4 K and warming the tropical troposphere over 2 K during DJF. During JJA, responses are weaker but the additive effect of the forcings is still clearly evident.

The modeled wind responses to the combined forcings ('all'; Figure 2h) very nearly match the linear combination of the responses to individual forcings (Figure 2j), with ozone depletion, greenhouse gas increases, and SST warming all acting to shift the tropospheric jets poleward for the '2000' climate simulation. The clear similarities between the 'SST' and 'all' figures reiterate the importance of the indirect SST effect in shaping the overall circulation response to external forcings.

The '2000' DJF temperature and zonal wind responses to the combined forcings broadly agree with the linear temperature and wind changes during 1979–2000 in the European Centre for Medium-Range Weather Forecasts 40-year Reanalysis Project (ERA-40; Figure 2k, l). ERA-40 data are generally noisier, and include some localized cooling in the tropical mid-troposphere, as well as a deceleration of the surface easterlies in the deep tropics. More importantly, the SH lower stratosphere exhibits a linear cooling trend about

50% stronger than our '2000 all' simulated response. The cooling in the NH polar vortex, also a response to ozone depletion, is stronger in observations. sIf the observed trend is to be taken at face value, then this suggests that either the model's thermal response to ozone depletion is too small, or that the prescribed ozone depletion is too weak. The simulated tropospheric wind response, on the other hand, is quite realistic.

The changes from DJF to MAM can be understood as a shift towards equinoctial, tempered by the fact that the SH polar vortex is still present to some degree, and by the hemispheric contrast in land coverage. The ozone hole disappears (Figure 3a), and anomalous cooling begins to set in over the NH (Figure 3b). The effect of the SH ozone hole is still seen in surface winds, however. The weakening of the NH polar vortex due to stratospheric ozone depletion is absent from this season. This feature was not originally described in detail with the publication of Staten et al. (2011), but is seen again in Chapter 5, and is described below.

Stratospheric cooling due to CO_2 also shifts northward (Figure 3c), producing a more latitudinally uniform pattern of cooling, and thus a weaker westerly acceleration over the SH (Figure 3d). The overall pattern of warming and cooling due to warming SSTs (Figure 3e), and the associated wind response (Figure 3f), are largely similar to those during DJF. The similarity of the combined response (Figure 3g, h) to the linear sum of responses (Figure 3i, j) and to observations (Figure 3k, l) is immediately apparent, although there is little observed tropical stratospheric cooling, implying only a weak anomalous meridional temperature gradient over the SH, and thus the SH zonal wind response.

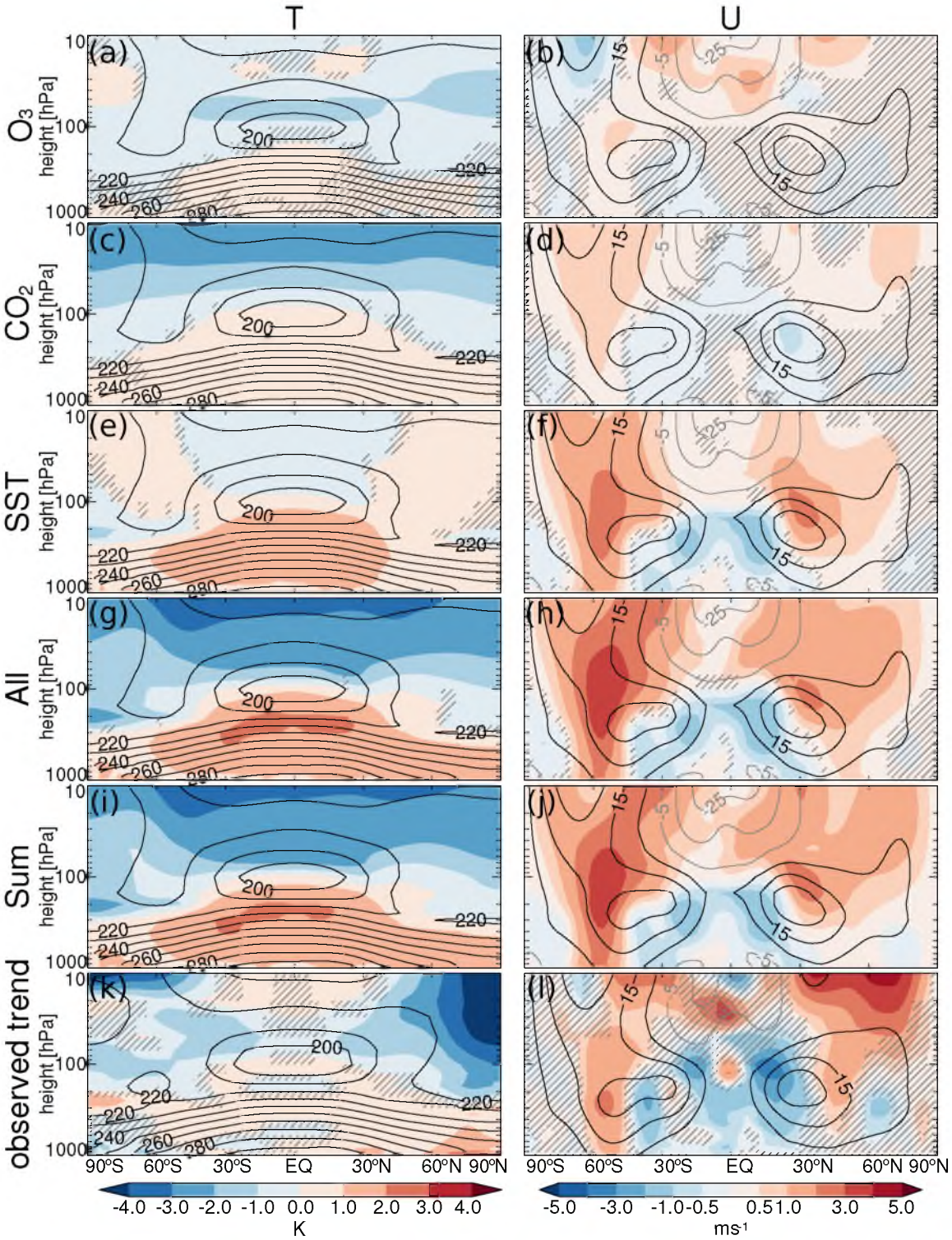

Fig. 3: March-April-May 1870–2000 temperature and zonal wind, by column, for the experiments and observations labeled, by row. Control climatologies are contoured every 10 K or 10 ms^{-1}, with negative contours in gray. Anomalies are shaded as shown. Gray hatching represents lack of significance at the 5% level.

The O_3 response during JJA (Figure 4a, b) is quite similar to the MAM response, albeit with weaker westerlies over the SH stratosphere, similar to the deceleration seen over the NH during DJF. The ozone hole over the NH is indistinct. The JJA CO_2 response (Figure 4c, d), like the MAM CO_2 response, appears similar to the DJF CO_2 response, although it is important to note here that the acceleration of zonal winds in the tropics is well removed from the zonal wind SH tropospheric wind maximum, suggesting that the CO_2 response over the SH during this season mainly acts to accelerate winds along the poleward flanks of the eddy-driven jet. An interesting question is why the cooling anomalies in the SH stratosphere extend further down during JJA than during DJF. (The stratosphere and troposphere are more strongly coupled over the winter-time pole, so there is certainly room for speculation.)

The particular influence of the applied forcings to the eddy-driven jet is evident in the SST response as well (Figure 4e, f). This is of particular interest, as SST warming has the potential to modify tropospheric stability and tropical tropopause height—both parameters included in the Hadley cell scalings discussed in Section 1.4. In spite of this, it seems that SSTs influence the Hadley cell largely via the extratropics. Indeed, this is indirectly analyzed in Chapter 4, and seen in Chapter 5. The tropical stratospheric cooling and extratropical stratospheric warming are still present. The zonal wind dipoles about the midlatitude jet in the SST response are stronger over the SH than for the NH during both DJF and JJA. Again, the combined response (Figure 4g, h) resembles the linear sum (Figure 4i, j) of responses, but neither of these strongly resembles the observed

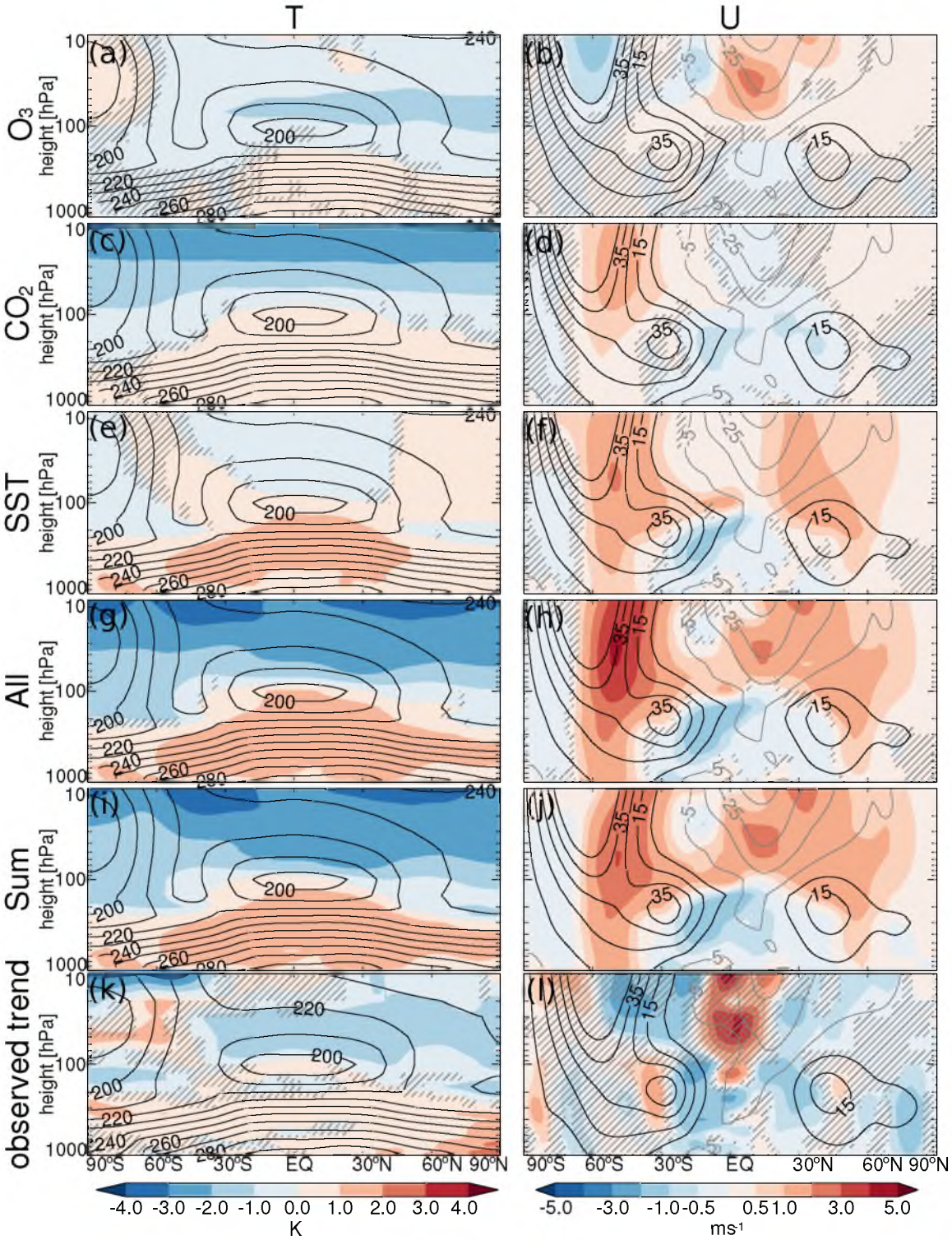

Fig. 4: June-July-August 1870–2000 temperature and zonal wind, by column, for the experiments and observations labeled, by row. Control climatologies are contoured every 10 K or 10 ms^{-1}, with negative contours in gray. Anomalies are shaded as shown. Gray hatching represents lack of significance at the 5% level.

trend (Figure 4k, l).

The reduction of ozone is strongest during September-October-November (SON; see Figure 5a, b), towards the end of the polar night, but the zonal wind response takes time to propagate down to the troposphere, and is strongest during DJF. An important question is whether this indicates a slowly downward propagating effect, or whether the troposphere and stratosphere are simply more strongly dynamically connected during DJF. Son et al. (2008) argue the former, and these results corroborate their claim, with important ramifications for the work in Chapter 5.

The SON CO_2 response (Figure 5c, d) is perhaps the nearest to solstitial, being nearly latitudinally symmetric, although still strongest over the SH. The SST response (Figure 5e, f) is likewise largely symmetric about the equator, except for the asymmetric heating and cooling over the Tropics. The combined response (Figure 5g, h) has a notably more intense SH stratospheric wind anomaly then does the linear sum (Figure 5i, j). The resemblance to the observed trend (Figure 5k, l) is, as with JJA, poor.

3.3.2 The tweny-first century temperature and wind response

This discussion so far has focused on the temperature and wind responses to individual forcings during the past century. It now turns to the corresponding changes during the next century, considering ozone to have recovered by the year 2050; in fact the response to ozone recovery pictured here is identical to that in the '2050' results described in Staten et al. (2011), and can expected to be nearly equal and opposite to the temperature and wind

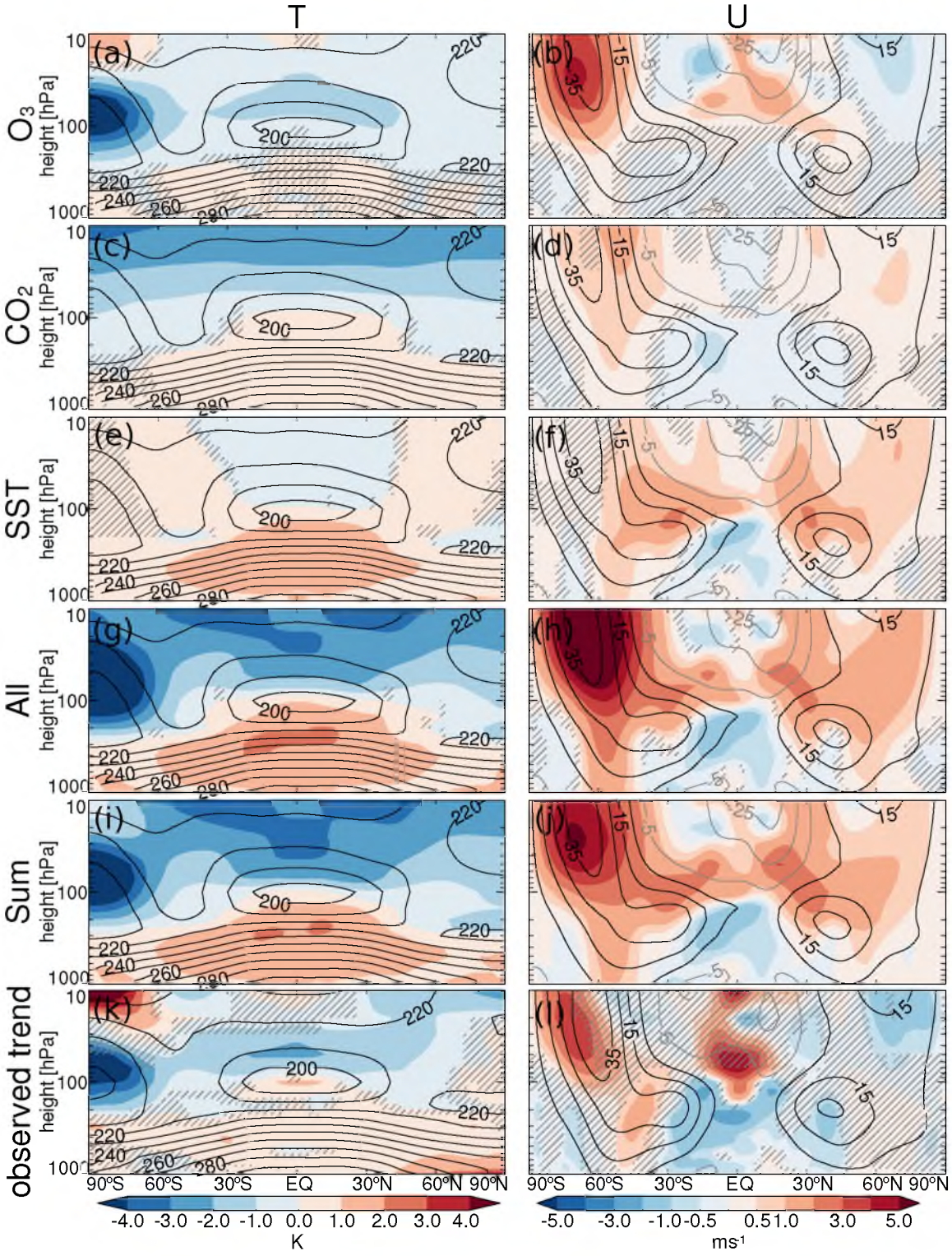

Fig. 5: September-October-November 1870–2000 temperature and zonal wind, by column, for the experiments and observations labeled, by row. Control climatologies are contoured every 10 K or 10 ms^{-1}, with negative contours in gray. Forced anomalies are shaded as shown. Gray hatching represents lack of significance at the 5% level.

response due to ozone depletion. The greenhouse concentration increases over the next century in this scenario are double that over the previous century, so one may expect a similar but stronger response for CO_2. The SST responses are likewise intense, but their structure is not the same; the SST response, then, is the most likely to depart significantly from the response in the '2000' experiments.

As expected, the '2100' DJF O_3 response (Figure 6a, b) is nearly equal and opposite to the '2000' DJF O_3 response; differences exist, but they are mostly statistically insignificant. The '2100' DJF CO_2 response (Figure 6c, d) is considerably strong in the stratosphere, but in the troposphere it is similar as that for the '2000' response. Net warming over the SH lower stratosphere due to ozone recovery and greenhouse gas increases occurs between 2000 and 2050 but changes to slight but significant cooling by 2100. Note that the tropospheric impact of ozone recovery and greenhouse gas increases oppose each other. This has been a theme of recent research.

The '2100' SST response (Figure 6e, f) is again strong, and the local maxima of the zonal mean temperature anomaly are shifted, and the resulting zonal wind anomalies in the tropics and over the NH bear little resemblance to those for '2000', except for a dipole about the jet axes over both hemispheres, indicative of a poleward shift. There also exists a particularly intense localized strengthening of winds about the SH tropical tropopause.The combined responses (Figure 6g, h) are, as with the previous century, very similar to their respective linear sums (Figure 6i, j), supporting the linearity this study relies upon to interpret the '2100' experiments. (This linearity is confirmed directly in the

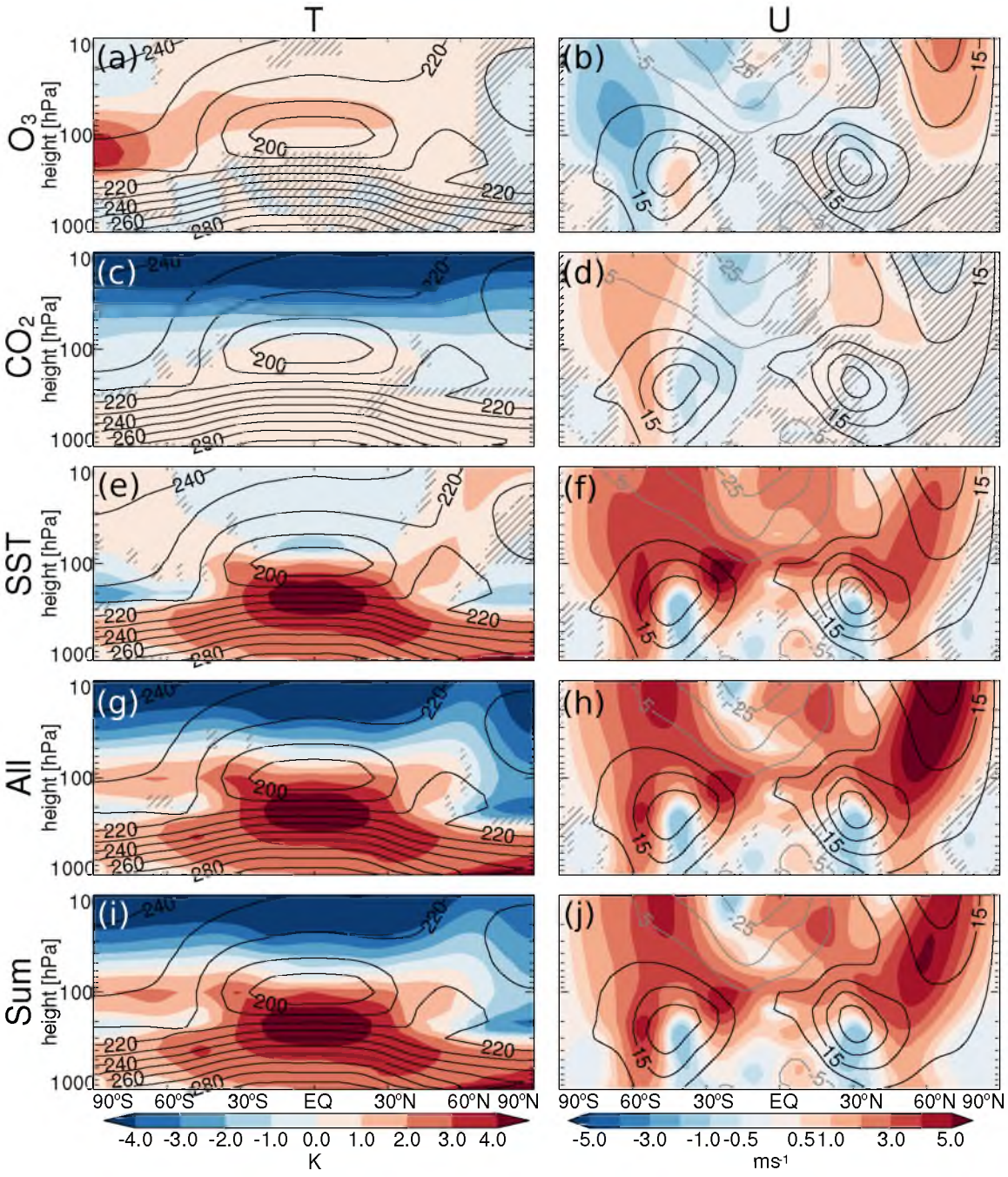

Fig. 6: December-January-February 2000–2100 temperature and zonal wind, by column, for the experiments and observations labeled, by row. Control climatologies are contoured every 10 K or 10 ms^{-1}, with negative contours in gray. Forced anomalies are shaded as shown. Gray hatching represents lack of significance at the 5% level.

'2050' response, as in Staten et al. (2011).) In these future simulations, greenhouse gas increases and SST warming act together to overcome the response to ozone recovery, still shifting the tropospheric jets poleward.

'2100' MAM O_3 and CO_2 responses (Figure 7a–d) are similar to those for the previous century, except the O_3 response is reversed, and the CO_2 response is again intensified, mainly in the stratosphere. The increased westerlies about the tropical tropopause are again a differentiating feature of the '2100' SST response (Figure 7e, f). The combined response (Figure 7g, h) is again roughly linear and very similar to the SST response (Figure 7i, j).

The '2100' JJA response to O_3 is as expected (Figure 8a, b); the CO_2 temperature response (Figure 8c, d) is as well, except that the zonal mean zonal wind response over the SH is not noticeably more intense; it may even be slightly weaker. Again the SST response (Figure 8e, f) is strong, and includes noticeable tropical westerly anomalies. The similarity between the SST response, the combined response (Figure 8g, h), and the linear sum (Figure 8i, j) are as above.

The '2100' SON responses (Figure 9) can be described similarly, although the '2100' CO_2 tropospheric wind response is stronger than the '2000', as during DJF and MAM.

3.3.3 Some generalizations regarding the temperature and wind response

In general, SH winds respond more strongly than NH winds to each type of forcing. The weak SH DJF wind response in '2100 all' (Figure 6) appears to be an exception at first glance. Upon closer examination, however, the weak SH response to the combined

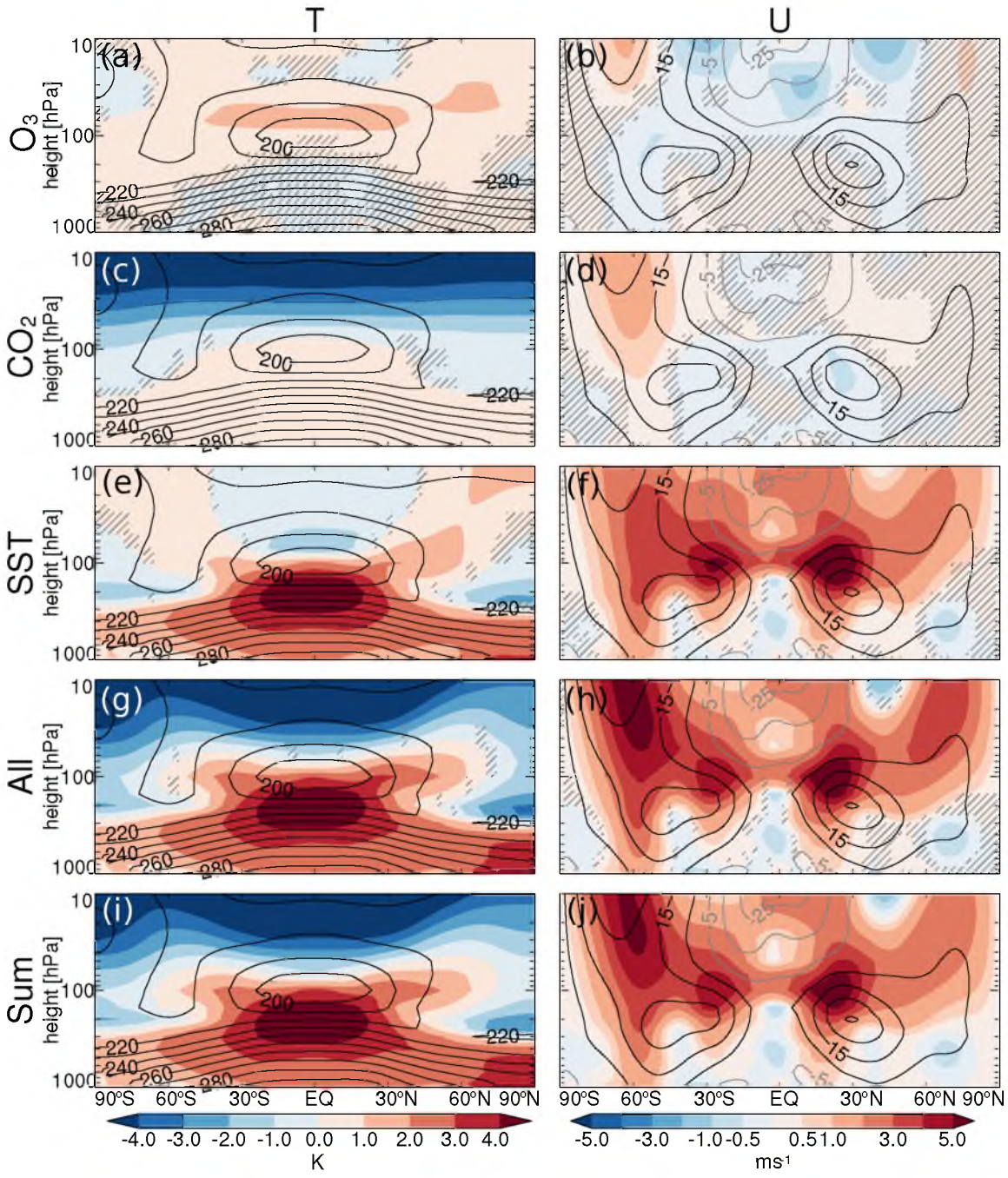

Fig. 7: March-April-May 2000–2100 temperature and zonal wind, by column, for the experiments and observations labeled, by row. Control climatologies are contoured every 10 K or 10 ms^{-1}, with negative contours in gray. Forced anomalies are shaded as shown. Gray hatching represents lack of significance at the 5% level.

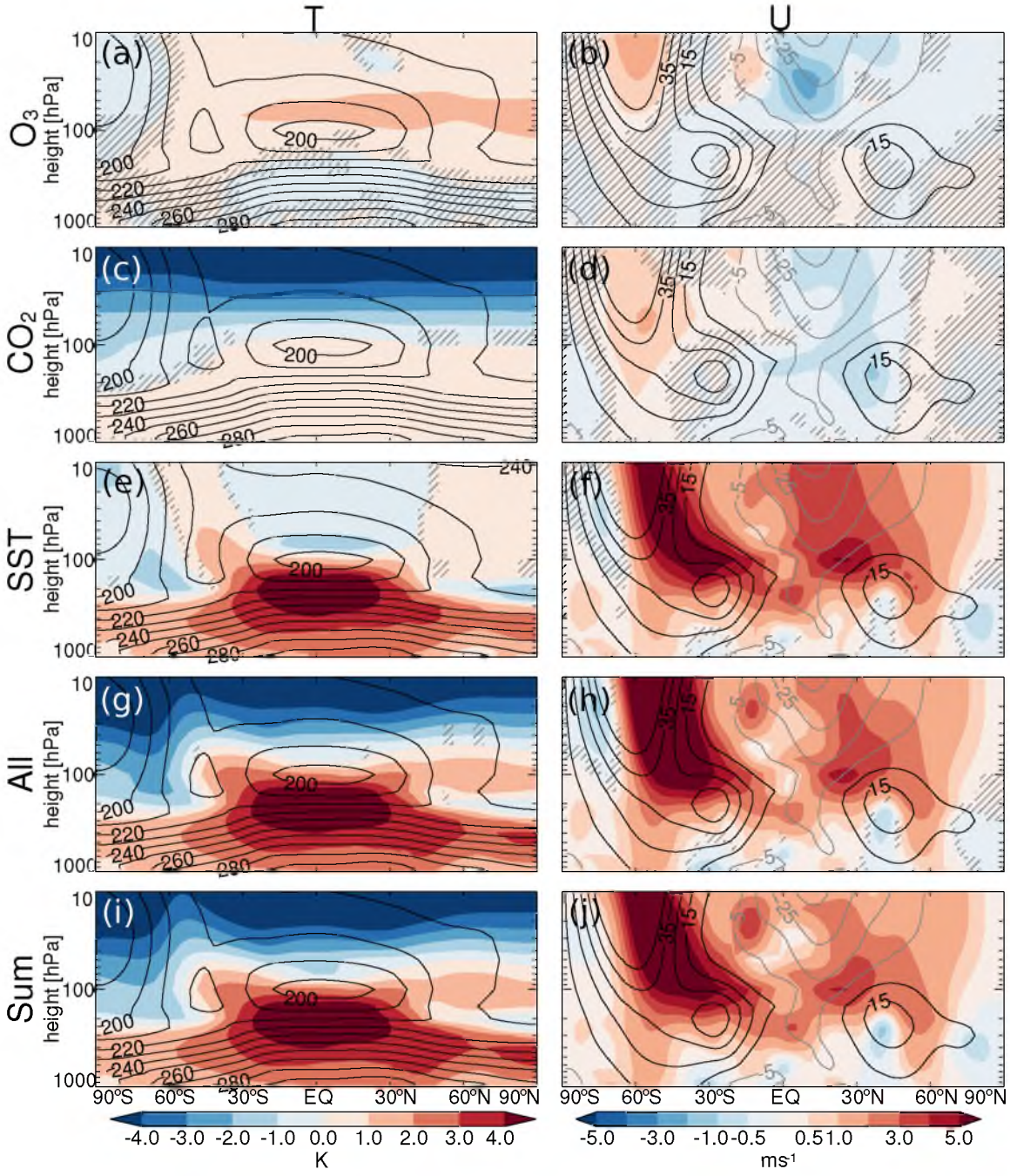

Fig. 8: June-July-August 2000–2100 temperature and zonal wind, by column, for the experiments and observations labeled, by row. Control climatologies are contoured every 10 K or 10 ms^{-1}, with negative contours in gray. Forced anomalies are shaded as shown. Gray hatching represents lack of significance at the 5% level.

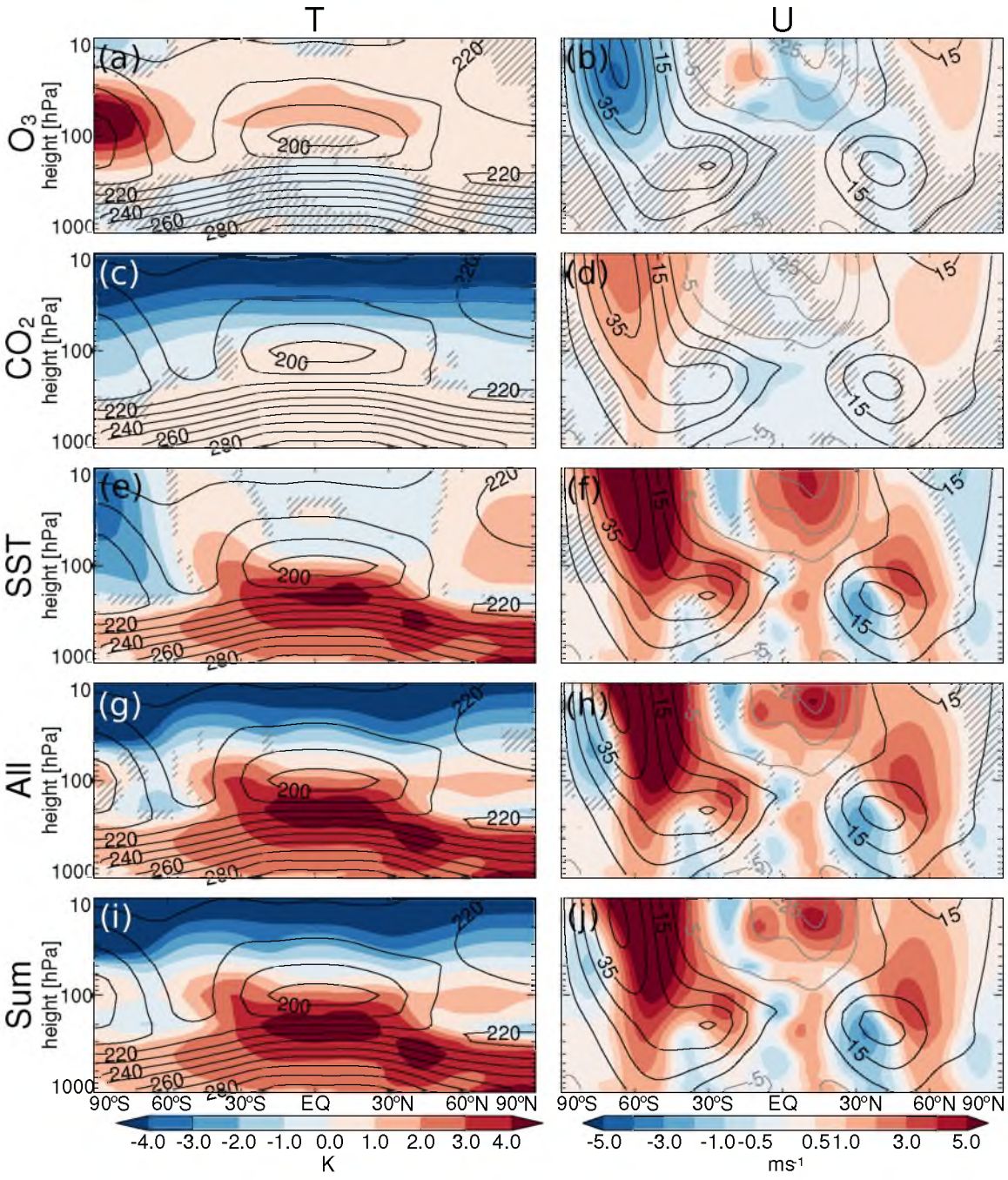

Fig. 9: September-October-November 2000–2100 temperature and zonal wind, by column, for the experiments and observations labeled, by row. Control climatologies are contoured every 10 K or 10 ms^{-1}, with negative contours in gray. Forced anomalies are shaded as shown. Gray hatching represents lack of significance at the 5% level.

forcings turns out to be a cancellation of (1) a strong positive response to SST warming and (2) a strong negative response to ozone recovery (Figure 6b). Thus the net SH response is weak compared to the net NH response.

The seasonal change in the temperature and wind responses to greenhouse gas increases is much smaller than that due to ozone depletion or recovery or to SSTs, since greenhouse gas concentrations are largely constant during the course of the year.

The continued poleward shift of the SH midlatitude jet during the 21st century is an important result of this work, and stresses the importance of the SST response to increasing greenhouse gas concentrations. The fact that the jet continues to shift poleward even during the first 50 years of the 21st century (as seen in Staten et al. (2011)) further emphasizes the role of SSTs.

3.4 The hydrological response

Key points in this section include:

- Global mean precipitation changes agree with energetic constraints.
- Zonal mean precipitation changes in midlatitudes reflect shifting circulation patterns.
- The "rich-get-richer" mechanism can explain some of the changes we see in the tropics.
- The pattern of SST warming dominates the tropical precipitation response.

While precipitation shifts are among the most difficult results of climate change to predict, Allen and Ingram (2002) describe some constraints on the change in global mean

precipitation. Rather than precipitation change being limited by the amount of available moisture, they posit that global mean precipitation is limited by the atmosphere's ability to radiate away the latent heat released during condensation. They demonstrate some modeled evidence for this constraint, and argue that CO_2 increases (barring surface temperature increases) should decrease the amount of precipitation, as less radiation escapes the troposphere. Warming sea surface temperatures, all else being equal, should increase the amount of radiation leaving the troposphere, and so should increase global mean precipitation.The effect of ozone depletion on the global tropospheric radiative balance should be small.

One difficulty in comparing observed and modeled precipitation changes, is that the amount of global mean precipitation is sensitive to the presence of aerosols (Previdi and Liepert, 2008; Liepert and Previdi, 2009). Decreasing aerosols over the past decades have helped to produce a stronger increase in precipitation than often seen in models. Liepert and Previdi (2009) argue that the atmosphere is more sensitive to aerosol forcing than to greenhouse gas forcing. Thus, if aerosol forcing stabilizes over the coming decades, the amount of precipitation change per degree celcius warming is likely to change. The present model framework may be helpful in this regard, since ozone and greenhouse gas forcings are examined separately; aerosols remain fixed in all of our simulations.

Moving beyond global mean precipitation changes, Held and Soden (2006) explain that as the earth climate system warms, and the amount of atmospheric water vapor increases, the atmosphere should become more efficient both at evaporating and precipitation. They

also argue that models do not show the general circulation intensifying proportionally. Together, these facts imply that regions of climatologically negative precipitation-minus-evaporation should tend towards becoming dryer, and conversely, regions of intense precipitation should experience trends towards increased precipitation. In other words, trends in precipitation and evaporation should resemble, to some degree, the climatological pattern of precipitation and evaporation. This is the so-called "rich-get-richer" thermodynamical mechanism.

In Section 3.5 we will examine shifts in zonal mean precipitation and evaporation thresholds. For now, we take a more broad view, examining global precipitation changes by forcing, time period, and season. Figure 10 depicts the DJF precipitation responses by forcing and time period.

The global mean response to ozone depletion (Figure 10a) includes slight drying in the global mean, with a few regions of intense drying in the tropics. While the zonal mean temperature and wind responses to ozone depletion and recovery are nearly equal and opposite, the zonally varying precipitation response between the two show less symmetry. However, the dipole in SH midlatitude precipitation anomalies due to ozone depletion is clear, and suggestive of a poleward shift of the jet. An oppositely signed dipole is present in the '2100' experiment (Figure 10b), emphasizing the sensitivity of precipitation changes to the structure of SST warming. Even comparing just the zonal mean profiles, we see substantial departures from symmetry between '2000' and '2100'.

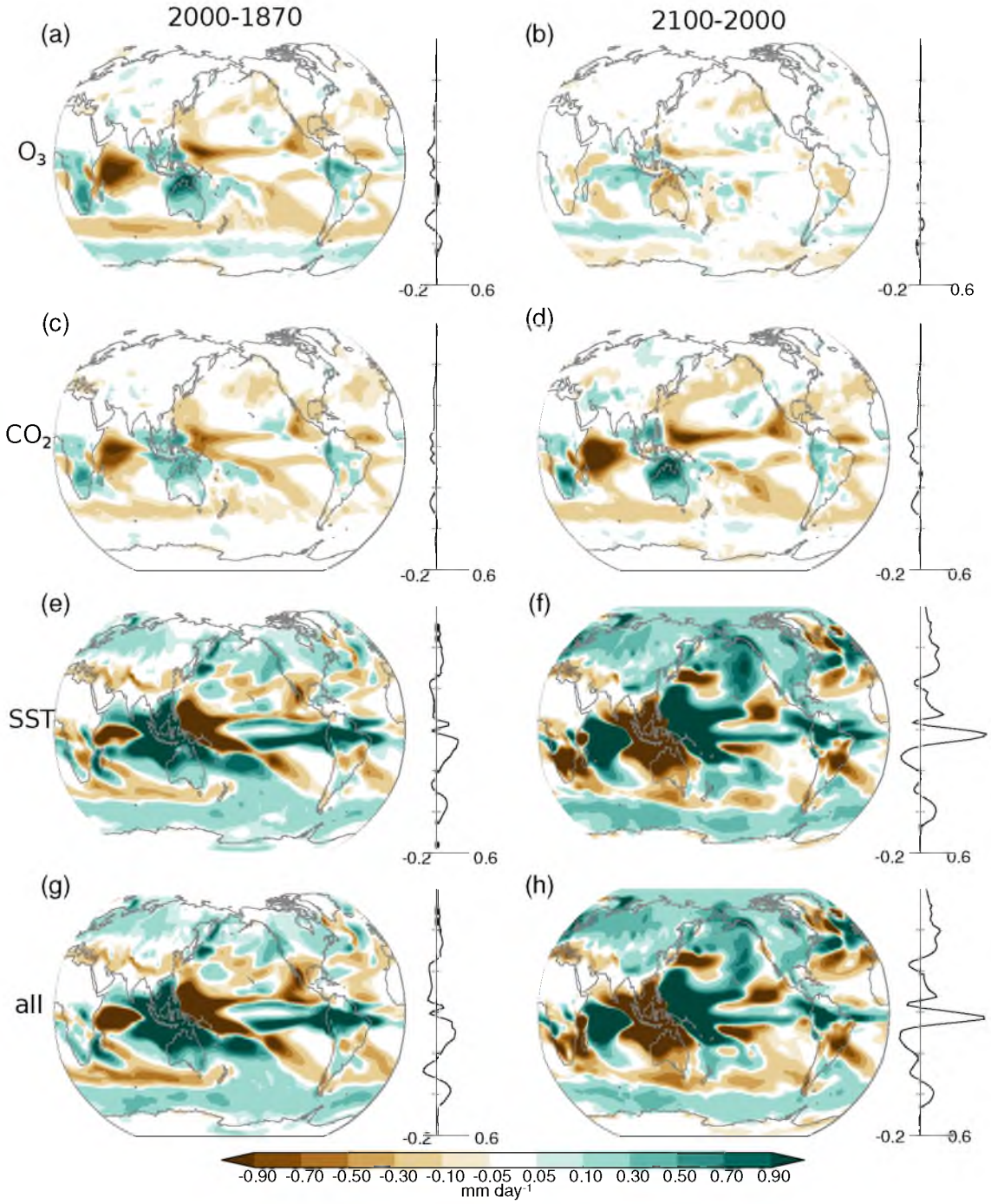

Fig. 10: Changes in December-January-February precipitation (in mm day^{-1}), for the time periods shown at the top, and the forcing type shown at the left. The zonal mean changes are depicted to the right of each map (also in mm/day), with the global mean change listed next to each latitudinal profile.

The global mean precipitation response to CO_2 (Figure 10c, d) includes drying over both centuries, coinciding with Allen and Ingram (2002). Features include drying along the poleward flanks of the subtropical dry zones resembles that in observations, and a pattern in the tropics similar to that in the O_3 experiment. The precipitation responses to CO_2 during the coming century are similar to that in the past, but more severe.

SST warming (Figure 10e, f) strongly increases global mean precipitation both in '2000' and '2100', with the structure of zonal mean anomalies being similar over both time periods, but the pattern in the tropics varying strongly; indeed, many of the most intense anomalies in the deep tropics are oppositely signed in '2100' compared to '2000'. Moistening over high latitudes is a feature of both time periods, and over the southern hemisphere (SH), and slight drying along the poleward flanks of the subtropical dry regions is also present in both hemispheres for both time periods. The drying on the poleward flanks of the dry regions, rather than at their centers, suggests midlatitude shifts are more closely related to circulation shifts than to the "rich-get-richer" mechanism.

If the "rich-get-richer" thermodynamical mechanism is valid, then it ought to be evident in the tropical precipitation response to warming SSTs, as this is the experiment in which tropospheric temperatures and water vapor concentrations increase most sharply. Comparing the anomalies to the climatology (not shown), there does seem to be a visual correlation, although there are some significant departures between 60°–120°E, in the region of the Indian Ocean and the Western Pacific. This can be seen also by comparing the '2000' and '2100' precipitation responses to SST warming. This suggests that the

"rich-get-richer" mechanism does play a role, but is likely to be more obvious in an idealized simulation.

The midlatitude drying and high latitude moistening captured in the combined response are also present in 43-year linear precipitation trends from ERA40 (not shown), and the dipole over the SH is particularly clear during DJF, but the intense drying regions in the tropics are not reproduced in reanalyses trends. This is an area where the choice of prescribed SSTs evidently plays a large role. Observations do agree that the Indian Ocean and Western Pacific are regions of particularly strong changes; the difference being that these regional trends in observations are nearly universally positive. Interestingly, the broad positive trends in the tropics match our modeled climatology. Perhaps this modeled result is not so much a criticism of the "rich-get-richer" mechanism, but rather the departures from "rich-get-richer" in the tropics serve as a reality check for our model.

The most notable difference between the DJF and MAM precipitation responses may be the weakening dipole in precipitation anomalies in the O_3 experiment (see Figure 11a, b). This is to be expected as the influence of ozone depletion over the SH wanes during MAM. What's more striking than the differences between the two seasons is perhaps their similarity.

The response during JJA (see Figure 12) contrast more strongly with that during DJF, although the subtropical drying and high-latitude moistening persist. The boundary between the two over the SH is shifted northward, here. By SON (see Figure 13), the response seems to again be similar to that during DJF. The SH dipole in the O_3 experiment can be

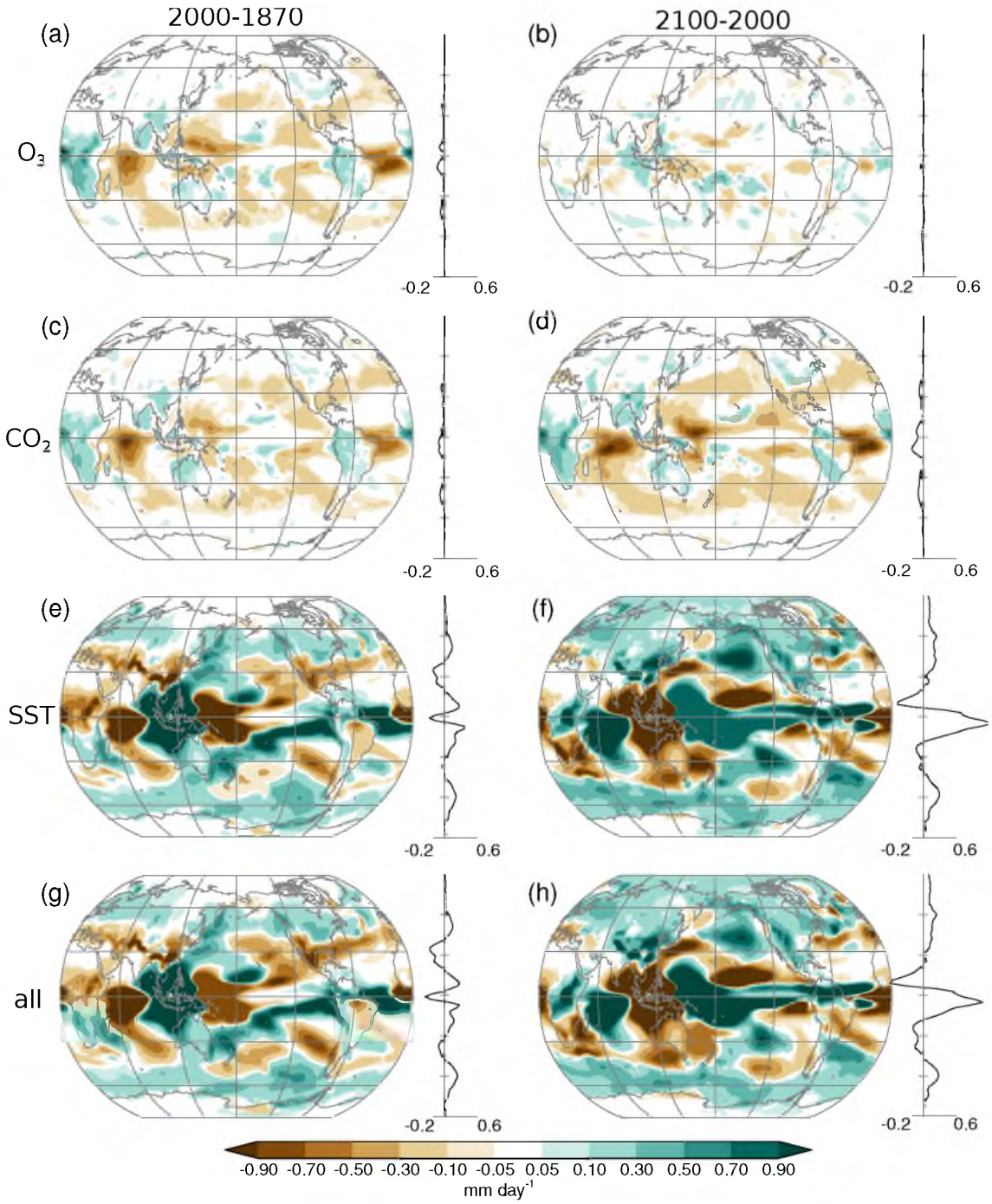

Fig. 11: Changes in March-April-May precipitation (in mm day^{-1}), for the time periods shown at the top, and the forcing type shown at the left. The zonal mean changes are depicted to the right of each map (also in mm/day), with the global mean change listed next to each latitudinal profile.

seen returning, as the influence of the ozone hole begins to propagate downward.

3.5 Changes in zonal mean indices

Key points in this section include:

- Ozone shifts both the Hadley and Ferrel cells over the SH, particularly during DJF.
- Greenhouse gas increases shift cells poleward year-round, with SH shifts being stronger.
- Sea surface warming dominates the combined shift response across latitudes.
- Cell shifts are generally stronger during summer over their respective hemispheres.

This section quantifies shifts in indicators of the general circulation, beginning with the Hadley cell edge. The following sections will refer extensively to Figures 14 and 15. The precise descriptions of the indicators discussed are explained in Chapter 2. The time periods and forcings are listed in Table 2, and annual mean changes for each experiment and forcing are quantified in Table 3.

During the past century, the Hadley cell edges shift slightly poleward (less than 0.3°) under the influence of radiative forcings alone, but substantially (up to 1°) under the influence of warming SSTs. Shifts are largest during the summer of each hemisphere, in agreement with the observational study by Hu and Fu (2007), amplifying the seasonal swings in Hadley cell extent. Ozone depletion produces its largest shifts during austral spring and summer, and smaller, mostly insignificant changes during the rest of the year, owing to the seasonal nature of ozone depletion.

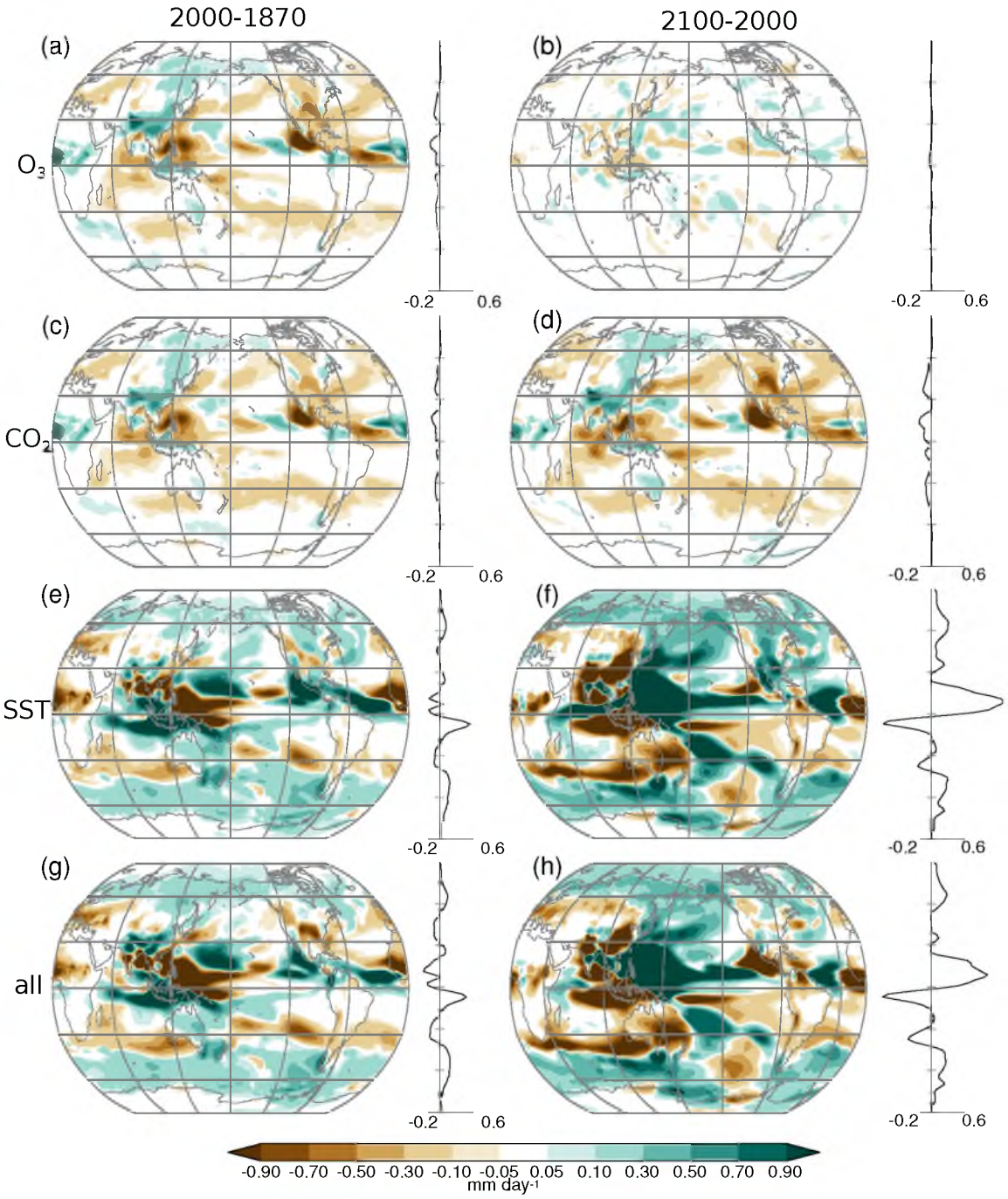

Fig. 12: Changes in June-July-August precipitation (in mm day^{-1}), for the time periods shown at the top, and the forcing type shown at the left. The zonal mean changes are depicted to the right of each map (also in mm/day), with the global mean change listed next to each latitudinal profile.

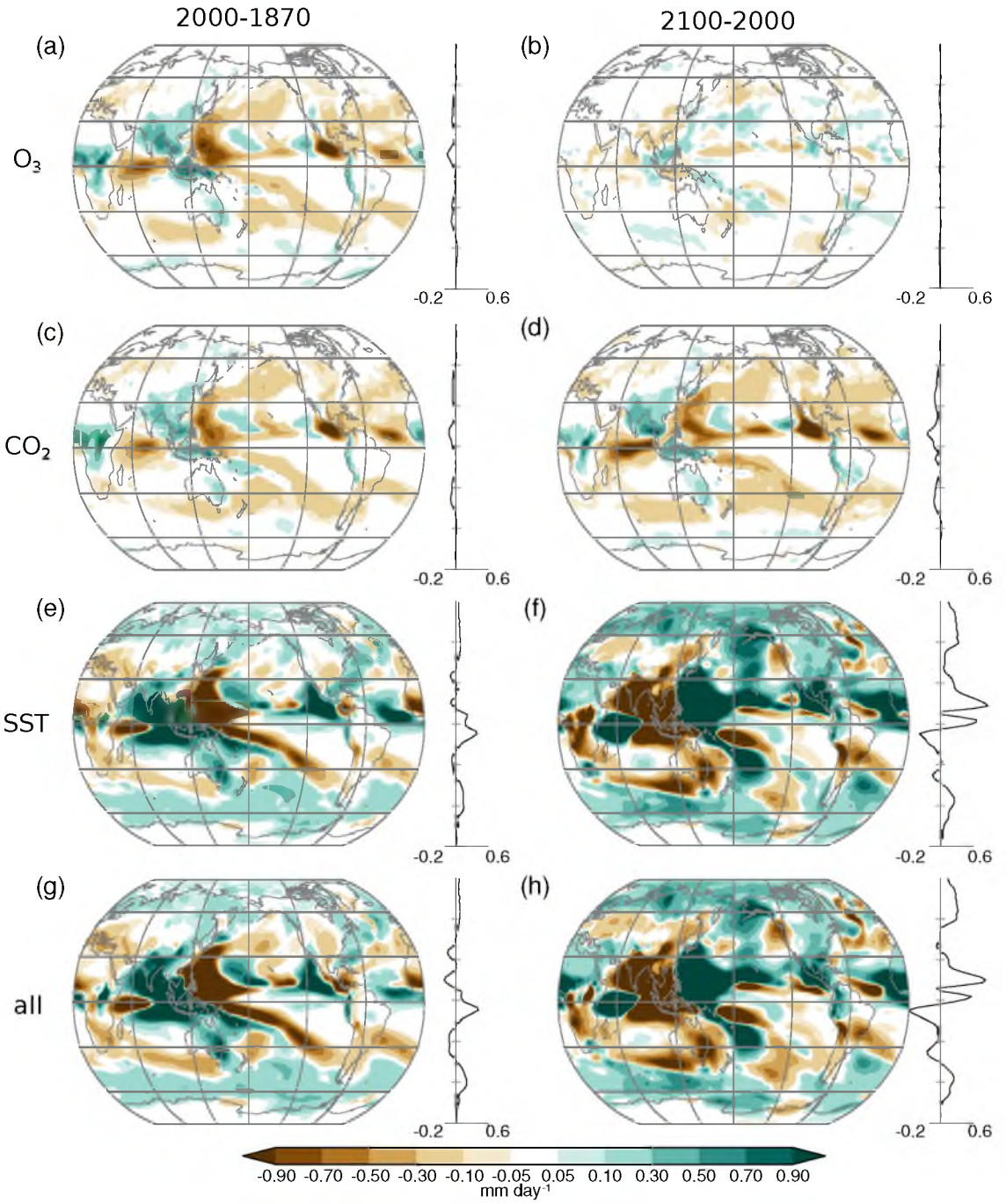

Fig. 13: Changes in September-October-November precipitation (in mm day^{-1}), for the time periods shown at the top, and the forcing type shown at the left. The zonal mean changes are depicted to the right of each map (also in mm/day), with the global mean change listed next to each latitudinal profile.

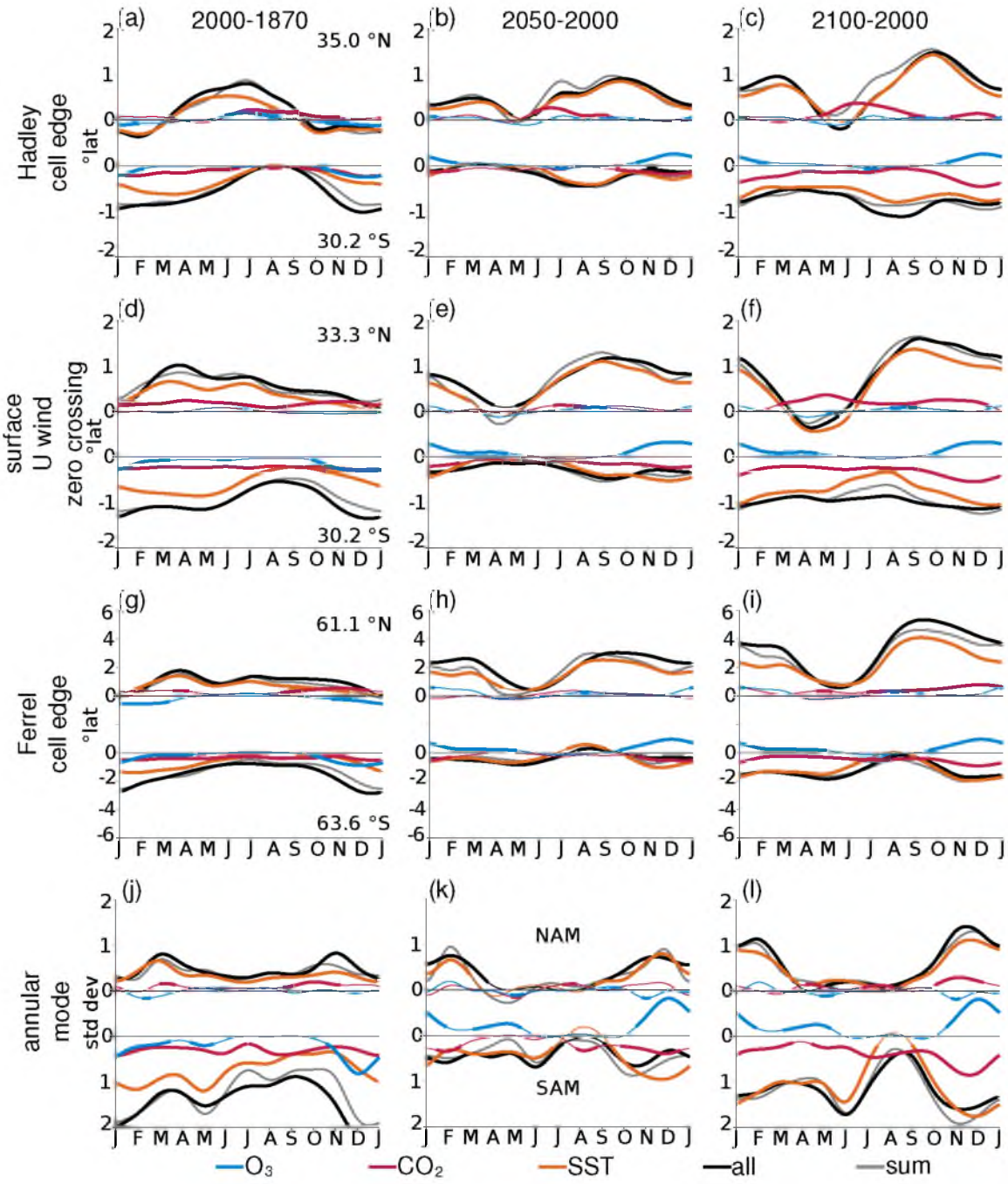

Fig. 14: The seasonality of shifts in the zonal mean circulation indicators (by row; see Section 2.5) for specified time periods (by column). Shifts are shown in degrees latitude, except for the annular mode (bottom row), which is shown in in standard deviations. Note the different scale used for the Ferrel cell edge (third row). The color of each curve denotes the type of forcing, as shown at the bottom. Thick lines highlight statistically significant shifts at the 5% level. Each panel is divided into two parts, with the upper half showing NH changes, and the lower half showing SH changes. Numbers in the first column indicate the preindustrial annual mean latitudes for each feature.

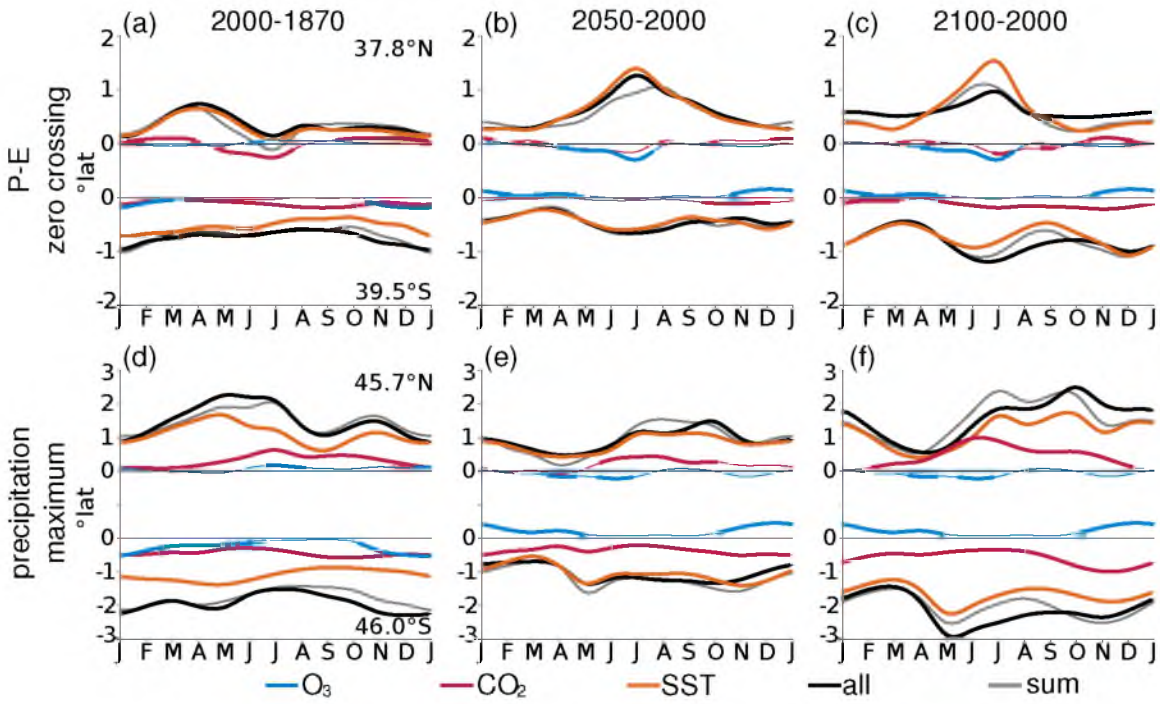

Fig. 15: The seasonality of shifts in the zonal mean hydrological indicators (by row; see Section 2.5) for specified time periods (by column). Shifts are shown in degrees latitude. Note the different scale used for the precipitation maximum (second row). The color of each curve denotes the type of forcing, as shown at the bottom. Thick lines highlight statistically significant shifts at the 5% level. Each panel is divided into two parts, with the upper half showing NH changes, and the lower half showing SH changes. Numbers in the first column indicate the preindustrial annual mean latitudes for each feature.

Table 3: Annual mean NH and SH latitudinal shifts

	O_3			CO_2			SST			All		
	2000	2050	2100	2000	2050	2100	2000	2050	2100	2000	2050	2100
HC	(-0.01)	-0.02	-0.02	0.08	0.07	0.13	0.07	0.43	0.68	0.18	0.5	0.74
edge	-0.07	0.06	0.06	-0.12	-0.1	-0.21	-0.32	-0.16	-0.61	-0.57	-0.17	-0.78
sfc U_0	-0.01	-0.02	-0.02	0.17	0.05	0.19	0.39	0.57	0.6	0.56	0.7	0.79
	-0.12	0.11	0.11	-0.23	-0.14	-0.31	-0.56	-0.26	-0.73	-0.98	-0.28	-0.98
FC	-0.18	0.14	0.14	0.3	-0.06	0.4	0.7	1.54	2.37	1.01	2.06	3.27
edge	-0.27	0.27	0.27	-0.39	-0.25	-0.49	-0.7	-0.36	-1.15	-1.52	-0.34	-1.25
AM	-0.01	-0.01	-0.01	0.09	-0.03	0.09	0.34	0.26	0.48	0.47	0.33	0.57
	0.2	-0.21	-0.21	0.3	0.2	0.39	0.75	0.42	1.02	1.4	0.42	1.17
$P–E_0$	0.07	-0.08	-0.08	0.31	0.18	0.46	1.11	0.81	1.16	1.53	0.92	1.55
	-0.23	0.21	0.21	-0.44	-0.36	-0.58	-1.1	-1.04	-1.67	-1.92	-1.06	-2.16
P_{max}	-0.01	-0.07	-0.07	-0	-0	-0.01	0.3	0.62	0.6	0.35	0.6	0.61
	-0.07	0.05	0.05	-0.11	-0.06	-0.13	-0.53	-0.44	-0.73	-0.74	-0.45	-0.84

During the 21st century (see Figure 14b, c), the effects of ozone recovery (blue curve) over the SH neatly oppose those from ozone depletion. Recovery-induced changes over the NH are small and almost nowhere significant, even in the annual mean. By '2100', greenhouse gas increases (red curve) shift the Hadley cell edges poleward significantly year-round over both hemispheres (0.7°-0.3° in the annual mean).

SST warming (orange curve) shifts the Hadley cell edges significantly during most seasons, in all three time periods studied. Annual mean poleward Hadley cell edge shifts due to SST warming (tab:ann) span nearly an order of magnitude, from less than 0.1° during the 20th century to 0.7° during the 21st century. This dominant SST impact holds for all indicators analyzed in this study.

During '2000', in addition to the expected summertime shift, SST warming also strongly affects the Hadley cell edges during May in both hemispheres, producing over 1° of widening of the tropics. In contrast, future changes during May over the NH are close to zero, and are strongest instead during the boreal fall. The effects of future SST warming on the SH Hadley cell are overall relatively weak in '2050', only becoming strong year-round by '2100'. We note that the structure and seasonality of the SST forcing used to drive the '2000' and '2100' simulation sets also differ (see Figure 1), which may help to explain some of the differences.

The linear sum of the effects of the individual forcings (gray) is very similar to the effect of the combined forcings (black), even in many minor details. It is significant that the linear sum for '2100' approximates the combined response as well as it does, considering that

the linear sum for the '2100' includes (1) errors of the sum, as with the '2050' and '2000' cases, and (2) errors of the substitution, or errors from using purely forced experiments to approximate mixed forcing experiments (see Section 2 and Table2). The match between the '2100' linear sum and combined-forcings run validates the assumption of linearity, as well as the choice of substitution in this study. That said, departures from linearity can be seen during JJA in the future scenarios (Figure 14b, c), and they appear to be real and systematic.

In summary, the Hadley cell boundary shifts poleward in response to the forcings imposed in this study, with strong seasonalities. Over the past century, this seasonal cycle peaks in the summertime over both hemispheres, although the largest overall widening occurs in May due to the phase difference of the NH and SH shifts. This detail in seasonality is a slight departure from that in observations (Hu and Fu, 2007), in which similar shifts during the summer and fall of each hemisphere produce fairly consistent year-round tropical widening. Future simulations produce more year-round widening, and a different seasonality. Shifts over the NH become stronger than shifts over the SH, even during seasons with no cancelling effect from ozone depletion over the SH; changes in the SST response are mostly responsible for the strong NH shift. The reasons for this change in seasonality from '2000' to '2050' and '2100' are unclear. We suspect that nonlinear behavior, as well as changes in the structure of the driving SSTs and sea ice, might play a role; such structural changes may include the direct effect of aerosols on SSTs. In general, the SST effect dominates shifts in the Hadley cell, producing a response

similar to that of the combined forcings, which in turn very closely resembles the linear sum of the individual responses.

The descending branches of the Hadley cell are roughly co-located with the subtropical high pressure cells and consequently with zero crossings of the zonal wind at the surface. Here the surface wind zero crossing (hereafter $U = 0$; see Figure 14, second row) is used further examine tropical widening. Overall, latitudinal shifts in the Hadley cell and $U = 0$ are similar in magnitude, but differences exist in the details and seasonality. For example, shifts occur earlier in the year over the NH than for the Hadley cell edge. This NH-SH phase difference produces tropical widening in most seasons during '2000'. By '2100', strong NH changes contribute to widening of as much as 2° latitude.

The Ferrel cell edge shifts strongly due to ozone depletion and recovery during SH Spring (Figure 14, third row; note the differing axes). In '2000' and '2050', ozone changes at times shift the Ferrel cell more than either greenhouse gas increases or SST warming. But in these simulations, the combined effect of the latter two forcings consistently and strongly outweighs the effect of ozone recovery in '2050' and '2100', in contrast to Deser and Phillips (2009).

The present study shows that the Ferrel cell edge shifts more strongly (at nearly 6°) than the Hadley cell edge (at about 1.5°), implying a widening of the Ferrel cell. This widening is substantial in both hemispheres throughout most of the year, except over the SH during JJA, giving rise to a seasonality distinct from that of the Hadley cell.

The AMs (Figure 14, bottom row) can be seen as an integrated measure of the circulation over each hemisphere (poleward of $\pm 20^\circ$). Positive values here reflect a decrease in sea level pressure over the poles and a poleward shift of midlatitude westerlies, similar to what one would expect with a poleward-shifting Ferrel cell. It is interesting to note, therefore, that the seasonalities of the above described extratropical circulation changes over the NH differ markedly from that of the NAM. The NAM response is very muted in summer but strong during early winter and spring, particularly in '2050' and '2100'. In contrast, the SAM response is strongest during SH summer as with the Ferrel cell edge response. The strong responses over the NH are roughly coincident with the active seasons of the NAM, when coupling between the stratosphere and the troposphere is expected to be strongest (Thompson and Wallace, 2000). It is also noteworthy that, as with the other circulation indicators, the seasonality of the AM response to SST warming changes sharply between the '2000' scenario and the '2050' and '2100' scenarios.

While the circulation features described above have fairly similar seasonalities, the hydrological indicators in this study (see Figure 15) do exhibit somewhat different seasonalities than their dynamical counterparts, as with Hu et al. (2011). It is conceivable that this difference is related to thermodynamical constraints on the hydrological cycle. Not surprisingly, the seasonality of $P - E = 0$ more closely resembles that of $U = 0$ at the surface, rather than the mid-tropospheric Hadley cell edge at 500 hPa. One can see a similarity in the seasonality of $P - E = 0$ to the observed subtropical precipitation minimum trends described in Hu et al. (2011), with a NH peak during March-April-May, and a SH peak

during DJF, but there is little agreement with the observed seasonality of the subtropical dry zone trends presented in Zhou et al. (2011).

SST warming produces poleward $P-E=0$ shifts in '2000' with a seasonality similar to that for $U=0$ (Figure 14d), but in '2050' and '2100' it produces poleward $P-E=0$ shifts year-round, with a pronounced 1.5° latitude peak in July over the NH; the 0.7° shift over the SH is substantial as well. Again, SST warming explains the shifts in the combined response to a large extent; the effects of direct radiative forcings alone are similar to those described for the dynamical indicators above, and are particularly weak for $P-E=0$.

Shifts in the midlatitude precipitation maxima (Figure 15, bottom row), which are indicative of shifts in the location of stormtracks, are reminiscent of shifts of the edge of the Ferrel cell (Figure 14, third row). Over the NH, warming SSTs shift the Ferrel cell edge more than the precipitation maximum, while over the SH, warming SSTs shift the SH precipitation maximum more than the SH Ferrel cell edge.

Figure 10 can be compared to Figure 12 in Polvani et al. (2011b), to Figure 11 in Deser and Phillips (2009), and to Figure 2 in Kang et al. (2011). All three of these other studies use CAM3, although Kang et al. (2011) also take data from the CMAM model. Deser and Phillips (2009) examine ensembles of 50-year transient simulations, while Polvani et al. (2011b) and Kang et al. (2011) perform 50-year time-slice simulations. Despite methodological differences between these other studies, all three depict an extratropical precipitation change due to ozone depletion or radiative forcings using CAM3 that is generally stronger than we show here due to 'O_3' or 'CO_2' using AM2.1 (Figure 10,

first and second rows, respectively). On the other hand, one can see a much stronger extratropical precipitation response to SST changes (Figure 10, third row). As with these other studies, the experiments here produce overall subtropical drying and high-latitude moistening, but also suggest that the direct effects of ozone and greenhouse gases play only a secondary role compared to the indirect SST effect.

Why the indirect SST effect is so much stronger in this study than in Deser and Phillips (2009), Polvani et al. (2011b), or Kang et al. (2011) is not clear. While SST variability is expected to be the dominant source of atmospheric variability in the tropics (Deser et al., 2012), it is somewhat surprising to see such a powerful effect at high latitudes, especially when prescribing decadally averaged SSTs taken from coupled model 20C3M and A1B scenarios. Deser and Phillips (2009) perform ensemble transient experiments with observed SSTs, but Polvani et al. (2011b) and but Kang et al. (2011) both use multiyear averaged SSTs as we do, so it is unlikely that natural SST variability is confounding our results or the results of Polvani et al. (2011b) or Kang et al. (2011). The effect of aerosols (which is not examined in this study) may provide some clues.

To understand the differing ozone responses in this work compared to Polvani et al. (2011b), the reader is referred to Figure 3 in Son et al. (2008). CM2.1 (the coupled model companion to AM2.1) has a weaker polar cap temperature response than CCSM3 (the coupled model companion to CAM3). Assuming the differences between prescribed ozone changes in the two studies are small, CM2.1 is less sensitive to ozone depletion than CCSM3, and by extension AM2.1 may be less sensitive than CAM3 as well. However, data

from the standard 24-level configuration of CM2.1 were examined in Son et al. (2008), while this work uses a 48-level version of AM2.1. The author estimates that the SH lower stratosphere temperature response to the combined forcings is 30% stronger in the high-top configuration of AM2.1 than in the standard 24-level AM2.1 configuration. This increasing sensitivity with vertical resolution is somewhat expected (Karpechko et al., 2008), and may 'close the gap' in sensitivity somewhat between AM2.1 and CAM3.

3.6 The effect of melting sea ice

Key points in this section include:

- Strong 21st century zonal mean circulation shifts during SON are not due to sea ice melt.
- Sea ice melt produces a weak equatorward shift of the jet.
- Melting of the sea ice during May influences the general circulation the following winter.

The strong circulation shifts seen during fall in the future scenarios due to SST warming (orange curves in Figure 14, third column) are coincident with the season of strongest sea ice decline. To investigate the role of melting sea ice on the general circulation, the author performed an additional simulation, with year-2100 sea surface temperatures, but with sea ice coverage at the preindustrial levels. By comparing this simulation with an SST_{2100} simulation, one can isolate the role of changing sea ice (with sea surface temperatures

held constant), and by comparing with a preindustrial control, one can isolate the role of changing sea surface temperatures (with sea ice held constant).

The effects of sea ice and of sea surface temperatures individually on the zonal mean temperature and wind structure of the atmosphere during DJF is depicted in Figure 16. (The results during SON are very similar.) The effect of sea ice on the temperature and wind structure of the free atmosphere is very small, although there is some statistically significant warming and deceleration that propagates up into the stratosphere on the poleward flanks of the midlatitude jet.

This study also finds that the atmosphere during SON is not particularly sensitive to the amount of sea ice cover. Rather, changes in sea ice cover during May were correlated

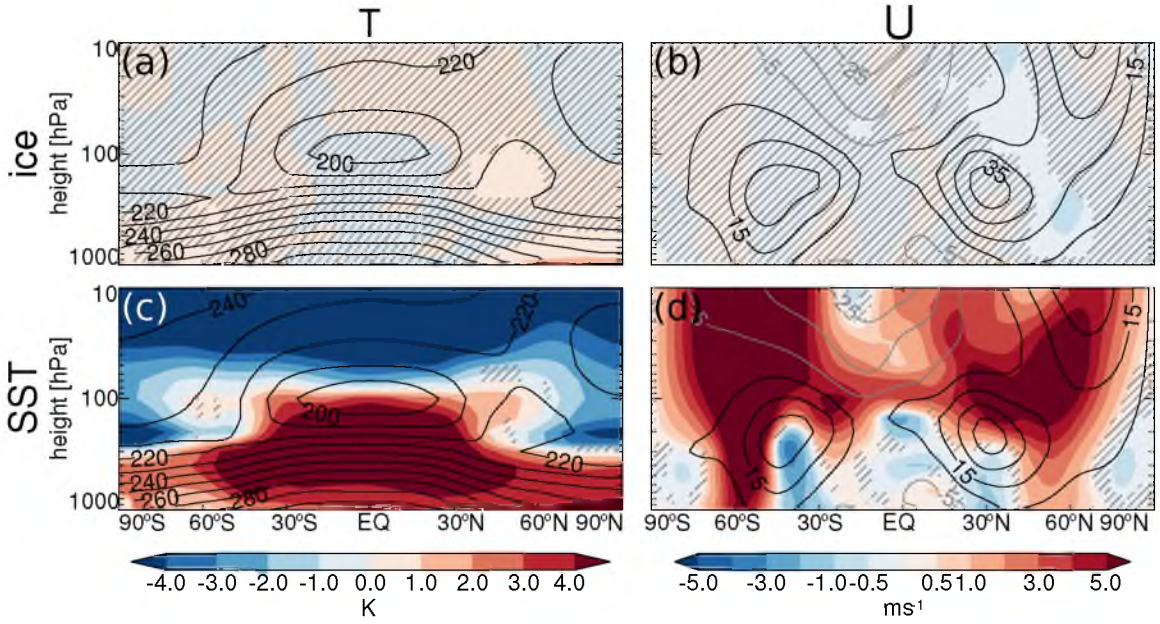

Fig. 16: December-January-February 1870–2000 temperature and zonal wind, by column, for changes in sea ice coverage only (first row), and sea surface temperature changes only (second row). Control climatologies are contoured every 10 K or 10 ms^{-1}, with negative contours in gray. Forced anomalies are shaded as shown. Gray hatching represents lack of significance at the 5% level.

with the heat flux into the atmosphere during the following winter. These results agree with other recent work (Deser et al., 2010; Screen et al., 2012).

3.7 Low- versus high-top configurations

Key points in this section include:

- L24 and L48 model results are very similar.
- L48 exhibits stronger sensitivity to ozone depletion.
- We cannot say from this work alone which most realistically simulates climate.

The results presented in this chapter have mainly been those produced using the enhanced, 48-level version of the AM2.1 model. Staten et al. (2011) presented results from the 24-level model, since it is the standard formulation. To illustrate the similarity of the two model versions, Figure 17 depicts the differences in the combined model response by forcing, superimposed on the control climatology (from the high top control simulation). Differences are small, but often statistically significant. It is notable that the westerlies in the SH polar stratosphere are stronger, illustrating the increased sensitivity to O_3 in the high-top model.

It is tempting to argue from this that the L48 model's superiority in this respect is a result of a better resolving of stratospheric dynamics. However, another possibility is simply that the level of maximum ozone depletion, which is between vertical levels in the L24 models, is better resolved in the L48 model. Sigmond et al. (2008) also suggest that the realistic representation of climatological winds in the stratosphere is a better indicator

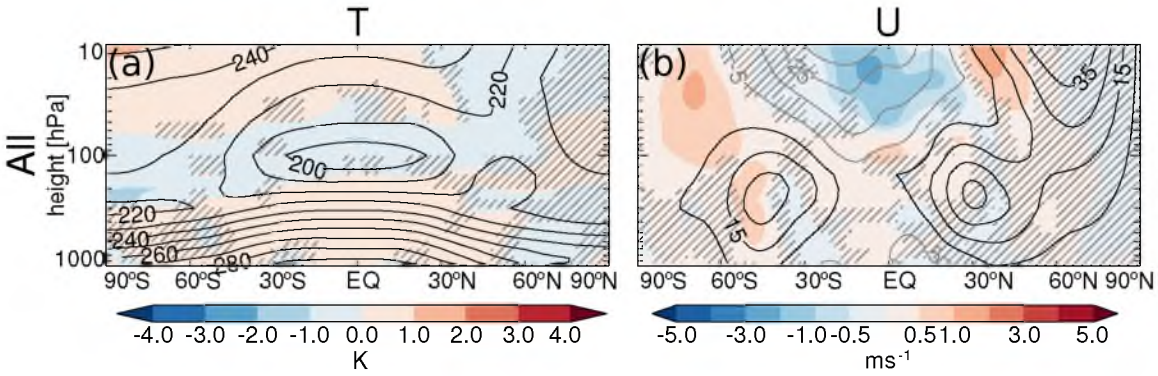

Fig. 17: December-January-February 1870–2000 temperature and zonal wind, by column, for the difference between the combined forcing experiments in the low-top and high-top model configurations. Low-top control climatologies are contoured every 10 K or 10 ms^{-1}, with negative contours in gray. Differences in the forced anomalies are shaded as shown. Gray hatching represents lack of significance at the 5% level.

of the realism of modeled trends, than the stratospheric resolution alone. Gillett et al. (2002) also model greenhouse gas-induced climate change, and find little difference in the surface arctic oscillation response between their high-top and low-top model versions. Wilcox et al. (2012) further note that the high-top version of HadGEM2-ES tends to show a continued poleward shift of the SH DJF jet during 2006-2050, while the low-top models show an equatorward shift. We cannot, simply by examining the mean response in this work, be certain that the high-top model is more realistic.

3.8 Examining possible mechanisms

Key points in this section include:

- Momentum flux convergence spectra suggest that ozone depletion and greenhouse gas increases may shift the eddy-driven jet by increasing eddy phase speeds.
- We cannot discount any mechanisms in the shift due to SST warming; rather, we see

evidence for several.

The work presented in this chapter provides some evidence for several circulation shift mechanisms, although it discredits none—at least not in the combined response. For an individual forcing, however, some mechanisms can probably be ignored.

Increasing subtropical tropospheric stability due to greenhouse gas increases and warming SSTs should serve to widen the Hadley cell, and indeed widening occurs in both cases, and the width of the Hadley cell seems to be correlated to the increase in stability for a given simulation. Yet ozone depletion, which affects subtropical static stability very little, shifts the Hadley cell as well. Some other mechanism is likely at play for ozone depletion.

To better understand the changing circulation, this study examines changes in the structure of eddy momentum flux convergence and divergence in latitude-phase speed space, as in Chen and Held (2007). Eddy-mean flow interactions are complex and inherently nonlinear, but some understanding can be gained through a linear treatment, considering how waves of a given wavenumber and phase speed propagate meridionally, given a prescribed background flow.

This section addresses the role played by the critical latitude for wave absorption. Specifically, this discussion relates the changes seen in the eddy momentum flux convergence to mechanisms proposed by Robinson (2002), Chen and Held (2007), and Kidston et al. (2010). Each of these mechanisms addresses changes in the critical latitude for the absorption of midlatitude waves. Robinson (2002) describe how anomalous subtropical westerlies should permit the propagation of midlatitude waves into the Hadley circulation.

Even if tropical winds remain constant, however, the critical latitude may still shift, depending on the phase speed of the midlatitude waves. The mechanism proposed by Chen and Held (2007) suggests that increasing eddy phase speeds (in response to global climate change) are responsible for an increase in the critical latitude of wave absorption, and a poleward shift of dissapation and of the zone of maximum baroclinicity. This mechanism is generally cited to explain shifts on the equatorward side of the eddy-driven jet, as zonal winds on the poleward flanks of the jet generally increase, and the flow-relative phase speed of midlatitude eddies changes less compared to the zonal winds poleward of the jet, than compared to those equatorward of the jet.

Kidston et al. (2010) focus on the flow-relative phase speed of the jets, noting that the observed and modeled increase in eddy length scale should be accompanied by a decrease in the flow-relative phase speed of midlatitude waves. This should allow waves to propagate further from the jet core before dissipating. Although most midlatitude waves propagate equatorward from the jet, some do propagate poleward. The poleward flanks of the jet are sites of significant eddy generation and dissipation. If some of this eddy dissipation is displaced further poleward, the net convergence increases, and the jet is likely to shift poleward.

Summarizing, applying linear wave theory, we may expect to see a poleward shift (or an equatorward shift, applying the same principles in reverse) of the eddy driven jet due to one or more of the following:

- anomalous tropical easterlies, and a poleward shift in the subtropical critical latitude,

- increased ground-relative phase speeds, and a poleward shift of the subtropical critical latitude, or
- larger eddy length scales, decreased relative phase speeds, and increased net convergence on the poleward flanks of the jet.

Figure 18 depicts the eddy momentum flux convergence by latitude and angular phase speed for specified forcings, along with the zonal mean zonal wind (divided by the cosine of the latitude). Note that these are not the same prescribed forcings as those used earlier in this chapter; the forcings here include double the observed stratospheric ozone depletion, SST changes over 1870–2100, and four times the present greenhouse gas concentrations, in order to produce a stronger signal. This is also for convenience, as these figures will be referred to in Chapter 5, and the forcings here match the forcings in that chapter.

Note that these are not the same prescribed forcings as those used earlier in this chapter; the forcings here include double the observed stratospheric ozone depletion, SST changes over 1870–2100, and four times the present greenhouse gas concentrations, in order to produce a stronger signal. This is also for convenience, as these figures will be referred to in Chapter 5, and the forcings here match the forcings in that chapter.

Tropical wind speeds do not change in the $2\times O_3$ experiment (Figure 18), so the Robinson (2002) mechanisms are probably not active here. There is some extra divergence along the poleward flank of the jet, but this is at similar phase speeds as the peaks in the climatological convergence, suggesting it is probably of a similar wavenumber, unless the wavenumber has decreased as the background flow has accelerated. But there is

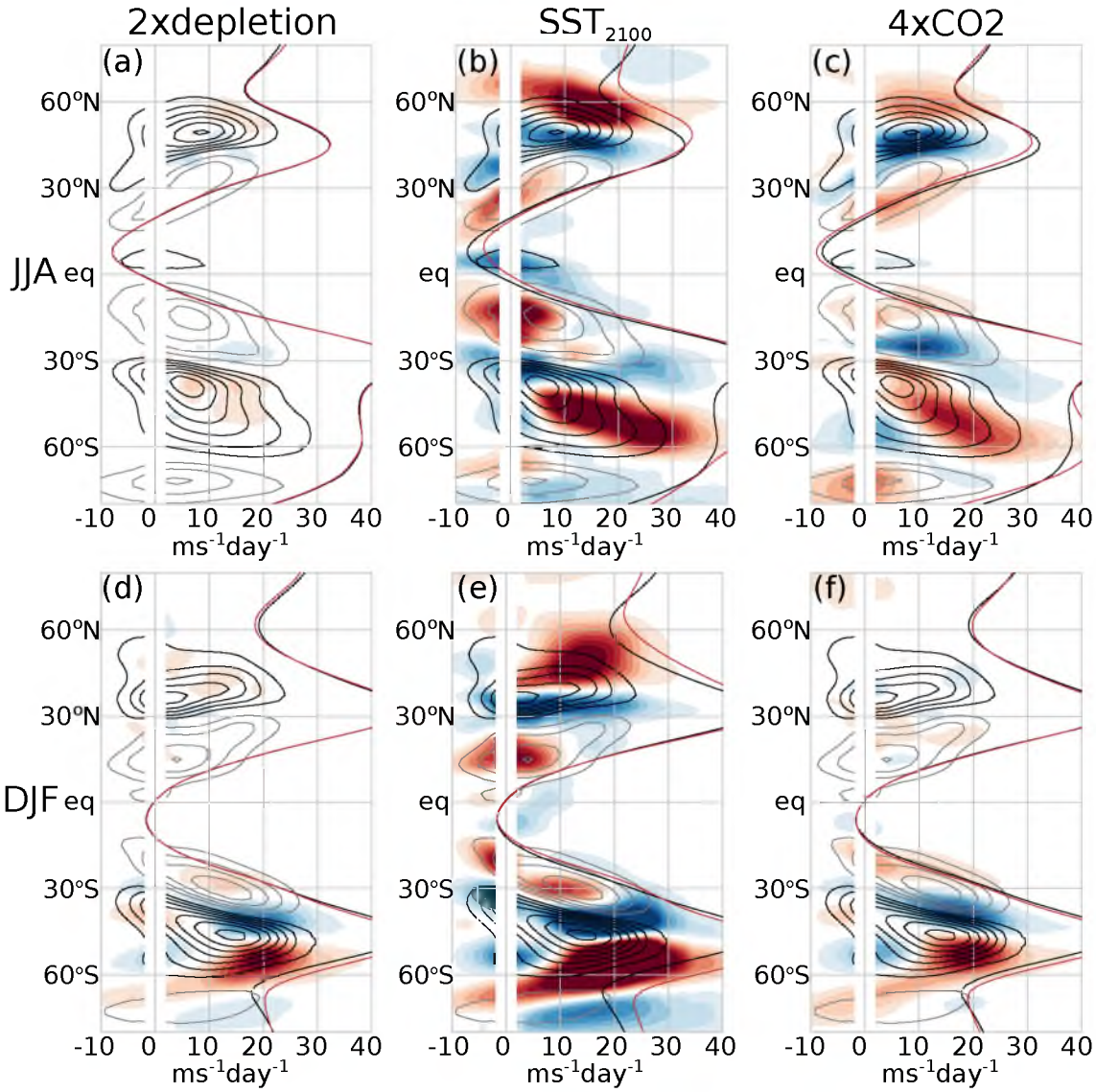

Fig. 18: The climatological mean (contours, negative values in gray) and forced change (shading, negative values in blue) trends of the eddy momentum flux convergence at 250 hPa in the season shown on the left, for the forcings shown at the top, as a function of latitude and angular phase speed. Climatological values are contoured at 0.03 $\mathrm{ms}^{-1}\mathrm{day}^{-1}$, and the response is shaded at 0.003 $\mathrm{ms}^{-1}\mathrm{day}^{-1}$. The black (red) solid line shows the control (experiment) zonal mean zonal wind divided by $\cos\theta$ for comparison.

no noticeable divergence anomaly on the equatorward flank of the existing divergence maxima, so the Kidston et al. (2010) mechanism seems unlikely as well. The signs of the phase speed mechanism, however, are clear. Whenever there is a noticeable increase in divergence or convergence, it is poleward of the climatological maxima of either, and it generally takes place at faster phase speeds as well.

The same interpretation applies to the $4\times CO_2$ experiment results. During DJF, tropical wind speeds do not increase, there is no notable anomalouse divergence on the outer flanks of the climatological jet maxima, and the signs of the phase speed mechanism are clear. One difference, however, is that tropical wind speeds during JJA decrease. As the Robinson (2002) mechanism would predict, there is a decrease in divergence in the tropics.

The response of the momentum flux convergence to SST warming is considerably more complicated. However, the evidence for the Chen and Held (2007) phase speed mechanism is clear, as with the other experiments. Here, however, we also see anomalous divergence poleward of the climatological divergence maxima, at time below maximal phase speeds, so we cannot discount the Robinson (2002) mechanism in this case. Finally, in this experiment, zonal winds on the flanks of the tropics increase somewhat, and anomalous divergence can be seen along the background 'angular wind' curves, possibly as a result.

3.9 On mean jet position and climate sensitivity

Key points in this section include:

- Mean jet position in our model compared to more sensitive models does not fit with

the previously proposed relationship.

This section investigates the possibility that the relative insensitivity of the AM2.1 model to ozone depletion is related to the annular mode timescale in our model. Fluxuation-dissipation theory predicts that the forced climate response along a given mode of variability should increase with the timescale of the mode (Ring and Plumb, 2008). Gerber and Vallis (2007), Kidston and Vallis (2010), and Kidston and Gerber (2010), furthermore, show the timescale of the annular mode to be related to the mean latitude of the jet. The argument goes something like this. The timescale of the annular mode increases as the jet becomes more self-maintaining. A poleward-shifted jet is broader, and less self-maintaining. Thus, one would expect a more sensitive climate response in simulations with an equatorward bias in the jet.

The L48 model framework appears more sensitive to ozone depletion than the L24 framework, and neither of these is as sensitive to ozone depletion as CAM3 model. If the difference in timescales is the source of our differing sensitivities, then the models should be ordered, from the most equatorward to most poleward mean jet latitude, as CAM3 (or the other NCAR models), L24, and L48. However, examining $\overline{\mathrm{HC}}$ and $\overline{\mathrm{FC}}$ data in the appendix reveals that the order is L48, L24, and CAM3 (and other NCAR models). Thus, while the differences in the climatological bias in jet latitude may explain the small differences between the L24 and L48 models, they do not explain the difference in sensitivity between our model and the NCAR models.

3.10 Discussion; comparing our forced shifts to those in other work.

Key points in this section include:

- Forced shifts in AM2.1 are on the small end of observed estimates.
- Poleward circulation features shift most strongly.
- The effects of individual forcings are approximately additive.
- This work demonstrates the importance of the SST response to external forcings.

This work uses GFDL AM2.1 time-slice simulations diagnose anthropogenically induced shifts in the general circulation during the 20th and 21st centuries. Forcings over the past century have produced statistically significant poleward shifts in upper level circulation patterns, as well as surface circulation and hydrology patterns. Estimates of tropical widening are within the range of previous modeling studies. These simulations suggest that SST warming, and its dominant impact on the thermal structure and moisture distribution in the troposphere, play a crucial role in the response of the general circulation and global hydrological cycle to anthropogenic forcings. Perhaps the most important outcome of this chapter is the projection that poleward shifts over the coming century will continue over both hemispheres, and will remain significant, despite the competing effect of ozone recovery.

Annual mean tropical widening estimates in this chapter from all forcings combined are mostly below 1° latitude over the past century. Assuming most of this widening occurred during the last 25 years, this amounts to 1° per 25 years, or 0.4° per decade. This is small compared to the 2.0–4.8° per decade widening seen in observational studies reviewed by Seidel et al. (2008), and at the bottom end of the 0.3–3.0° per decade range

of observational estimates listed in Reichler (2009). However, the changes are typical for the model-derived estimates discussed in Reichler (2009). This study is unique in its use of very long time-slice simulations, all but eliminating natural variability. The results from this chapter validates the results of other modeling studies, in that our circulation shifts can be attributed with high confidence to external forcings.

In agreement with Deser and Phillips (2009), this work reveals that the effects of individual forcings on the circulation are nearly additive. We use this result to estimate '2100 SST' and '2100 CO2' changes, as described in Section 2. The linear sum of the '2100' purely-forced changes approximates the '2100 all' changes quite well, validating this approach. Exceptions to linearity in '2050' and '2100' are strongest in general during NH summer, while in the '2000' comparisons, we see more departures from linearity during SH summer. The consistency of these departures between model formulations suggests that they are realistic.

The circulation shifts seen in this chapter are also reflected by changes in the AMs. The seasonality of the change in the SAM is roughly in line with that of other circulation features, while the seasonality of the change in the NAM bears little semblance to the seasonality of the Hadley or Ferrel cell edge shifts. The mismatch in the seasonality between the NAM and other circulation features illustrates that caution is needed when using AMs to examine mean changes in circulation. An increase in the AM does not clearly distinguish between changes in the structure of the circulation (e.g., the location of the midlatitude jet) and the intensity of the circulation (e.g., the strength of the jet).

In contrast with several recent studies (Deser and Phillips, 2009; Polvani et al., 2011b,a; Son et al., 2010), these results suggest that the poleward shifts in SH circulation features observed over the past century will continue throughout the next century, and remain significant despite ozone recovery. This is likely to be at least somewhat model-dependent and may be described as a combination of (1) a relatively strong indirect SST response, and (2) a relatively weak direct radiative response to changing ozone concentrations.

Which of the many projections is more accurate remains to be seen (Perlwitz, 2011). What this chapter demonstrates is that even among realistic models, with carefully prescribed ozone recovery and a well-resolved stratosphere, the halting or reversing of the poleward SH jet shift during the coming century is strongly model dependent.

CHAPTER 4

THE RELATIONSHIP BETWEEN CIRCULATION FEATURES

The scalings and proposed mechanisms described in Chapter 1 are intended to help to understand shifts in the Hadley cell *or* the eddy-driven jet. It is important to keep in mind, however, that a mechanism for the dynamics for either cell is incomplete without including the effects of the other (Schneider et al., 2010), as tropical and extratropical circulation elements are themselves dynamically connected. This chapter attempts to improve our understanding of the relationship between the Hadley cell and the eddy-driven jet, by analyzing the ratio between correlated shifts in the two features from year to year.

4.1 Expanding on previous ratio studies

Key points in this section include:

- Previous work has found
  - a 2:1 ratio of jet and Hadley cell edge shifts from year to year during austral summer
  - inconsistent ratios between the trends in the jet and Hadley cell edge shifts

- Improved methodology allows us to to extend previous work to other seasons and timescales.
- This work examines the ratio by timescale, as well as in trends and in the forced equilibrium response.
- Results in this chapter shed light on the role of the tropical mean state and of midlatitude eddies in setting the ratio.

Kang and Polvani (2010) investigate the relationship between the eddy-driven jet and Hadley cell edge in multiple CMIP3 datasets, examining the ratio between shifts in the latitude of the eddy-driven jet and shifts in the poleward boundary of the Hadley cell. They find (1) an approximate 2:1 ratio in their respective shifts from year to year, during austral summer, and (2) inconsistent ratios of trends in the eddy-driven jet and Hadley cell. Thus, while the 2:1 ratio seems to describe year-to-year shifts well, it does not seem to characterize climate trends accurately. However, the circulation indices used in Kang and Polvani (2010) are sensitive to changes in circulation structure, and the linear regression method used is sensitive to the correlation between shifts.

In this chapter, empirical orthogonal function (EOF) analysis is used to investigate the relationship between the eddy-driven jet and the Hadley cell edge. Circulation indices are calculated, which are less sensitive to subtle changes in cell structure. For example, the eddy-driven jet latitude in this chapter is estimated from weighted Ferrel cell center, rather than a local wind maximum.

Aside from methodological improvements, the work presented in this chapter expands on previous work by examining the ratio of Ferrel cell center and Hadley cell edge shifts (hereafter the FC:HC ratio) not only on interannual timescales, but also across timescales, hemispheres, and seasons. The examination of the FC:HC ratio in these various settings is done in the interest of understanding how meaningful the ratio is physically, and what factors set the ratio. Specifically, this section addresses the following questions. How does the FC:HC ratio vary by season, hemisphere, and timescale? What circulation changes are associated with a typical ratio? What does the ratio tell us about the dynamical connections between the Hadley and Ferrel cells? How important is a realistic representation of the ocean to reproducing a realistic FC:HC ratio? Are interannual ratios the same as the ratios of trends?

The FC:HC ratio for SH DJF is calculated as in previous work, and the ratios are documented by hemisphere, season, and model formulation. We ascribe the FC:HC ratio to be a measure of the influence of extratropical eddies on the Hadley cell. The ratios of trends and of equilibrium shifts due to prescribed forcings, however, vary from 1:1 to 4:1.

This work explores the role of the tropics in setting the interannual FC:HC ratio, and finds that it depends on the strength of the westerlies in the tropics, which are discussed in Robinson (2002), Seager et al. (2003), Bordoni and Schneider (2009), Schneider and Bordoni (2008), and Kang and Lu (2012). It is found that the modeled ratio is not critically dependent on tropical sea surface temperature variability or to the choice of coupled or prescribed SSTs, but it does depend on the time-mean sea surface temperature, whether

the ocean is coupled or not. This dependency is manifested in a strong correlation between the FC:HC ratio and the time-mean Hadley cell edge.

4.2 Data and methods for examining the ratios of shifts

The coupled model framework described in Chapter 2 includes both ocean heat storage and ocean dynamics. To delineate the role of the two in setting the FC:HC ratio, this study also examines output from the CM2.0 model, coupled to a mixed layer slab ocean (also as described in Chapter 2). This allows one to directly examine the effect of oceanic heat storage, and to gauge the importance of ocean dynamics by comparing these results with those from the fully coupled model.

This section the 4000-year-long coupled preindustrial control simulation produced using CM2.1, in addition to several uncoupled time-slice simulations created using AM2.1 (see Table 1). As a reminder, prescribed SSTs are calculated from multiyear average SSTs in CM2.1 preindustrial, 20th century, and A1B scenario integrations. All of the uncoupled experiments in this chapter are performed and analyzed with both L24 and L48.

In order to understand the effects of external climate forcings on the general circulation, (as in Section 4.5), this work examines pairs of time-slice simulations from Table 1 which differ in just one of the three listed forcings (see Table 4). 24 such pairs are examined. Note that the forced response in these experiments is an equilibrium response, rather than a transient response.

Table 4: Simulations pairs, differing by one forcing.

Forcing	Control	Experiment
CO_2	$0.5\times CO_2SST_{1870}$	CO_2SST_{1870}
CO_2	$0.5\times CO_2SST_{1870}$	$2\times CO_2SST_{1870}$
CO_2	$0.5\times CO_2SST_{1870}$	$4\times CO_2SST_{1870}$
CO_2	O_3SST_{1870}	$CO_2O_3SST_{1870}$
CO_2	O_3SST_{2000}	$CO_2O_3SST_{2000}$
CO_2	SST_{2050}	$CO_{2,2050}SST_{2050}$
CO_2	SST_{2100}	$2\times CO_2SST_{2100}$
O_3	CO_2SST_{1870}	$CO_2O_3SST_{1870}$
O_3	CO_2SST_{2000}	$CO_2O_3SST_{2000}$
O_3	$-0.4\times O_3SST_{1870}$	SST_{1870}
O_3	$-0.4\times O_3SST_{1870}$	O_3SST_{1870}
O_3	$-0.4\times O_3SST_{1870}$	$2\times O_3SST_{1870}$
O_3	SST_{2000}	O_3SST_{2000}
SST	$2\times CO_2SST_{1870}$	$2\times CO_2SST_{2100}$
SST	$CO_2O_3SST_{1870}$	$CO_2O_3SST_{2050}$
SST	$CO_2O_3SST_{1870}$	$CO_2O_3SST_{2000}$
SST	$CO_2O_3SST_{2000}$	$CO_2O_3SST_{2050}$
SST	CO_2SST_{1870}	CO_2SST_{2000}
SST	O_3SST_{1870}	O_3SST_{2000}
SST	SST_{1870}	SST_{2050}
SST	SST_{1870}	SST_{2000}
SST	SST_{1870}	SST_{2100}
SST	SST_{2000}	SST_{2050}
SST	SST_{2000}	SST_{2100}

To validate the results from the GFDL model, results are compared to those from the NCAR CAM3, CAM4, CCSM3, and CCSM4 simulations (see Table 5). Calculations are also performed on data from the NNR, ERA Interim, ERA40, and 20CR reanalyses. For the sake of consistency, all four analysis time series are truncated to 1979-2001.

4.2.1 Ratio estimation

Previous work characterized the interannual relationship between the eddy-driven jet (or of the Ferrel cell center, hereafter FC) and the Hadley cell edge (hereafter HC) as a ratio of the latitudinal shifts in the two. This ratio was calculated from the slope of the least squares best-fit line of the eddy-driven jet latitude versus HC scatter field (Kang and Polvani, 2010). However, the slope of a best fit line is a monotonic function of the correlation between the dependent and independent variables. That is, as the scatter increases, the slope decreases. (This also implies that the slope of the best-fit line depends on which of the two variables is considered independent. Thus, linear regression can address how the Ferrel cell varies with the Hadley cell, or vice versa, but it cannot address

Table 5: The models used in this chapter

model name	SSTs	vertical levels	length (years)
CM2.1	coupled	24	4000
AM2.1, L24	prescribed	24	$\geq$500 (each)
AM2.1, L48	prescribed	48	$\geq$500 (each)
CM2.0	mixed layer	24	50
CCSM3	coupled	26	209
CCSM4	coupled	26	500
CAM3	prescribed	26	100

how both cells vary with each other.) The author posits that a more appropriate ratio to describe two co-varying fields is that which explains the most variance in the FC and the HC. Visually, this is the slope of the longest axis of a FC versus HC scatter plot. This slope is calculated from the first empirical orthogonal function (EOF) of the FC and HC time series, and is here called the FC:HC ratio, or simply 'the ratio.' This amounts to a linear regression, but the residual orthogonal to the best-fit line is minimized, rather than the residual strictly in the y-direction.

The EOF method is useful mainly for describing the ratios of anomalies from year to year (hereafter termed interannual ratios), ratios of anomalies from decade to decade (decadal ratios), and ratios of anomalies from day to day (daily ratios). However, it works less well for describing the mean shifts in the Ferrel and Hadley cells brought on by external forcings. This forced ratio is here calculated as $(\overline{FC_2} - \overline{FC_1})/(\overline{HC_2} - \overline{HC_1})$, where overbars represent time-mean quantities, and subscripts 1 and 2 denote data taken from control and experiment datasets, respectively. Ratios of trends in the two cells (e.g., in reanalyses) are calculated as the FC trend divided by the HC trend. For all three of our ratio calculation methods, confidence intervals are calculated by bootstrapping. For each ratio estimation, data are randomly subsampled 1000 times, without replacement, and the ratio is calculated for each subsample, using the appropriate method as described above. The median value is taken as the FC:HC ratio, and 2.5th and 97.5th percentiles of the calculated ratios as the 95% confidence interval limits. These ratios for the various datasets are documented in the appendix.

4.3 Documenting interannual and decadal FC:HC ratios

Key points in this section include:

- DJF ratios are similar to those in previous studies.
- Ratios during other seasons are higher.
- Sea surface coupling effects ratios little, lowering them slightly.
- Ratios on decadal timescales are similar, and may be higher.

This section begins by characterizing the ratios of year-to-year FC and HC anomalies for SH DJF, as has been done in previous work. The EOF method described in Section 4.2.1 obtains a median interannual ratio (95% confidence interval) of 1.48 (1.46, 1.50) during DJF for CM2.1, which is on the low end of the range of previously recorded estimates (Kang and Polvani, 2010). If the slowly varying wind field is not filtered prior to these calculations, the ratio is closer to 1.7, in agreement with previous studies.

Seeing the methods in this work produce meaningful values for SH DJF, results for all four seasons over both hemispheres is examined. Figure 19 shows FC versus HC scatter plots, including the FC:HC ratio estimates for the different seasons. As explained in Section 4.2, these methods work well in most seasons; NH JJA is a striking exception. During NH JJA the Hadley cell edge is poorly defined, and a near-zero seasonal mean stream function routinely extends over (30°N, 40°N). This results in a tri-modal distribution of Hadley cell edges during NH JJA (note the differing axes for the SH). Interestingly, however, inspection of Figure 19 reveals that the middle cluster of NH JJA (centered at about 35°N, 50°N) has a slope roughly similar to that for SH DJF, hinting at a similarity in the behavior of the FC and HC during summer over both hemispheres, as with other

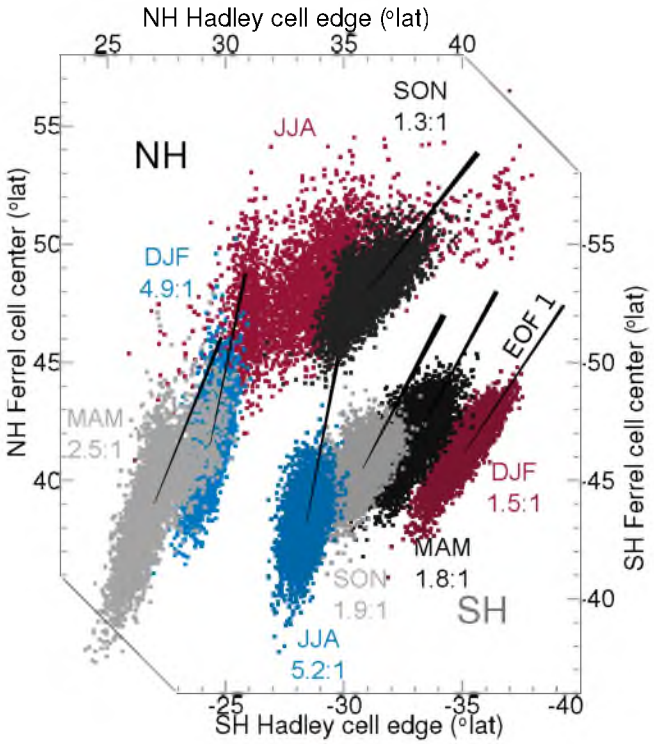

Fig. 19: Seasonal mean FC versus HC latitudes for the CM2.1 preindustrial control for given seasons and hemispheres. The NH (SH) data are plotted on the upper-left (lower-right) axes; note that the SH axes are reversed and shifted to aid comparison. The first EOF eigenvectors for SH DJF are also shown, with the thickness increasing away from their respective origins, reflecting the estimated uncertainty in the calculated slope, or in the FC:HC ratio.

seasons. Note also that the 1.48:1 ratio quoted above for DJF is far from universal; the ratio is generally higher for other seasons and hemispheres. Mean HC and FC positions and ratios are similar for the NCAR model data and reanalyses (not shown).

The ratios documented above are calculated from coupled simulation data, which include internally generated tropical SST variability (e.g., El Niño and the Pacific decadal oscillation, or PDO). Tropical SSTs have been linked to the width of the Hadley cell (Robinson, 2002; Seager et al., 2003; Lu et al., 2008), which begs the question: how does the prescribing sea surface temperatures affect the FC:HC ratio? It is conceivable that,

since tropical SSTs have been linked specifically to Hadley cell width, that the HC should shift less from year to year in an uncoupled simulation than in a similar coupled simulation. From this, and assuming FC and HC shifts remain correlated, we would expect ratios to be higher in an uncoupled simulation than in a coupled simulation.

To investigate the role of coupling, we perform our EOF analysis as above, but for uncoupled preindustrial control simulations using both the GFDL and the NCAR models. Figure 20 shows the interannual and decadal FC:HC ratios calculated for our various datasets, along with their 95% confidence intervals. SH DJF and SH JJA are shown. Results for NH JJA are not shown, as the HC calculation is unreliable. NH DJF results are not shown, as to a first order they are similar to those for SH JJA, but they are less certain. Examining uncoupled GFDL AM2.1 model data (AM2.1 L24 and AM2.1 L48 in Figure 20a) reveals that the uncoupled interannual FC:HC ratio during SH DJF is indeed slightly – but statistically significantly – higher than the coupled ratio, with a median estimate (95% confidence interval) of 1.68 (1.61, 1.76) for L24, and 1.71 (1.68, 1.75) for L48.

Interannual ratios are significantly higher in AM2.1 compared to CM2.1 for all seasons over the SH. The same is true over the NH, except for JJA (in which HC calculations are problematic) and SON (for L24). But this coupled versus uncoupled relationship does not hold on decadal timescales, nor does it hold for the NCAR models. If one examines scatter plots similar to Figure 19 for uncoupled data (not shown), the immediate impression is of similarity. For example, while the standard deviations in HC and FC are reduced by 39%

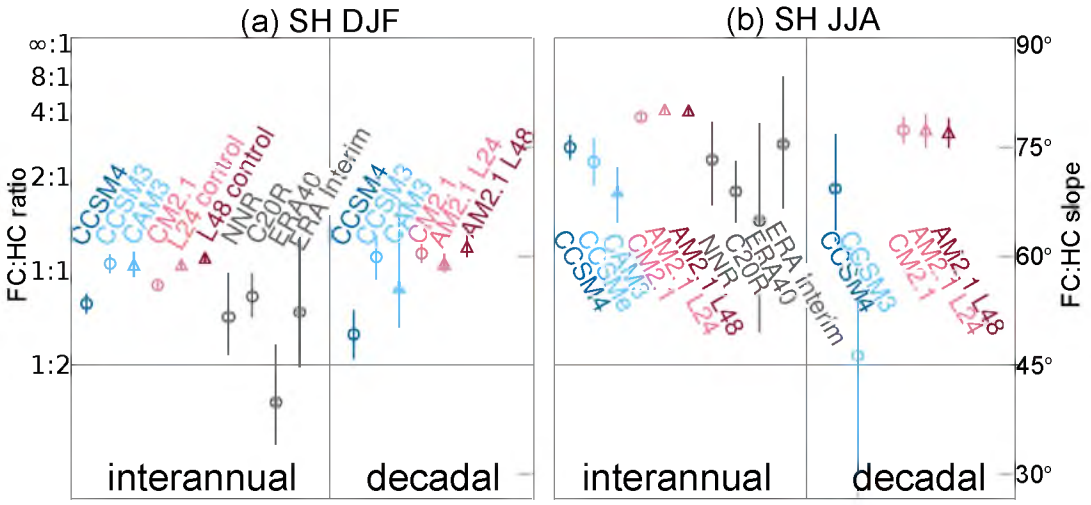

Fig. 20: FC:HC ratios and confidence intervals associated with interannual and decadal anomalies over the SH during (a) DJF and (b) JJA. The y-axis is not linear in the ratio m, but in $\tan^{-1}(m)$, and ranges from 0° to 90°. Points are only plotted if their confidence interval is reasonably narrow (less than 45°, or half the height of the plot). The axis shows interannual ratios, while the right-hand axis shows decadal ratios. NCAR model points are shown in blue, GFDL model points in red, and reanalyses in gray. Uncoupled model data are marked with triangles.

and 28% respectively, the FC:HC ratios change little, as seen in Figure 20.

It is important to remember that the uncoupled simulations use prescribed 10-year mean SSTs. While this ought to filter out a substantial portion of natural SST variability, it is possible that any remaining longer-term SST variability (e.g., the PDO) may alter the FC:HC ratio. This would explain not only the statistically significant differences in the ratio between the coupled and uncoupled simulations in some seasons, but also why these differences do not appear to be systematic between seasons and models.

In addition to investigating the role of SST coupling in determining the FC:HC ratio, this section examines how the ratio varies by dataset. Although the NCAR model data used here cover a shorter timespan (at 100–500 years) than the GFDL model data (at 2000–4000

years), and thus have wider confidence intervals (see Figure 20), differences in the FC:HC ratio appear to be significantly model-dependent. These differences in the ratio are even larger between the model datasets and reanalyses (the gray signatures in Figure 20). While this may indicate that the models produce a somewhat unrealistic FC:HC ratio, it may also be due to the time period examined in the reanalyses. All four reanalyses cover the same 23-year period, which may be too short a time to reliably characterize the interannual ratio. If the ratios from reanalyses can be taken at face value, however, the ratios from the NCAR models, particularly CCSM4, would appear to be more realistic than those from the GFDL models.

Finally, Figure 20 also depicts differences in the FC:HC ratios by timescale. Interannual ratios are broadly similar to decadal ratios in models, but the decadal ratio in reanalyses is not shown, due to the shortness of the record. Note that the decadal ratio for CAM3 over the SH during JJA is also absent from Figure 20b, as the 95% confidence interval for the slope varied by over 45°.

Although daily FC:HC values are also calculated, the meaning of the zonal mean wind field on a day-to-day basis is questionable, and over-interpretation is deliberately avoided. For completeness, however, daily values for the CM2.1 and AM2.1 (L24) control simulations are included in the appendix. Over the SH, the daily ratios are lower for each season than the interannual ratios. Upon inspection, no such generalization can be made for the NH.

4.4 The meaning of the FC:HC ratio; a regression analysis

Key points in this section include:

- The FC:HC ratio captures annular mode variability, as well as some La Niña when SSTs are coupled.
- Tropical variability (e.g., La Niña) does affect the extratropics, but it changes the ratio little.
- Extratropical variability (midlatitude eddies) affects the deep tropics little, but appears to be closely associated with the 1.5:1 ratio.

One advantage of employing EOF analysis is that, along with each EOF, the method produces a corresponding principal component time series. The interpretation of this time series is geometrically straightforward. Since this analysis is performed on two one-dimensional time series (FC and HC), say of length n, EOFS are being calculated from a $2 \times n$ dataset, yielding two EOFs, each a 2-element vector. The first EOF points along the direction of maximum variance, and its slope is the FC:HC ratio described previously (see the vector labeled "EOF 1" in Figure 19). The second is orthogonal to the first, and represents a residual term, corresponding to a poleward Hadley cell edge shift, but an equatorward shift in the Ferrel cell center (or vice versa). The principal component time series associated with each EOF (named PC1 and PC2, respectively) is simply the projection of each point in FC-HC space onto the vector defined by that EOF. Over-interpretation of PC2 should be avoided, as it is purely a residual, rather than a physical mode.

In order to physically interpret the FC:HC ratio, sea level pressure, SSTs, and zonal mean zonal winds are regressed onto PC1, or the time series associated with the FC:HC ratio, and onto PC2, or the time series associated with the residual. Figure 21 shows the zonal mean zonal wind regression on PC1 and PC2. In the coupled case (Figure 21a), shifts along the FC:HC ratio (PC1) correspond to a combination of (1) a poleward shift of the jet and decreased pressure over the pole (not shown), reminiscent of a positive annular mode, and (2) anomalous cool SSTs in the tropical Pacific (not shown) and easterlies in the tropical upper troposphere, similar to the negative phase of the El Niño-Southern Oscillation (ENSO), or to La Niña. Shifts along the residual (Figure 21b) depict a contrasting sharpening and an intensification of the jet, but a similar La Niña-like signal in the tropics. From this, one may suppose that regressing the zonal wind field onto the FC time series alone would produce an annular mode-like pattern, while regressing onto a HC time series would produce mainly tropical easterlies. However, the tight correlation between the Ferrel and Hadley cells implies that both of these regressions (not shown) yield a pattern very much like that in Figure 21a.

In the uncoupled regressions, the tropical easterlies are absent (see Figure 21c; the regression along PC2 for the uncoupled case is not shown). To investigate whether ocean dynamics are required to produce the tropical signal, or whether heat storage is sufficient (see Clement et al. (2011)), the same regression analysis is performed on 40 years of data from a mixed-layer ocean simulation (not shown). As with the uncoupled data, the tropical signal is absent. Unfortunately, this simulation is too short to clearly say whether

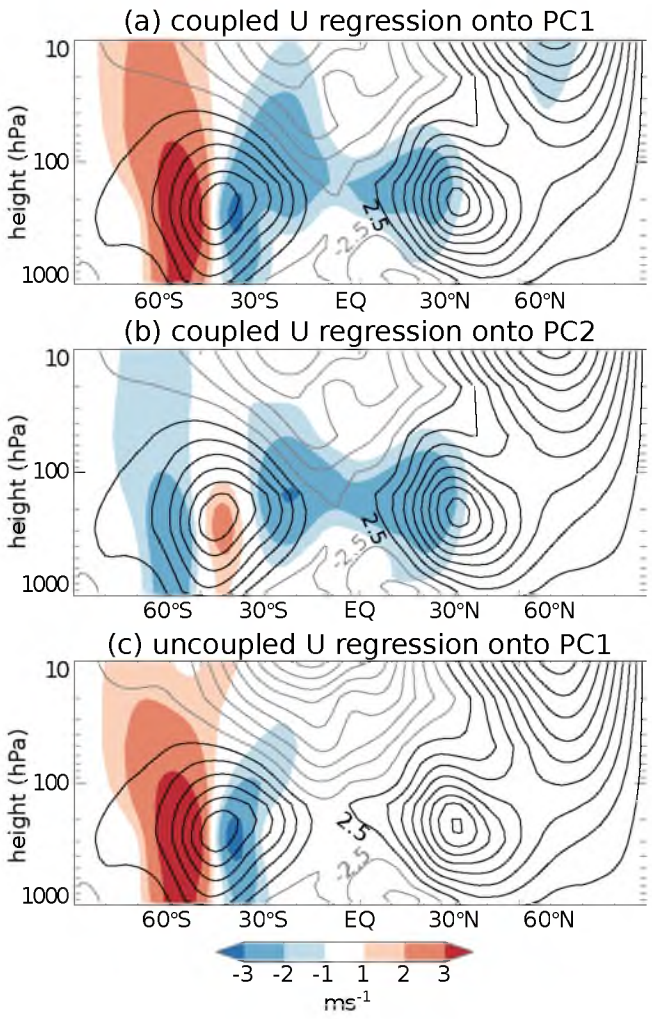

Fig. 21: Climatological DJF zonal mean zonal winds (contours every 5 ms^{-1}) for (a, b) coupled and (c) uncoupled control simulations, along with a regression (shading) of zonal mean zonal wind anomalies onto the time series of the (a, c) first EOF and (b) second EOF of the SH FC versus HC time series. The regression patterns are scaled in each case to represent the wind anomalies corresponding to a 1° poleward Hadley cell edge shift.

the interannual FC:HC ratio from the mixed-layer simulation is different from either the coupled or uncoupled interannual ratios. But it seems clear that ocean dynamics are necessary in order to capture the tropical upper-tropospheric zonal wind shifts associated with HC and FC shifts.

These figures, and the coupled versus uncoupled ratios, illustrate three important points. First, tropical SSTs control the strength of westerlies within the tropics, as can be seen by comparing Figure 21a and c. Second, tropical westerlies contribute to both tropical and extratropical variability from year to year; if they did not, they would not project onto the PC1. Third, in spite of the contribution from tropical westerlies, extratropical eddies dominate correlated year-to-year shifts in the HC and the FC, and thus the FC:HC ratio, judging from the similarity in the coupled and uncoupeld ratios in Figure 20.

4.5 Forced responses and observed trends

Key points in this section include:

- Ratios of observed shifts are small.
- Different forcings produce different ratios.
- The same forcing can produce very different ratios for different seasons.
- Even for the same forcing and season, the ratio can vary substantially.

Climate change often manifests itself in trends along existing modes of variability. Climate projections, for example, include surface temperature trends resembling El Niño and sea level pressure trends resembling the arctic oscillation. Thus, there may be reason to

suppose that the ratio between forced shifts in the FC and HC is similar to the interannual FCC:HC ratio. Kang and Polvani (2010) investigated this, and found that the ratios of trends varied by model, although Chapter 3 showed evidence for ratios of externally forced shifts during DJF were similar to the 2:1 ratio. This section revisits the question of whether the ratios of the externally forced shifts in the FC and HC bear any similarity to the interannual ratios.

Figure 22 shows the ratios of trends in reanalyses, and the ratios of forced shifts in pairs of time-slice simulations (see Table 1). From this figure, four generalizations can be made. First, the ratios of past trends in reanalyses are small (about 1:1) and uncertain. Second, different forcings produce different ratios. That is, some forcings have a more focused effect on either the FC or on the HC. During SH DJF, for example, ozone depletion produces noticeably higher ratios than do greenhouse gas concentration increases. Third, the effects of each forcing differ by season. SST warming produces higher ratios of shifts than do CO_2 increases during SH DJF, but this relationship is reversed during SH JJA. Fourth, the ratio of shifts even for a given forcing type (e.g., for changing CO_2 concentrations) varies substantially.

Why the ratios vary so much for a given forcing is unclear. No single parameter seems to predict what the shift ratio for a given forcing will be. Some correlations exist between the ratios of shifts and the tropical tropospheric mean state in the control simulation, but this relationship is inconsistent between forcings and model formulations. For example, ratios of FC and HC shifts due to CO_2 for SH DJF are positively correlated with tropospheric

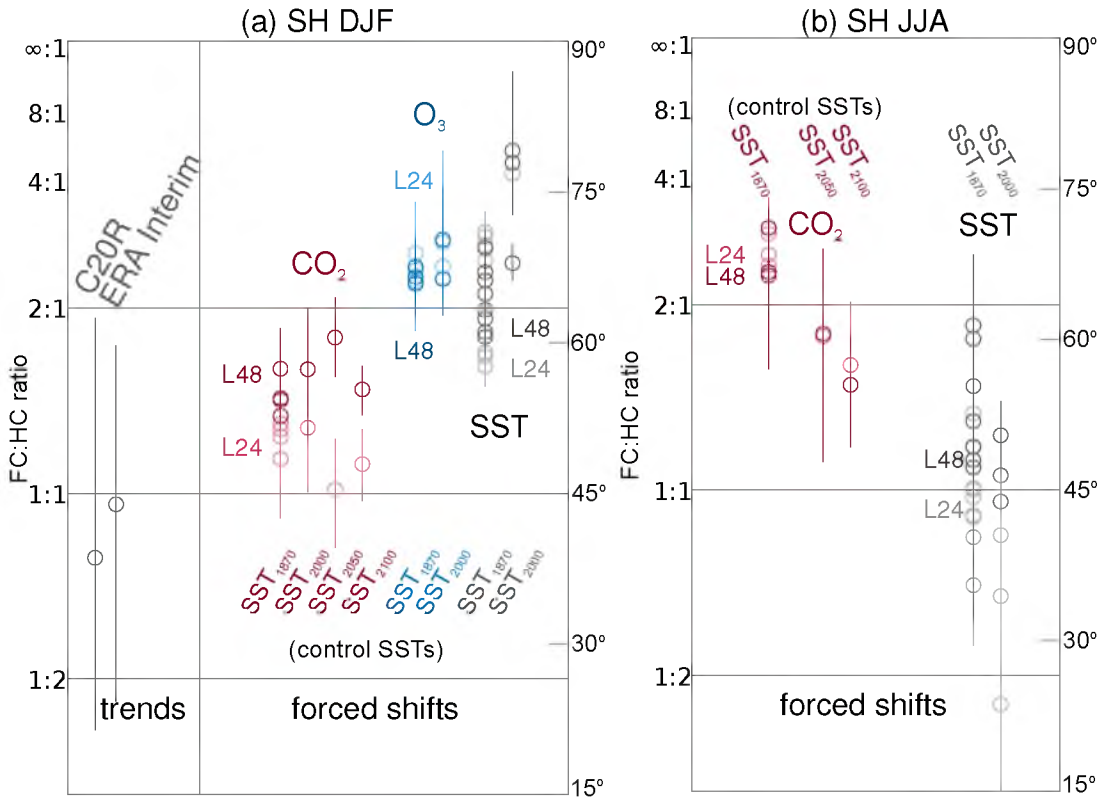

Fig. 22: Ratios of observed trends and modeled forced shifts in the FC and HC, along with the confidence interval for the ratio, calculated via bootstrapping, for the SH during (a) DJF and (b) JJA. Points are only plotted if their confidence interval is reasonably narrow (less than 45°, or half the height of the plot). In the first panel, the left-hand column shows the ratios of trends for reanalyses (gray) as labeled. Ratios of trends are omitted from the second panel because the confidence intervals were wider than 45°. The right-hand column shows the ratios of forced shifts, calculated using the GFDL AM2.1 L24 (light shades) L48 (dark shades) models, with forcing types labeled by color. Data points are staggered horizontally according to the control SST climatology, as labeled. Points within one column may vary by the respective strength of the applied forcings, or by the background climatology aside from prescribed SSTs.

temperature in L48, but negatively correlated in L24. This tentative relationship can be seen in Figure 22a, as the CO_2 points are staggered, left-to-right, by the SST climatology in each respective control experiment.

Two data points in Figure 22 are not shown, but are worth mentioning. These points both involve SST changes from 2000 to 2050 during SH DJF, and both points are negative FC:HC ratios. SST changes between 2000 and 2050 are caused by a superposition of CO_2 increases and O_3 recovery, which have competing affects on the midlatitude jet (Perlwitz, 2011). The resulting SSTs may likewise have an ambiguous effect on the FC. The existence of a negative ratio in the shifts during this season and for the given SST changes is thus less surprising.

Comparing the ratios of modeled forced responses to the ratios of observed trends reveals that, for SH DJF and SH JJA, CO_2-forced ratios appear to be the most similar to the ratio of trends, although these trend ratios from reanalyses have more in common with the interannual FC:HC ratios, than to the ratios of forced shifts. With just 23 years of data, the ratios of trends in reanalyses may reflect a mix of natural variability and the transient climate response. Uncertainties in the reanalysis trends are large; Hadley cell width trends over the past several decades in reanalyses are not even all of the same sign (Stachnik and Schumacher, 2011).

4.6 On the role of the tropics

Key points in this section include:

- Internal tropical year-to-year jet variability only explains a portion of the total Hadley cell variability.
- Even with a coupled ocean, the Kang and Lu (2012) scaling underestimates Hadley cell shifts from year to year, even though it has been shown to perform well when examining mean state.
- The mean Hadley cell latitude is well-correlated to the FC:HC ratio between and within seasons and hemispheres.
- We interpret these results to mean that, from year to year, internal atmospheric variability from the extratropics overpowers the effect of tropical sea surface variability in setting the FC:HC ratio, in a manner modulated by the tropical mean state.

Given the established connection between ENSO and the Hadley cell width, and the clear tropical signal in the regression analysis in Section 4.4, the similarity between the coupled and uncoupled FC:HC ratios may be surprising. The following sections elaborate on the role of the tropics. The role of tropical variability is first examined, followed by the role of the tropical mean state.

4.6.1 The insensitivity of the FC:HC ratio to tropical variability

To better understand the role tropical variability in determining the Hadley cell width from year to year, a scaling from Kang and Lu (2012) is employed, which is essentially a modification of the traditional Held and Soden (2000) scaling, but with an additional term to account for the mean action of eddies. The goal here is to examine how the Hadley cell

would shift from year to year, if the action of eddies on the tropics remained constant.

The traditional scaling approach is to consider, assuming angular momentum conservation, the latitude at which the overturning Hadley circulation becomes baroclinically unstable and eddy generation terminates the cell. In reality, eddy momentum conservation does not hold, in large part because of the action of eddies. Kang and Lu (2012) modify the traditional equations to include the local Rossby number, which describes the degree to which angular momentum conservation is valid (Walker and Schneider, 2006).

The functional parameters in the Kang and Lu (2012) scaling are the lapse-rate tropopause height, the fractional difference in potential temperature between 1000 hPa and the tropopause, and the local Rossby number *Ro*. This section follows their procedure for the SH, calculating the tropopause height after Reichler et al. (2003), averaging the height and stability terms over the interval (20°S,40°S), and tuning *Ro* such that the predicted DJF time-mean HC matches the modeled DJF time-mean HC in each simulation. This work then examines the year-to-year anomalies in the predicted and actual Hadley cells (see Figure 23). This predicted Haldey cell is well-correlated to the actual HC in the coupled simulation ($r^2 = 0.55$), confirming that the thermal structure of the tropics plays a direct role in modulating the Hadley cell width. But the predicted HC varies too little, roughly by a factor of 3, as evidenced by the steep slope in Figure 23a. Furthermore, the correlation disappears in the uncoupled simulation, where conditions in the deep tropics are not influenced by SST variations from year to year.

We suspect that the underwhelming performance of the Kang and Lu (2012) metric in

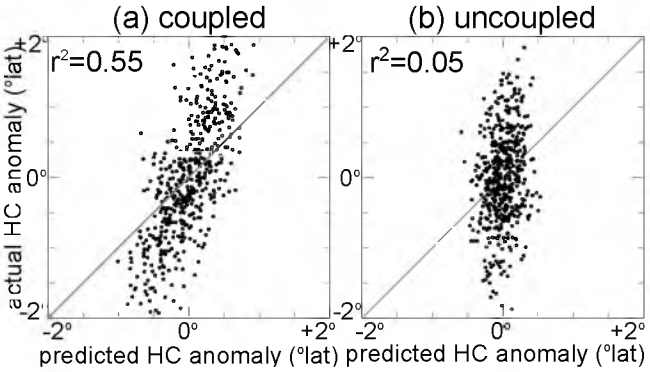

Fig. 23: Scatter plots of actual versus predicted Hadley cell anomalies over the SH during DJF in the coupled CM2.1 (gray) and uncoupled AM2.1 (black) datasets, with the explained variance shown.

our case is because, while tropical SSTs do play an important role in setting the width of the Hadley cell in the long term, the role of eddies in modifying the HC from year to year is dominant. Kang and Lu (2012) focus on long-term trends, in which the internal variability due to eddies is averaged out to a degree, and the direct influence of the tropics is more likely to be seen. The work in this chapter has focused on year-to-year changes; hence the insensitivity of the FC:HC ratio to SST coupling. This difference in timescales may also explain the discrepancy between the interannual ratios and ratios of trends or shifts. In the former case, internal variability is manifested as the roughly 2:1 FC:HC ratio. In the latter cases, internal variability is removed by averaging, leaving systematic mean changes to contribute more strongly to the FC:HC ratio.

4.6.2 The importance of the tropical mean state

So far, the present investigation of the role of the tropics in setting the FC:HC ratio has been centered on tropical variability. The following section more closely examines the role

of the tropical mean state. The strong change in the FC:HC ratio from season to season (see Figure 19) is one indicator that the tropical mean state may be related to the FC:HC ratio.

Bordoni and Schneider (2009) and Schneider and Bordoni (2008) argue that the summertime Hadley cell extends further poleward than the cross-equatorial wintertime cell, because the lack of easterlies in the summertime cell allows extratropical eddies to penetrate into the cell, removing more angular momentum, and delaying the onset of baroclinic instability. In the context of the present study, this suggests that while midlatitude eddies may be primarily responsible for the Hadley and Ferrel cell shifts from year to year, the mean zonal wind structure of the tropics may govern the degree to which these eddies can influence the Hadley cell.

These studies suggest that seasons with a more poleward time-mean Hadley cell edge ($\overline{\text{HC}}$) are the seasons where the Hadley cell is most susceptible to midlatitude eddies. In terms of the FC:HC ratio, seasons with a poleward $\overline{\text{HC}}$ are likely those where extratropical eddies cause year-to-year shifts in the HC which are most comparable to shifts in the FC, or when the FC:HC ratio is the lowest. More succinctly, the $\overline{\text{HC}}$ ought to be negatively correlated with the FC:HC ratio. These correlation values for the 18 time-slice simulations listed in Table 1, for given hemispheres and seasons, are shown in Figure 24.

This figure neatly confirms the expectation that the $\overline{\text{HC}}$ and the FC:HC ratio are negatively correlated ($r^2 = 0.85$), even with data from both model formulations included. The relationship between the Hadley cell edge latitude and the FC:HC ratio (in degrees, or

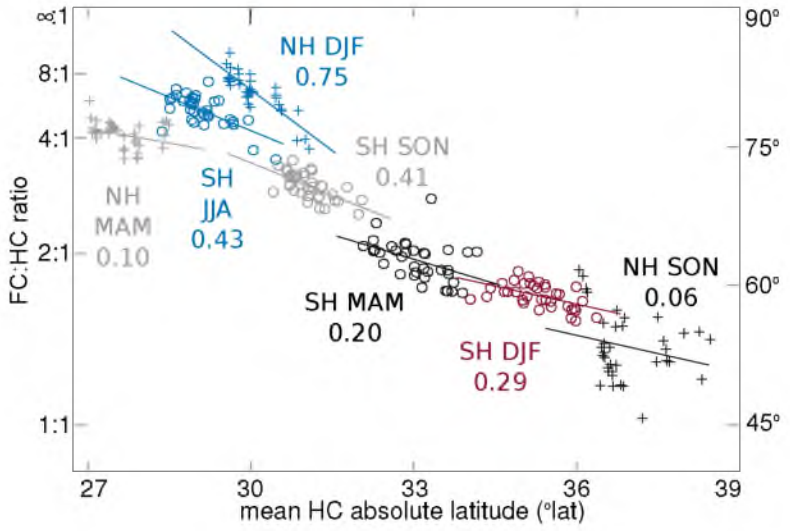

Fig. 24: The interannual FC:HC ratio versus the absolute value of the mean Hadley cell edge latitude, for the time-slice simulations shown in Table 1. NH (SH) data are marked by a + (○), and colors correspond to respective seasons as in Figure 19. The y-axis varies as in Figure 20, although the range is truncated, as shown. All 18 time-slice simulations are performed using L24 and L48, making 36 data points for each hemisphere and season. r^2 values for each season and hemisphere are shown under each respective label.

$\frac{180}{\pi}\tan^{-1}(\text{ratio})$) appears to be roughly linear (at least in the modeled climate regimes), with the slope decreasing about 3° for every 1° latitude poleward shift of the HC. Correlations are likewise high for NCAR model data ($r^2 = 0.64$) and for reanalyses ($r^2 = 0.57$). Within seasons, correlations are moderate for the different experiments (with r^2 values shown in Figure 24), confirming the importance of the tropical mean state not only for describing FC:HC ratio differences by season and hemisphere, but also for describing ratio differences by background climatology, within one season and hemisphere.

Although this work focuses on the relationship between the $\overline{\text{HC}}$ and the FC:HC ratio, correlations are also moderately high between the $\overline{\text{FC}}$ and the FC:HC ratio ($r^2 = 0.56$). In fact, when examining only reanalyses or NCAR model output, the correlations are slightly higher for the $\overline{\text{FC}}$ than for the $\overline{\text{HC}}$. However, within seasons, correlations are usually lower

for $\overline{\text{FC}}$, compared to $\overline{\text{HC}}$ in AM2.1, and the best-fit slopes for each season do not match the slope for the seasonal cycle as well as those in Figure 24. Correlations for $(\overline{\text{FC}} + \overline{\text{HC}})/2$ are similar to $\overline{\text{HC}}$, but correlations for $\overline{\text{FC}} - \overline{\text{HC}}$ are substantially lower ($r^2 = 0.22$).

An alternative explanation for the correlation between the $\overline{\text{HC}}$ and the FC:HC ratio is that, rather than anomalous tropical westerlies allowing waves to propagate further equatorward, the phase speeds of the eddies may decreasing, allowing them to propagate further equatorward even if tropical westerlies remain unchanged (see Chen and Held (2007)). Examining the correlation between the mean phase speed of midlatitude waves (weighted by eddy momentum flux convergence) and the FC:HC ratio, however, reveals no relationship, whether or not the seasonal cycle is retained.

4.7 Summary and interpretation of the FC:HC ratio

Key points in this section include:

- The tropical mean state modulates the influence of eddies on the Hadley cell.
- The FC:HC ratio mostly describes internal atmospheric variability.
- Trends and forced shifts include more subtle changes that the FC:HC ratio misses.

This chapter documents the modeled and observed ratio between shifts in the Ferrel cell center and Hadley cell edge on interannual and decadal time scales, as well as the ratio between trends in reanalyses and between externally forced shifts in time slice simulations. The interannual FC:HC ratio for SH DJF was calculated to be 1.58:1, which is in fair agreement with Kang and Polvani (2010), although the methodology used here yields

slopes that are generally slightly lower for SH DJF. Also in agreement with their study, we find that the ratios of observed trends and of modeled externally forced shifts are highly variable, and no single parameter appears to predict the ratio of trends or of forced shifts. Results for JJA, on the other hand, cannot be compared with those from Kang and Polvani (2010), as their methodology did not produce robust estimates for this season. Ratios during other seasons and over the NH have not, to the author's knowledge, been previously documented.

The FC:HC ratio varies by season and hemisphere, and a significant portion of the variability in the ratio within and between seasons can be accounted for by changes in the mean Hadley cell position. This suggests that mean tropical westerlies, which themselves are controlled by tropical SSTs, are critically important in determining the FC:HC ratio, which ratio we suggest is a manifestation of the effect of eddies on the Hadley cell, or a measure of the Hadley cell's susceptibility to the influence of midlatitude eddies. A metric by Kang and Lu (2012) is used to show that year-to-year changes in tropical temperature structure fail to explain most of the Hadley cell anomalies from year to year, which suggests that midlatitude eddies cause the largest Hadley cell shifts from year to year.

This work adds to an increasing body of evidence which implicates dissipation by extratropical eddies in widening the Hadley cell. The correlation between the two cells coincides with Previdi and Liepert (2007), who note that much of the variability in the extent of the Hadley cell can be explained by the state of the annular modes. The importance of zonal winds in the tropics in modulating meridional eddy propagation has

been discussed by Robinson (2002), Seager et al. (2003), Walker and Schneider (2006), Lu et al. (2008), Schneider and Bordoni (2008), and Bordoni and Schneider (2009). This work compliments Kang and Lu (2012), who use a modified scaling argument to show the importance of tropical temperature structure in widening Hadley cell edge over time. This work confirms that this tropical temperature structure directly influences the width of the Hadley cell, but it also shows that from year to year, the role played by dissipating extratropical eddies is dominant. Tropical-extratropical interactions are intricate indeed, and in a changing climate, the cited 2:1 ratio seems fortuitous, rather than fundamental.

One of the motivations for performing this work on the relationship between the Hadley cell and the eddy-driven jet was to improve our understanding of circulation shift mechanisms which act in a changing climate. However, the interannual ratio studied here appears to be a reflection of internal variability, and the differing ratios of forced shifts and trends suggests that other mechanisms play a large role in climate change, which from year to year are overshadowed by internal variability.

CHAPTER 5

THE ATMOSPHERIC ADJUSTMENT TO SWITCH-ON FORCINGS

5.1 Motivation behind switch-on experiments

Key points in this section include:

- Understanding the general circulation response to climate forcings requires analyzing the step-by-step response of the atmosphere.
- The study of circulation shifts in large ensembles of realistic switch-on forcing experiments is a relatively new practice, and few such studies have been performed.
- This work raises important questions regarding model differences and on the what controls the latitude of the ITCZ.

Although modeled climate change-induced circulation shifts have been studied for several years, it is often the trend over several decades or the time-mean response that is examined, and in order to separate cause and effect, transient simulations are needed (Chen and Held, 2007; McLandress et al., 2010). Idealized transient studies have been performed to understand connections between tropospheric and stratospheric circulation, and emphasize the importance of the role of eddies in setting the mean state and variability

of the axisymmetric circulation (Polvani and Kushner, 2002; Kushner and Polvani, 2004; Simpson et al., 2009, 2010, 2012; Song and Robinson, 2004; Wittman et al., 2004). However, these studies do not directly address the circulation response to anthropogenic climate change.

Although these studies are not explicitly focused on modeling the climate response to increasing greenhouse gas concentrations or stratospheric ozone depletion (for example, Polvani and Kushner (2002), Kushner and Polvani (2004), and Song and Robinson (2004) are interested in coupled troposphere-stratosphere variability, while Simpson et al. (2009), Simpson et al. (2010), Simpson et al. (2012) are concerned with solar heating of the tropical stratosphere), these studies highlight the role of eddies in both instigating and reinforcing general circulation change, and in providing a dynamical linkage between the troposphere and the stratosphere. Simpson et al. (2010, 2012) include topography, citing Gerber and Vallis (2007), who in turn demonstrate that the inclusion of even an idealized representation of topography helps to produce more realistic timescales of eddy-driven jet variability, and hence sensitivity.

Recently, studies have begun to address circulation shift mechanisms by studying the ensemble mean transient circulation response to switch-on climate forcings. Wu et al. (2011) document the transient circulation response to a doubling of CO_2, and suggest that the circulation response begins in the stratosphere, and produces (rather than results from) a broad mid and upper tropospheric temperature response in the subtropics. Wu et al. (2012) take a closer look at changes in the structure and behavior of eddies, and suggest

that the poleward shift of the tropospheric jet is due to a changing index of refraction due to changes in the stratosphere described in Wu et al. (2011).

Chen et al. (2012) examine an ensemble of switch-on uniform sea surface temperature (SST) warming experiments in an aqua-planet simulation, employing a novel quasi-Lagrangian analysis after Nakamura and Zhu (2010) and Nakamura and Solomon (2010). Their results show a fast initial widening of the Hadley cell edge, (on the order of days) even before the stability increases. This shift is well-diagnosed by examining eddies, suggesting the Hadley cell is widened by eddy activity. The poleward shift of the eddy-driven jet is attributed to decreased eddy diffusivity, which in turn changes the meridional potential vorticity gradient. However, the cause of the change in this gradient itself is not explored. It is thus unknown whether this mechanism is pertinent to forcings other than uniform SST warming.

The present study documents the daily transient axisymmetric response to several forcings, using ensembles created with multiple models. It examines the response to switch-on ozone depletion since 1980 (O_3), four-times the observed year-2000 preindustrial greenhouse gas increases ($4\times CO_2$), and a combination of observed and projected sea surface warming from our control simulations to the year 2100 (SST_{2100}). The analyses are performed in uncoupled simulations, so no mixing of signals from greenhouse gas warming and sea surface temperature increases is expected, as in Wu et al. (2011). This work examines results from both the low-top and high-top GFDL AM2.1 models, and the CAM4 model, building on the work in previous chapters. In order to understand the relationship

between eddies and the mean flow response, this work analyzes the changing structure of eddy momentum flux convergence. Of particular interest are mechanisms focused on linear wave propagation, such as the mechanism proposed by Chen and Held (2007), which Chen et al. (2012) did not specifically address, and which Wu et al. (2012) may have discredited, at least in their simulations.

Some important results of this work are the documentation of the different sensitivities of CM2.1 and CAM4 to ozone depletion and greenhouse gas increases. Although it is understood that the two models have differing sensitivities (refer to the model comparison figures in Son et al. (2008), for example), it is unusual for the sensitivities of the two to be examined in such a framework, with deliberately similar forcings. It is also significant that the transient response to SST warming is so similar to the idealized response to globally uniform SST warming in an aquaplanet simulation.

This study also raises important questions. Temperature and wind changes in the two models show significant differences, which are not easily explained. We also see temporary shifts in the latitude of the intertropical convergence zone (ITCZ) which are in the opposite direction of what we expect based on previous studies, and based on the equilibrium responses from Chapter 3.

Section 5.2 outlines the methodology for this chapter. Results are presented in a two-part fashion. Section 5.3 documents the ensemble mean zonal mean temperature, zonal wind, and meridional circulation response for our six experiments. Section 5.4 presents a series of diagnostic exercises to ascertain the roles of the zonally symmetric flow and

eddies in altering the general circulation. Section 5.5 summarizes these results.

5.2 The switch-on framework and analysis

This section examines output from transient simulations performed with AM2.1 and CAM4. The AM2.1 spinup simulations are first described, followed by the CAM4 spinup simulations. Some notes on the analysis method follow.

5.2.1 The AM2.1 model formulations

The AM2.1 experiments again use preindustrial simulation as a control (see 1870,$\overline{O_{3,1850}}$ in Table 6). For each of the spinup simulations performed, there also exist equilibrium simulations performed as described in Chapter 2.

Transient simulations are generated using archived initial conditions from January 1st of each year in the L24 and L48 uncoupled control simulations. The chosen switch-on forcing is prescribed, and the model is integrated forward through March 31st. The chosen forcings include four-times the observed CO_2 depletion to date ($4\times CO_2$ in Table 6), twice the observed ozone depletion calculated using zonal mean values from the Randel and Wu (2007) dataset ($2 \times \overline{O_3}$), and SSTs from the year 2100 in CM2.1 A1B scenario (SST_{2100}). Studying the transient response in this manner implicitly depends on the linear response of the climate system to varying forcings. The more moderate radiative forcings are likely sufficiently small that linearity is not strongly violated. The stronger SST forcing may violate linearity to some extent. Caution must be taken not to over-interpret initial "model

Table 6: Pairs of control and switch-on experiments.

experiment	model	control	spinup	members
O_3			$2\times\overline{O_3}$	460
$4\times CO_2$	AM2.1	$1870,\overline{O_{3,1850}}$	$4\times CO_2$	460
SST_{2100}			SST_{2100}	460
CAM4 O_3^*		2000	$O_{3,1870}$	460
CAM4 $4\times CO_2$	CAM4	2000	$4\times CO_2$	460
CAM4 O_3		$2000,\overline{O_{3,1870}}$	$2000,2\times\overline{O_3}$	460

shock" to the suddenly warmed ocean. The first 90-days of each simulation are analyzed; that is, for leap years, data through March 30th are considered. In this manner, 640-member ensembles are produced for each of the three forcings in both L24 and L48, although results are only shown for L24, due to the strong similarity between the two.

5.2.2 The CAM4 model formulation

Three CAM4 spinup experiments are also examined. In the first experiment, the control simulation has year-2000 forcings imposed, including zonally varying ozone levels at their year-2000 levels from the MOZART model (Horowitz et al., 2003) (2000 in Table 6), and the spinup simulations have ozone prescribed at 1870 levels ($O_{3,1870}$). The control simulation is the same for the second experiment, but the spinup simulations differ from the control in their prescription of quadrupled greenhouse gas depletion ($4\times CO_2$). The third experiment is intended to be an ozone experiment that is directly comparable to the AM2.1 $2\times\overline{O_3}$ depletion experiment, and has a control experiment identical to the '2000' experiment, except that ozone concentrations are taken from the Randel and Wu dataset

(Randel and Wu, 2007), and precisely match those in the AM2.1 control experiment. The spinup simulation in this experiment differs from the control in that it uses the same doubled ozone depletion prescription as with the AM2.1 experiment. Note that the control conditions differ between models. For example, the CAM4 control state includes some CO_2 concentration increases. However, Staten et al. (2011) show that the sensitivity of the forced responses to the background climatology (within the neighborhood of the present-day climate) are reasonably small, and the signal $4\times CO_2$ experiment is sufficiently strong, that the differing control simulations do not strongly affect the results in this section (the author verified this using additional equilibrium experiments from Chapter 3).

When comparing the spinup simulations to their respective equilibrium time-slice simulations, it is also important to remember that the equilibrium response includes the integrated effect of the forcing from the previous year. For example, we study the response to ozone depletion, switched on suddenly on January 1st. However, the southern hemisphere (SH) tropospheric circulation response to ozone depletion during January is understood to be to some extent the downward propagation of changes in the stratosphere seen during the previous spring, when the ozone hole is deepest (Yang et al., 2007). This also must be remembered when studying greenhouse gas increases, as these strongly cool the lower stratosphere as well. However, this procedure is also advantageous, as one may interpret differences between the transient and equilibrium January response (at least in the ozone depletion experiment) as due to downward-propagating effects from the stratosphere during previous months, and similarities as near-real time responses to the

current, switched-on forcing.

In this chapter, eddy co-spectra calculations calculated for 12- and 30-day time series are presented.For simplicity, the first, second, and third consecutive 30-day periods are referred to as January, February, and March respectively.

5.2.3 A note on uncertainty

Statistical significance in this chapter by assuming that differences between ensemble members are randomly distributed, and using a Student's t-test with 100 degrees of freedom (although we have 640 ensemble members for the AM2.1 simulations). However, in practice this underestimates the uncertainty, as the spinup response varies by model and by the structure of a given forcing. Intermodel consistency, temporal coherence, and the realism of the response are here considered to be better indications of the robustness of our results.

5.3 Documenting the transient response

Key points from this section include:

- Ozone depletion cools the SH stratosphere, weakening the NH polar vortex, but the cooling is too weak and too late to have a large effect on the SH circulation.
- Greenhouse gas warming produces strong upper tropospheric warming in AM2.1, a meridional cross-tropopause temperature gradient in both models, and a corresponding circulation change.

- SST warming affects stratospheric temperature and winds, and these changes can be seen to propagate downward into the troposphere as with ozone depletion and greenhouse gas increases.
- The SST response is strong, fast, consists of multiple stages, and bears a strong similarity to the idealized response in other work.
- The slow response to all forcings is largely barotropic.

5.3.1 Documenting the zonal mean wind and temperature response

As described in the introduction, the attribution of circulation shifts to specific mechanisms has been hampered in previous studies because the order of events was unclear. This study thus begins by documenting the overall temperature and circulation shifts under individual forcings, in the zonal mean. Figure 25 shows the zonal mean temperature response, Figure 26 shows the zonal mean zonal wind response, and Figure 27 shows a cross section of the same changes, so the change can be seen day by day.

Instantaneous greenhouse gas increases cause upper tropical tropospheric warming and lower stratospheric cooling. The stratospheric cooling is fairly uniform, latitudinally, but the upper tropospheric warming creates a meridional temperature gradient, and the wind response at and above 100 hPa responds with increased westerlies over midlatitudes in response. Since planetary waves are able to propagate into the northern hemisphere (NH) stratosphere, the effect of this acceleration is quickly felt in the troposphere, where in contrast, over the SH, it is not until the zonal wind anomalies propagate downward near

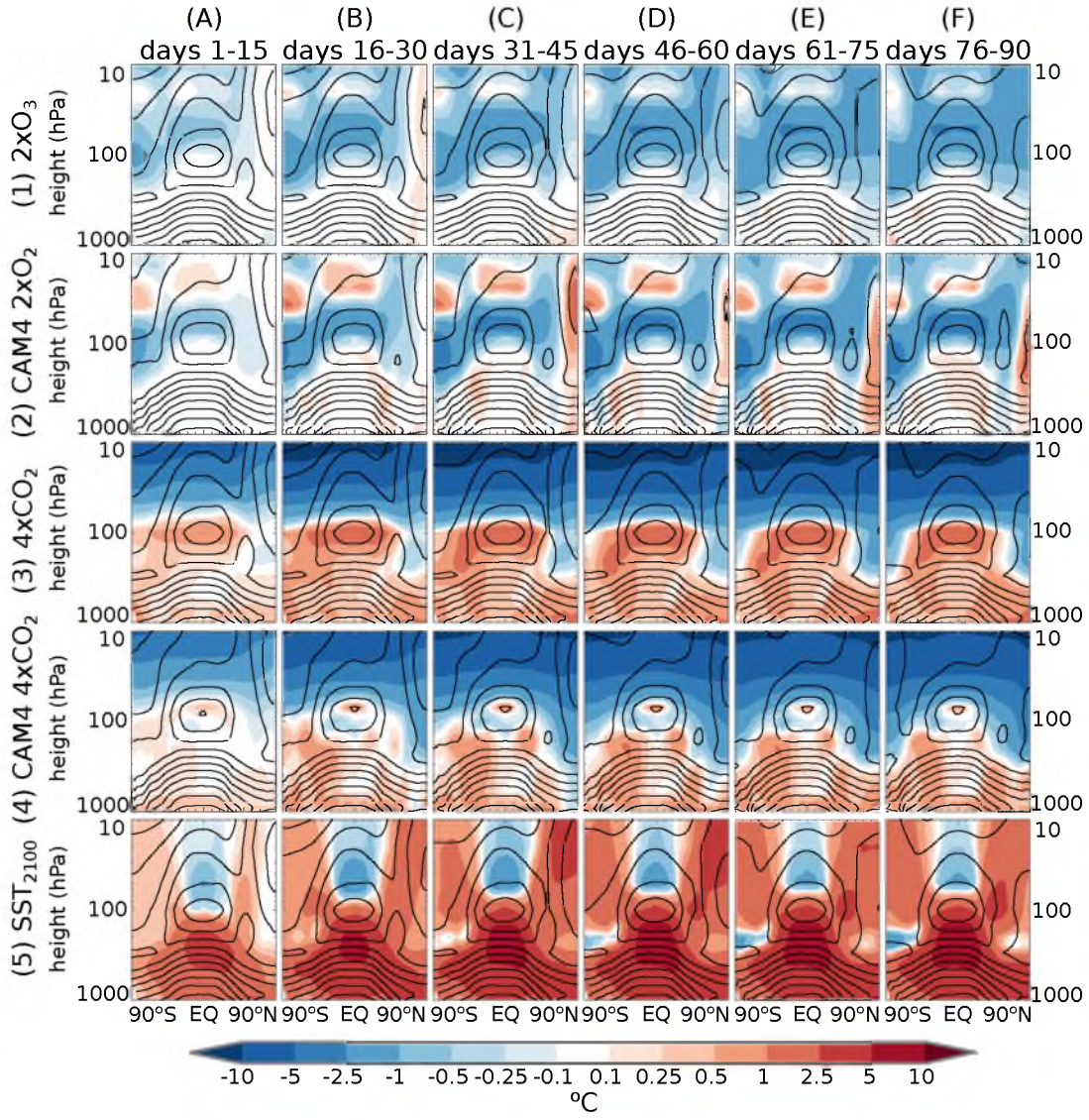

Fig. 25: Latitude-height plots of ensemble mean, zonal mean control temperature (contours) and spinup tempearture anomaly (shading) averaged over six successive 15-day periods (by column) of the spinup simulations (by row). Contours are plotted every 10 K, and shading denotes values as shown.

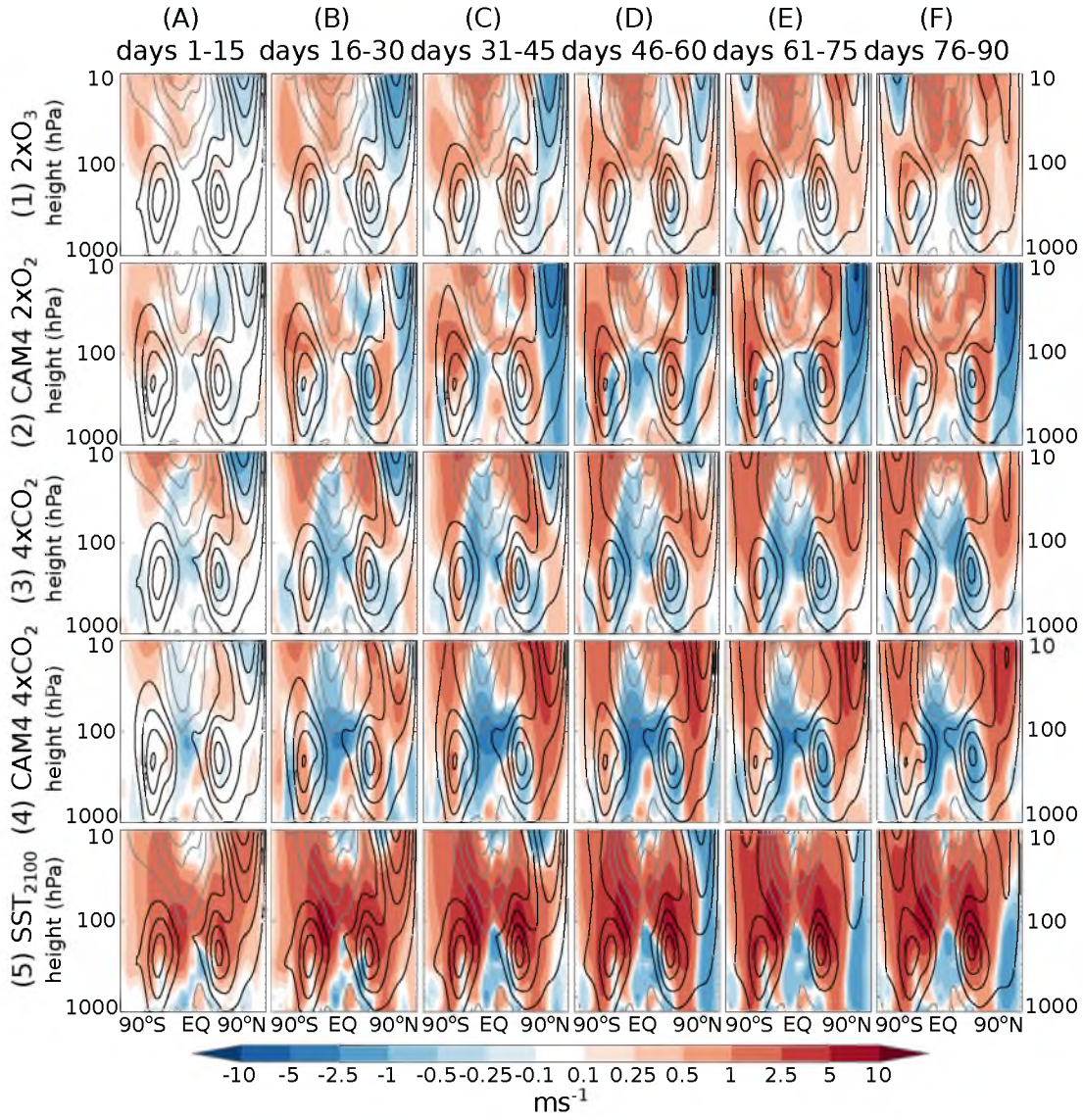

Fig. 26: Latitude-height plots of ensemble mean, zonal mean control zonal wind (contours) and spinup zonal wind anomaly (shading) averaged over six successive 15-day periods (by column) of the spinup simulations (by row). Contours are plotted every 10ms^{-1}, with easterlies contoured in gray, and shading denotes values as shown.

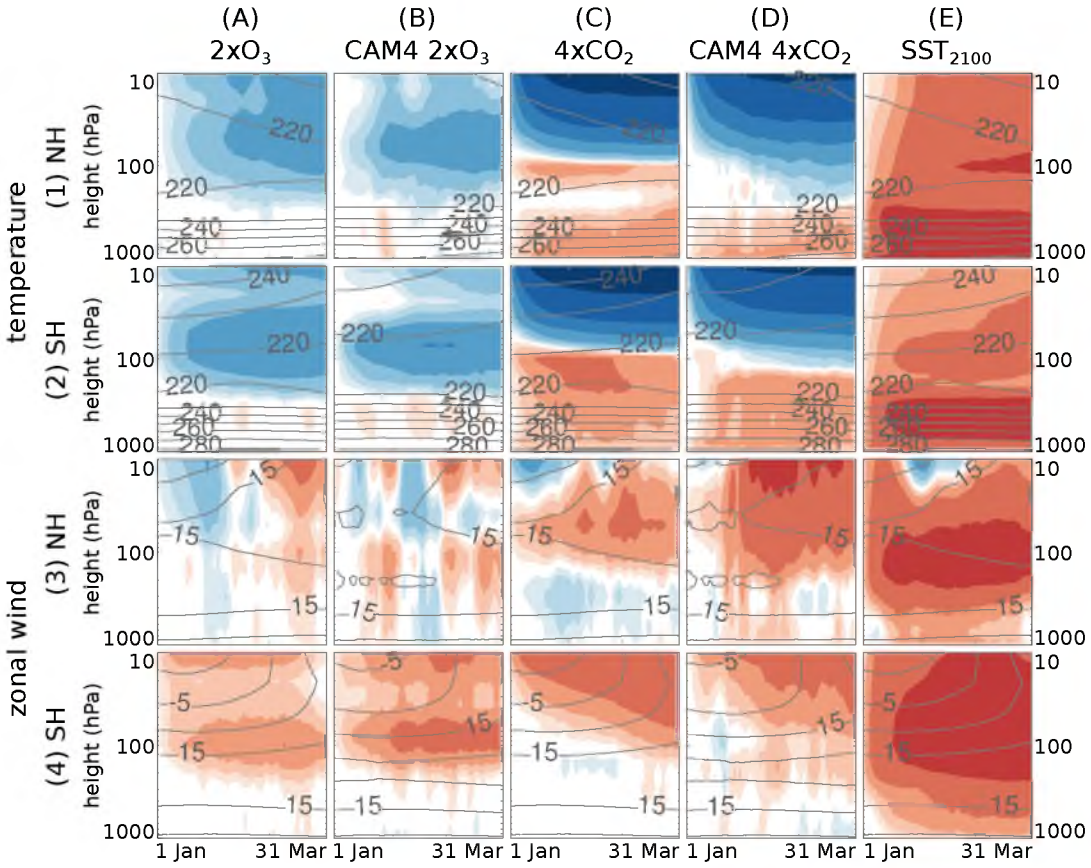

Fig. 27: Ensemble mean, zonal mean time-height plots of temperature (first two rows) and zonal wind (second two rows) control values (contours) and anomalies (shading) averaged over 30°N-70°N (odd rows) and 30°S-70°S (odd rows) for the spinup experiments shown (by column). Contours and shading are identical to those in Figures 25 and 26.

the tropopause that the troposphere responds.

The sequence in the extratropics can perhaps more clearly be seen in Figure 27, in which is shown the temperature and zonal wind response versus time and height for the switch-on experiments. As with Wu et al. (2011), our response to greenhouse gases includes cooling in the stratosphere, warming in the troposphere, an initial easterly wind anomaly in the stratosphere over the NH, and a westerly anomaly which strengthens and descends with time, descending rapidly (at least over the SH) once it reaches the tropopause region. Unlike Wu et al. (2011), our easterly anomaly does not propagate gradually down to the troposphere in our study; the two easterly anomalies are separated by a band of westerlies. However, in the supplementary animation, it can be seen that, from time to time, high latitude westerly anomalies do propagate suddenly down to the midlatitude troposphere, so we do not rule out a dynamical connection between the two.

Quadrupling CO_2 has a very different effect on the troposphere in the CAM4 simulations than in the AM2.1 simulations. Whereas the AM2.1 model depicts warming at around 100 hPa – the neighborhood of the tropical tropopause – over most latitudes in response to increased greenhouse gases, the CAM4 model shows very little warming either at these altitudes, or in the region of the tropical cold cold-point tropopause in this simulations, which is about 30 hPa higher in the year-2000 CAM4 control simulation than in the year-1870 AM2.1 control simulation. Some warming does occur over the equator at about 70 hPa, and below about 110 hPa higher latitudes. Stratospheric cooling is still present, and lower stratospheric cooling at high latitudes is stronger than in the AM2.1 model.

Together, the weaker upper tropospheric warming and stronger lower stratospheric cooling create a temperature gradient across the tropopause break, in cases comparable to that due to quadrupling CO_2 in the AM2.1 model. The large differences seen in the responses to CO_2 in the two experiments does not appear to be due to climatology. Comparing fixed-SST time-slice simulations differing only in their prescribed greenhouse gases (see Staten and Reichler (2013)) reveals that the response to greenhouse gases is very similar, whether SSTs are fixed at their year-2000 levels or at their year-1870 levels.

Figure 27, column C shows the zonal mean time-height anomalies due to greenhouse gas increases in CAM4. The stratospheric and lower tropospheric responses are initially fairly similar to the response simulated in AM2.1, but the weak warming signal in the upper tropospher-lower stratosphere (UTLS) region is quickly averaged out. The effects on the zonal winds are immediately apprent over the NH. Tropospheric winds accelerate early, and stratospheric winds accelerate most strongly well above the tropopause, rather than in its viscinity, as in the AM2.1 simulation. Over the SH, zonal wind differences between models are less severe.

At first, the most surprising response is that due to ozone depletion. Based on the equilibrium simulation (Staten et al., 2011), one would expect the strongest response to ozone depletion to be over the SH. However, as explained in Section 5.2, the switch-on ozone depletion experiment does not have an established cold stratosphere over the Antarctic. While the cooling over the arctic is noticeable, and happens fairly quickly, the thermal wind response is not tremendous. On the other hand, the induced south-to-north

temperature gradient decelerates the Arctic polar vortex, and this effect is again quickly communicated to the troposphere.

The CAM4 response to zonal mean double ozone depletion is considerably stronger than that in AM2.1, both in the magnitude of the cooling above the tropical tropopause and in the SH lower stratosphere and in the warming in the stratosphere about 60 hPa above the regions of cooling. The zonal wind response is also stronger in the troposphere, and propagates downward more quickly. The CAM4 simulation confirms a weakening of the NH polar vortex; in fact, the polar vortex weakens more in the CAM4 simulation. The response to observed, zonally varying ozone concentrations is surprising in its strength, and in its effect on the transition towards a summer-like polar vortex, although previous studies have shown that the response to zonal mean ozone depletion is weaker than the response to ozone depletion that is realistically zonally varying (Gillett et al., 2009; Waugh et al., 2009). The downward propagation of temperature and wind anomalies in the CAM4 ozone-depletion spinup simulations is broadly similar to that simulated in the AM2.1. The strength of the response to zonally varying ozone suggests its importance in climate projections, while the structural similarity between the the zonally varying and zonally symmetric ozone depletion responses suggests that zonally symmetric cooling in the stratosphere is sufficient for understanding the zonal mean circulation response.

The SST_{2100} temperature response is clearly distinct from the others, with temperature anomalies propagating upward from the surface. Strikingly, however, the wind response begins not at the surface, but in the extratropical lower stratosphere, again where merid-

ional heating gradients – this time due not to stratospheric cooling, but to exceptionally strong upper tropical tropospheric warming – produce strong westerly geostrophic wind anomalies. These anomalies very quickly strengthen near the tropopause region, and the effects are also quickly felt in the troposphere. It is as though the three-month adjustment process in the radiatively forced simulations occurs during the first month of the SST_{2100} experiment.

The high-top response (not shown) is very similar to the low-top response. The most obvious differences are that the sudden downward propagation into the troposphere is a little stronger, and thus is noticeable a few weeks earlier. Over the NH, stratospheric easterlies due to ozone depletion are also more persistent. Combined with stronger downward propagation, this produces noticeable easterly anomalies in the NH troposphere due to stratospheric ozone depletion nearly throughout the duration of these simulations. Notwithstanding, westerly anomalies can be seen descending through the stratosphere, reaching the troposphere in late March.

5.3.2 Meridional circulation change

Given the reliability of the L24 model, and the temporal and spatial coherence of the temperature and wind anomalies in the spinup simulations, one may expect to see some shifts in zonal mean indicators of the geometry of the general circulation as in Staten and Reichler (2013) from the zonal mean 500 hPa meridional stream funtion at 500 hPa ($\Psi_{500\ \mathrm{hPa}}$). Figure 28 shows the spinup anomalies for the various $\Psi_{500\ \mathrm{hPa}}$ zero crossings

(FC|PC, for example, denotes the zero crossing betwee the polar and Ferrel cells) and extrema (HCC, for example, denotes the center of the Hadley cell). Since these threshold indicators can be sensitive to small changes in $\Psi_{500\ \mathrm{hPa}}$, this figure includes the statistical significance of the anomalies on a day-to-day basis as described in 5.2. Here results are shown for AM2.1. Shifts were also calculated for the CAM4 simulations, but are ambiguous, probably due to the smaller number of ensemble members for CAM4. Even in AM2.1, there appears to be substantial variability from day to day, indicating that, even for 640 ensemble members, significant uncertainty remains. This is explicitly shown using line thickness; anomalies which are statistically significant at the 5% level of significance are plotted thick.

For ozone depletion, it appears that very few points are statistically significant in this sense; in fact, on the order of 5% are marked as significant, suggesting that these are the cases where the null hypothesis is likely incorrectly rejected. It appears that 5-day or 10-day smoothing may yield some clearer results, but we do not perform these calculations, choosing instead to examine the $\Psi_{500\ \mathrm{hPa}}$ field directly in Section 5.4.1.

Quadrupling greenhouse gas emissions produces a definite poleward shift of the intertropical convergence zone (ITCZ), along with the SH Hadley cell center, Hadley cell / Ferrel cell boundary, and the Ferrel cell center. Changes over the NH are uncertain. The response for the southward shift of the ITCZ are likewise not clear; Kang et al. (2008) find that when the NH is cooled and the SH is warmed, the ITCZ shifts southward as part of the atmosphere's response, acting to increase the flux of energy from the southern to

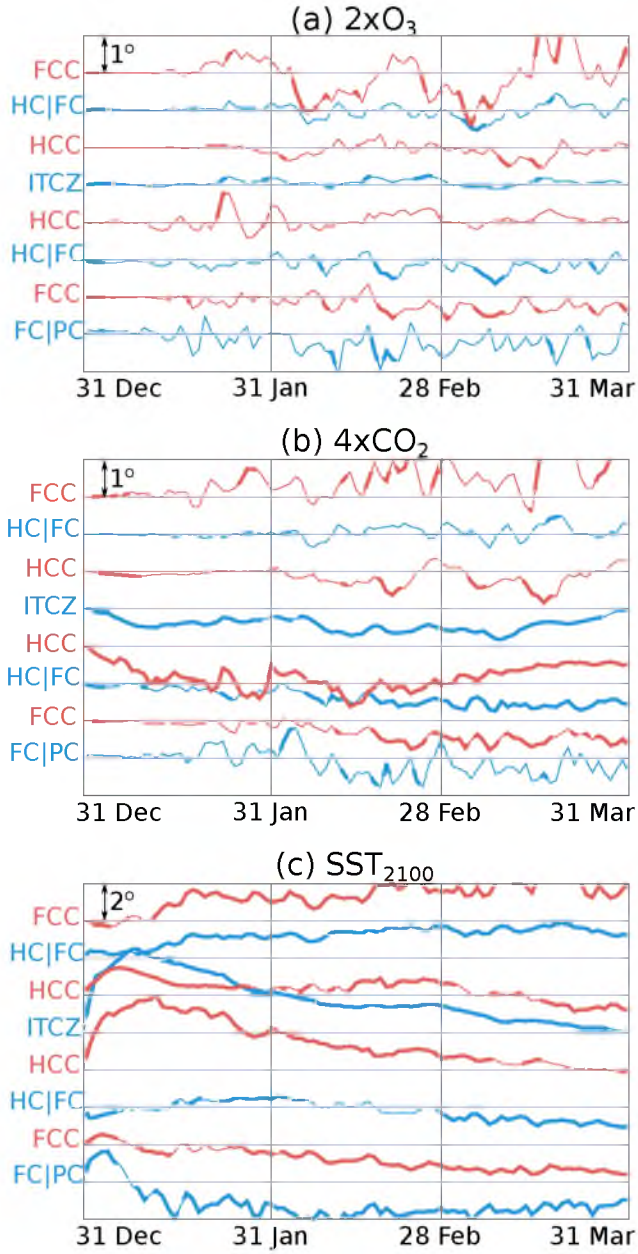

Fig. 28: Time-latitude plots of zonal mean $\Psi_{500\ \mathrm{hPa}}$ threshold anomalies for the L24 AM2.1 (a) $2\times O_3$, (b) $4\times CO_2$, and (c) SST_{2100} experiments. The zero-lines for each anomaly are spaced apart 1° or 2° as labeled, for readability. Thresholds include, starting from the south, the boundary between the Ferrel and polar cells (FC|PC), the Ferrel cell 'center of mass' as described in Staten and Reichler (2013), the boundary between the Hadley and Ferrel cells (HC|FC), the Hadley cell center (HCC), and the ITCZ. Thresholds north of the ITCZ are similar, but in reverse order. The NH FC|PC is not shown, as it is a poorly defined boundary, and varies strongly from day to day.

the NH. They add, however, that the response of the ITCZ is heavily dependent on the treatment of clouds in the model, and in our equilibrium response (not shown), the ITCZ shifts southward during January-March.

The immediate northward shift in the ITCZ is accompanied by northward shifts of both Hadley cell centers, suggesting a contraction of the ITCZ and the associated deep convection. The eddy-driven jets, as indicated by the Ferrel cell centers, seem to contract equatorward during these first few days as well. Interestingly, the boundaries between the Hadley and Ferrel cells shift poleward, even while the extrema on either side shift poleward. However, these changes are short-lived, may be considered "model shock," and are not resolved by the eddy analysis in Section 5.4.3.

By March, the SST_{2100} response involves poleward shifts in all of the indicators, other than the ITCZ and the Hadley cell centers (the NH center eventually shifts equatorward, while the SH center eventually tends towards a poleward shift, but not significantly). A first glance, it appears that the transient response to SST warming still has further to go. On the other hand, Staten et al. (2011) showed that the equilibrium response to SST warming includes a strong seasonal cycle. Seen here is a combination of the two; discerning the relative magnitude of each is, of course, more difficult.

The SST_{2100} response is broadly similar to the idealized response seen in Chen et al. (2012), including the initial contraction of the Hadley cell centers, the later widening of the cell edges, and the competing effects of tropical and extratropical effects on the Hadley cell edge. This adds certainty to the results from the present study, but it also again illustrates

that the precise pattern of SST changes, although very important in the deep tropics as seen in Chapter 3, may be less critical in determining the shifts in the extratropics. It furthermore suggests that idealized studies can capture the critical components of circulation widening, and are certainly worth performing.

5.4 Diagnosing the transient response

Key points from this section include:

- The subtropical warming seen in Wu et al. (2011) appears to be due to SST warming, rather than to the direct effect of $4\times CO_2$.
- The action of eddies is ubiquitous in the circulation response.
- Even during the first month (specifically, the second 12 days) eddy phase speed critical latitudes appear to play an important role in the circulation response.

5.4.1 Diagnosing meridional circulation change

In order to gain further insight into the changing meridional circulation, the mass meridional stream function at 500 hPa (Ψ_{500})is diagnosed, following Chen et al. (2012). Using Rossby number and small aspect ratio approximations, the zonal momentum equation can be written as

$$\Psi_{500} \approx \frac{2\phi a\cos\phi}{g}\frac{p_s}{f}\left(\frac{\partial \langle\overline{u}\rangle_U}{\partial t} + \frac{1}{a\cos^2\phi}\frac{\partial \langle\overline{v'u'}\rangle_U \cos^2\phi}{\partial\phi}\right), \tag{6}$$

where overbars denote zonal mean quantities, and $\langle\rangle_U$ denotes a top-down vertical integral, p_s corresponds to the pressure at the surface (here set to 1000 hPa), and other parameters

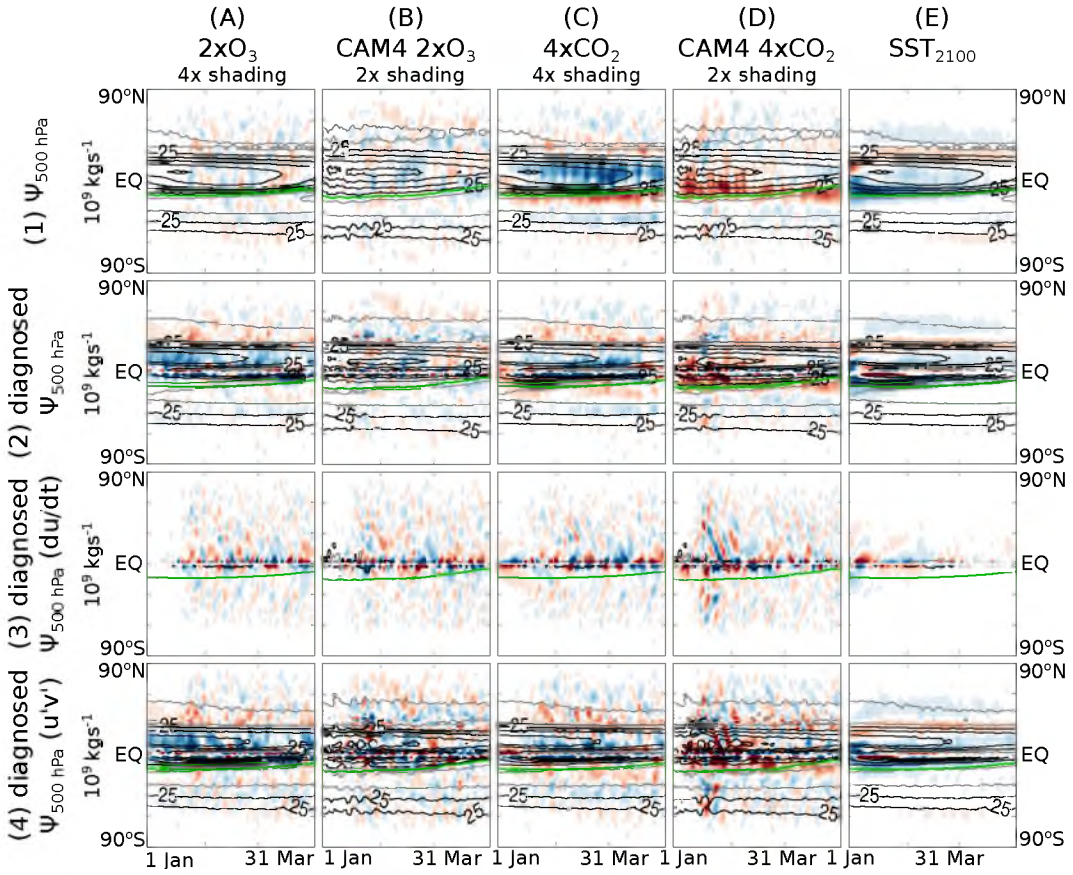

Fig. 29: The ensemble mean control (contours) and spinup anomaly (shading) of the meridional stream function at 500 hPa Ψ_{500} (first row), the diagnosed approximation (second row), and the contributions of the latter from to the first term (third row) and second term (fourth row) on the right-hand side of Equation 6. In all figures, latitude of the ITCZ is represented by a dashed line, for reference.

as is conventional. Figure 29 shows Ψ_{500}, the diagnosed approximation to Ψ_{500}, and the contributions of the two terms on the right hand side of Equation 6.

Changes in the meridional circulation due to ozone depletion, as depicted in AM2.1 (first column of Figure 29), are quite small. Diagnosed changes overestimate the actual changes in Ψ_{500} in the tropics, but it should remembered that much of this overestimation occurs between -20° and 20°, where the low Rossby number approximation is violated.

The response to double-ozone depletion in the CAM4 model (second column of Figure 29) is broadly similar, except over the NH, where the weakening polar vortex is considerably more severe, revealing itself here as a weakened Ferrel cell. The CAM4 modeled response also suggests a gradual influence of ozone depletion on winds in the deep tropics, becoming most notable near the end of February. Hints of this can also be seen in the AM2.1 response to ozone depletion, but the signal there is weaker. Possible reasons for this change in the tropical circulation are discussed in Section 5.4.2. For now, note that this diagnostic does not cleanly determine whether the change in the tropics is due to the changing zonal flow or to the action of eddies, and that it is possible that it is related to changing ozone concentrations in the Tropics, rather than at high latitudes. The response to zonally varying ozone looks quite similar, except for some intensification of the upwelling branch of the winter cell, which is, due to its latitude, poorly diagnosed.

For most fields examined in this study, the two formulations of AM2.1 produce very similar results to one another. The meridional circulation response to ozone depletion in L48, however, more closely resembles the CAM4 response. This is likely related to the more persistent stratospheric winds described above, which delay the propagation of westerlies down to the troposphere. The sensitivity of the NH tropospheric circulation response to ozone depletion suggests that the importance of stratospheric resolution depends on the season examined.

The $2\times CO_2$ AM2.1 experiment (third column of Figure 29) shows a decrease in the intensity of the cells, which is captured only roughly by the diagnosed stream function

(again, poleward of $\pm 20^{\circ}$lat), and is mainly related to changes in eddy momentum flux convergence. Also apparent is the southward shift of the ITCZ (judging from the positive anomalies at the ITCZ). At mid and high latitudes, the modeled response to quadrupling CO_2 is simlar to the ozone depletion response at mid and high latitudes, although the jet over the NH is shifted equatorward more strongly thanks to the action of eddies.

The warming in the upper tropical troposphere in AM2.1 in response to quadrupling CO_2 is largely absent in the CAM4 simulation and, accordingly, so is most of the weakening of the overturning circulation in the CAM4 model response. The energetic imbalance at the surface persists, however, as can be seen along the bottom edges of the fourth row of Figure 25. The greenhouse gas quadrupling in CAM4 also contrasts to that in AM2.1 in the strength and timing of the poleward shift of the SH jet. Whereas shifting eddy momentum flux convergence coincides gradually shifts the jet further south in the AM2.1 simulation, in CAM4 there is no coherent shift, but rather a vague intensification of the jet.

The SST_{2100} experiment produces a poleward shift of the winter Hadley cell, strongest during the first few weeks, likely in response to the sudden increase in convection, and then tapering off as the atmospheric stability increases. The zonal wind tendency gradually decreases after the first week, leaving the eddy term (not shown) to dominate the diagnosed Ψ_{500}. The changes in the zonal mean zonal wind are largely baroclinic, resembling a shift towards a more positive annular mode.

These diagnosed circulation responses emphasize the importance of eddies. Indeed, the only cases when the zonal mean term of Equation 6 plays a dominant role are during

the first few days of the SST_{2100} experiment (and this initial response may just be 'model shock') and the CAM4 the zonally varying ozone depletion experiment. This is in agreement with Staten and Reichler (2013), which suggests that the zonal mean temperature and wind structure in the tropics affects the circulation mainly by altering the propagation and dissipation of midlatitude eddies.

5.4.2 Diagnosing tropospheric temperature change

Ultimately, diabatic warming may be considered to be the trigger of circulation change. In fact, if one neglects the seasonal cycle, then in equilibrium, dynamical warming and cooling must be equal and opposite to the diabatic warming and cooling. Thus, the form of the diabatic warming is a powerful constraint on the changes in the general circulation; any changes in the circulation serve merely to balance the diabatic forcing. In this study, we are certainly not in equilibrium, but in principle, the dynamical response is a function of the applied diabatic forcing. However, a changing circulation modifies the structure of adiabatic warming and cooling, resulting in a feedback which has the potential to complicate the attribution of heating and cooling to a specific aspect of the structure of external diabatic forcing, and to the zonally symmetric and zonally varying components of the general circulation. This section takes a fairly linear approach, and considers the observed warming as the sum of the three terms described, examining the zonal mean temperature budget following Seager et al. (2003) and Wu et al. (2011). They write the budget as

$$\frac{\partial \langle \overline{T} \rangle}{\partial t} = \underbrace{-\left[\frac{\langle \overline{v} \rangle}{a}\frac{\partial \langle \overline{T} \rangle}{\partial \phi} + \langle \overline{\omega} \rangle \left(\frac{\partial \overline{T}}{\partial p} - \frac{R}{c_p}\frac{\langle \overline{T} \rangle}{p}\right)\right]}_{\text{(a) mean meridional circulation}} \underbrace{-\frac{1}{a\cos\phi}\frac{\partial}{\partial \phi}\left[\left(\langle \overline{vT} \rangle - \langle \overline{v} \rangle \langle \overline{T} \rangle\right)\cos\phi\right]}_{\text{(b) meridional eddy heat flux convergence}}$$

$$\underbrace{-\frac{\partial}{\partial p}\left(\langle \overline{\omega T} \rangle - \langle \overline{\omega} \rangle \langle \overline{T} \rangle\right)}_{\text{(c) veritcal eddy heat flux convergence}} \underbrace{+\frac{R}{c_p}\frac{1}{p}\left(\langle \overline{\omega T} \rangle - \langle \overline{\omega} \rangle \langle \overline{T} \rangle\right)}_{\text{(d) adiabatic eddy heat flux}} \underbrace{+\frac{\langle \overline{Q} \rangle}{c_p}}_{\text{(e) diabatic heating}}, \quad (7)$$

where overbars here denote monthly averages, and $\langle\rangle$ brackets denote zonal mean quantities, and variables follow convention. Here, results are shown only for the AM2.1 simulations, as the lower number of CAM4 simulations reduces the utility of these plots; the eddy term is particularly noisy.

Figure 30 shows the the component of zonal mean heating related to changes in the mean meridional circulation (term a in Equation 7), the component related to changes in the eddies (the sum of terms b, c, and d in Equation 7), and the diabatic component (term d in Equation 7) during January for the $2\times O_3$, $2\times CO_2$, and SST_{2100} experiments. The dynamical terms are calculated from model output, while the diabatic term is evaluated as the residual.

The previous section noted a gradual westerly acceleration in the deep tropical troposphere in the ozone depletion spinup experiments, and stated that it was unclear whether this was a direct result of diabatic forcing in the tropics, or the influence of the extratropics. From the breakdown of the temperature tendency due to ozone depletion in Figure 30, there does seem to be some strengthening of the Brewer-Dobson circulation, judging from the intensification of the existing cooling and warming pattern in the stratosphere in the MMC term, and the figure suggests that this cools the tropical UTLS region. This cooling

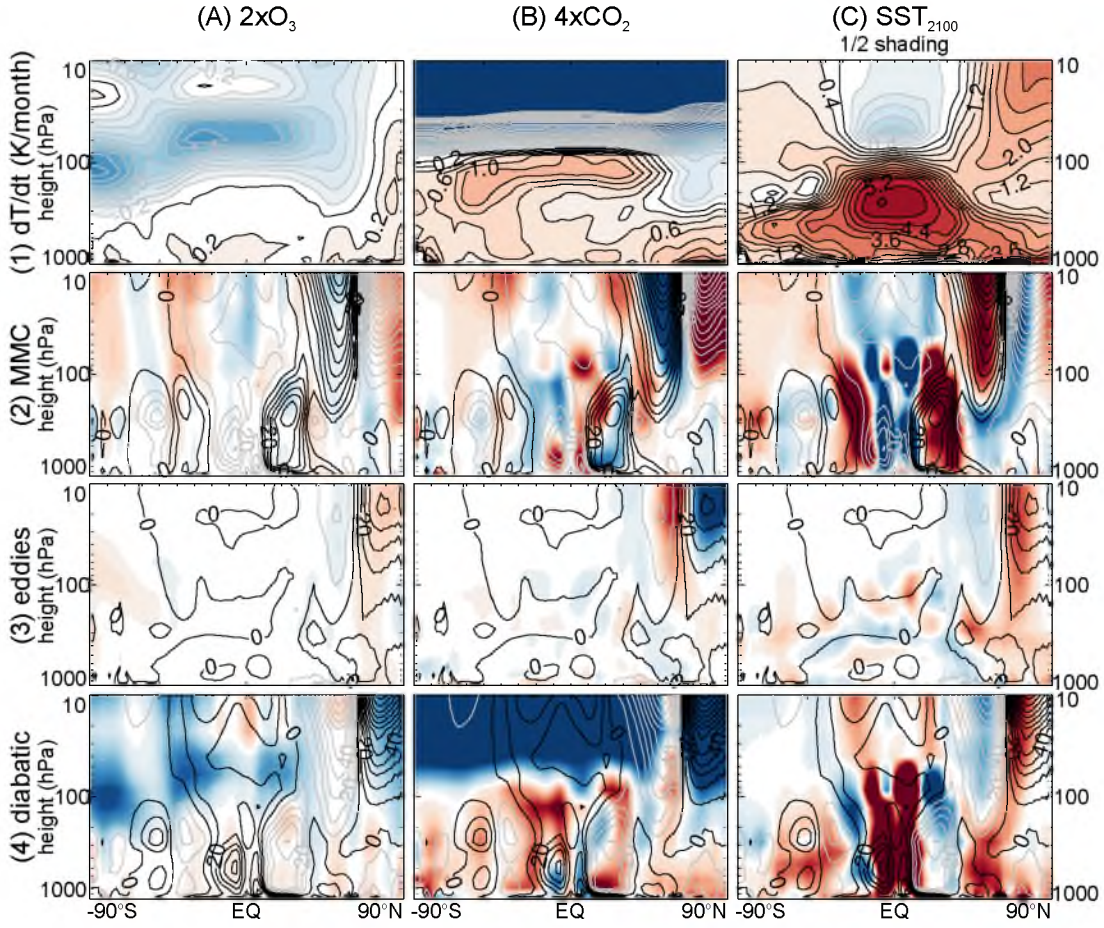

Fig. 30: Latitude-height plots of actual and diagnosed rates of temperature change (in Kelvins per month; see Equation 7). Ensemble mean control values (contours) and spinup anomalies (shading) are plotted by experiment (column). By row, shown are the total temperature change (row 1), the diagnosed component due to changes in the axisymmetric circulation (row 2), due to eddies (row 3), and to diabatic heating and cooling (row 3, calculated as a residual).

aloft may in turn decrease tropospheric stability, and be responsible for the strengthening of the tropical circulation as described above. The effect of eddies in the troposphere seems largely confined to mid-and high latitudes; that is, there is no striking increase in eddy activity near the Hadley regime. However, the weakened polar vortex over the NH allows wave activity to propagate into the stratosphere, and during February and March (not shown) this is coincident with even stronger cooling over the arctic due to the MMC term over the tropical stratosphere. Whether eddy-mean flow interactions in the troposphere alone can explain the change in the deep tropics cannot be discerned just from this linear breakdown. The diagnosed CAM4 response (not shown) to ozone depletion is similar, although rather than cooling in the deep tropical stratosphere and troposphere, we see cooling in the stratosphere and warming in the troposphere. This provides a counter example to the argument above, and leads one to believe that the westerly acceleration in the deep tropics probably indicates some influence of the extratropical wave activity on the deep tropics.

The CAM4 modeled temperature response to ozone depletion is similar to that AM2.1 modeled response, although the precise pattern of heating and cooling in the stratosphere over the arctic does show some model-dependency. Nevertheless, the response also demonstrates some dependency to the structure of prescribed ozone depletion, with the warming and cooling brought on by zonally varying ozone depletion during February resembling the warming and cooling brought on by zonal mean prescribed ozone in March.

During January, quadrupling greenhouse gas concentrations cools the stratosphere above

100 hPa, and warms most of the troposphere by about 0.4 K/month, with stronger warming in the tropical upper troposphere and at low-levels over latitudes with more land cover (as SSTs are held fixed). Most of this warming is a straight-forward result of diabatic heating, although there is some dynamical feedback during January, intensifying warming in the SH upper troposphere. During February and March, net heating rates have decreased substantially, as the general circulation has largely adjusted to the external forcing, although changes in the mean circulation do continue to produce some cooling in the stratosphere over the poles.

A vertical dipole in heating due to the eddy term at about 60°N, between 800–1000 hPa seems to hint at increased wave production at low levels, as well as dissipation at higher levels. There is a similar but much weaker signal over the SH as well. Perhaps increased land-sea temperature contrasts brought on by increased radiative forcing and amplified by our holding SSTs constant, amplify existing patterns of planetary wave activity. McLandress et al. (2010) note the eddy momentum flux divergence aloft at 60°N, and highlight the discrepancy between this divergence and that predicted by the Chen and Held (2007) phase speed mechanism. The present work may reveal a possible resolution to the dilemma; the phase speed mechanism may explain changes in the convergence on the equatorward flanks of the jet, while changing planetary wave activity may be related to the anomalous divergence seen on the poleard flanks. An analysis of convergence by wavenumber may help resolve the dilemma (see Section 5.4.3).

The 200 hPa warming in the viscinity of the jet noted in Figure 9a of Wu et al. (2011)

can be seen during January in the present study, but is absent from our $4 \times CO_2$ simulation during March. One possible reason for the apparent discrepancy is that their atmosphere is still adjusting during March, do to their choice to use a coupled ocean. The connectedness of the anomalous total warming at this level with the warming above the Arctic ocean begs the question of whether the March warming in their study is related to changing sea ice cover. The CAM4 response to $4 \times CO_2$ shows no warming at all at 200 hPa, between 25-30°N, even during January, as the (largely diabatic) upper tropospheric warming seen in AM2.1 is largely absent in CAM4. This suggests that, while the response to quadrupling CO_2 may depend on the model used, the March warming at 200 hPa depends on changing SSTs.

Since this warming depends on changing SSTs, we would expect it to be absent in March of our SST spinup simulation as well, since our SST warming is applied instantaneously, and the adjustment should be mostly complete by then. Indeed, the late warming signal near the NH eddy-driven jet in the study is absent from the SST_{2100} response for March (not shown). The existence of warming at this latitude during January is almost trivial, as the upper tropical and subtropical troposphere as a whole warms very strongly during January. Mean circulation and eddy transport extend warming into the mid- to high latitude stratosphere, while the strengthened Brewer-Dobson circulation produces cooling due to adiabatic ascent above the Tropics. Warming is also very strong over the arctic, where sea ice loss results in a very large increase in sensible and latent heat flux into the atmosphere.

In the tropics, strong latent heat release due to SST warming is balanced by intensified adiabatic ascent. By March, the upper troposphere has warmed, and relative humidities have recovered, reducing the condensational heating substantially, bringing it into balance with the dynamical term, which does not strongly increase from January to March. The heating over the arctic is largely dynamical, and subsides by February, such that dynamical and diabatic heating largely cancel during February and March.

Wu et al. (2011) noted that the broad warming of the upper-tropospheric subtropics was dynamically induced. However, term (a) in Equation 7 does not distinguish between changes in the dynamics versus changes in the temperature structure. That is, it is possible that the warming in the subtropics is due to identical advection across a steeper temperature gradient. However, we examine the effect of holding either the dynamics or the temperature at their climatological levels (not shown), and confirm that most of the warming in the subtropics is indeed due to the intensified meridional circulation during January. During later months in SST_{2100} (as all of our SST warming happens instantaneously, as in Chen et al. (2012)) the anomalous circulation brought on by the initial burst of convection settles, while the steeper temperature gradient, and the heating associated with it, remains.

In general, the effect of eddies in our SST_{2100} experiment qualitatively resembles the response to doubling CO_2 in the Wu et al. (2011) study—much more so than does eddy temperature tendency in our CO_2 experiment. This highlights the importance of the SST change in the circulation response, not just in the AM2.1 model, but in the CAM3 model as well, strengthening our results in 3. What we see is a poleward shift and lifting

of not only the eddy driven jets, but of the climatological eddy flux across nearly all latitudes. (In contrast, the CO_2 experiment only shows hints of a lifting of eddy activity at isolated latitudes.) Less of the anomalies here occur on the equatorward flanks of the jets, suggesting that the phase speed mechanism is unlikely to play a large role in the instantaneous SST response seen in this study; this certainly does not preclude the phase speed mechanism from playing a significant role under uniform SST warming. Again, the role of the changing eddy and mean flow structure here is completely dependent on the structure of the diabatic warming.

The eddy term in the temperature response to each of the three forcings is fairly small during January. We note that, in later months, the eddy term strengthens, playing a more important role in the dynamical-diabatic balance.

5.4.3 A close look at eddy momentum flux cospectra

Figure 31 shows the ensemble mean control eddy momentum flux convergence and spinup anomaly, along with the zonal angular phase speed in four experiments, for March. For the most part, February anomalies resemble those during March, although the signal is weaker. January anomalies are generally very weak for the ozone depletion and greenhouse gas increase experiments. The January SST warming response will be examined in more detail below.

The ozone depletion-induced convergence anomalies are strongest over the NH, which is in stark contrast to the anomalies based on time-slice simulations (not shown). As

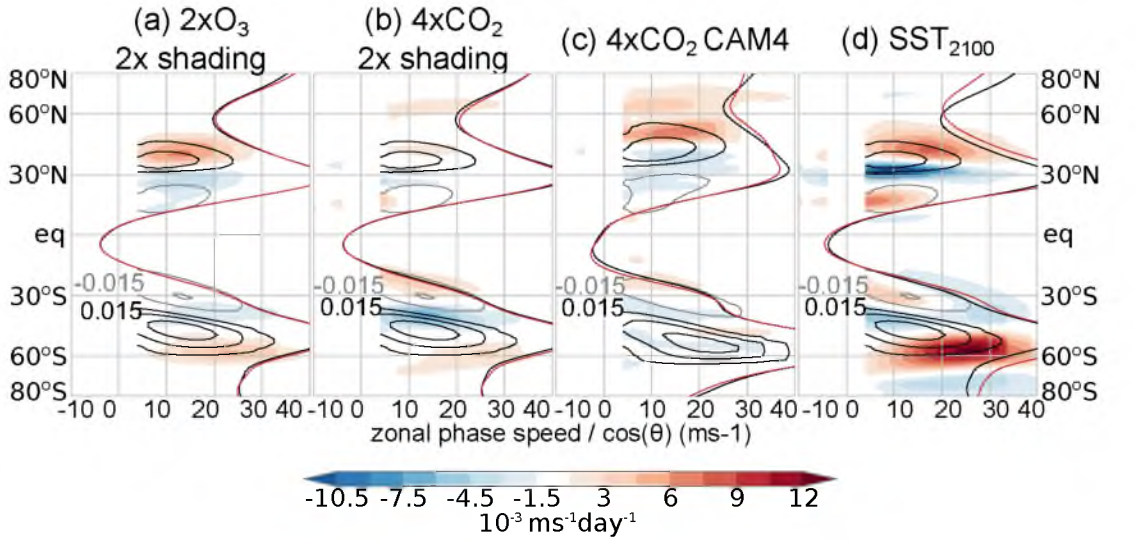

Fig. 31: Angular phase speed-latitude plots of ensemble mean, 30-day mean, control eddy momentum flux convergence (contoured every 1.5×10^{-2} $ms^{-1}day^{-1}$, divergence in gray) and spinup convergence anomalies (shaded every 1.5×10^{-3} $ms^{-1}day^{-1}$, after multiplication by the factors shown) at 250 hPa during March for several experiments in this study (by column). Zonal mean angular wind speeds are also plotted for the control (black) and spinup (red) experiments.

described above, time-slice simulations already have anomalously cold temperatures in place over the antarctic lower stratosphere, whereas in these spinup experiments, much of the effect of ozone depletion over the SH is missing, since ozone depletion begins to act after austral spring has already passed. That said, the figure shoes some shifts over the SH consistent with an increase in phase speeds and the hypothesized shift in convergence and divergence posited by Chen and Held (2007). Overall, the validity of the notion of critical latitudes can be seen by the lack of convergence and divergence at speeds faster than the background zonal wind.

Over the NH, a poleward shift in convergence is seen, but it does not fit with any of the above mechanisms. Convergence and divergence anomalies in the $4\times CO_2$ experi-

ments seem to eliminate all but the phase speed mechanism as possibilities, but even the phase speed mechanism is not strongly suggested; it seems morel likely that some other mechanism may be more likely; this is touched on in Section 5.5. The SST experiment, however, shows evidence for all three mechanisms. Over the NH, there is some anomalous divergence at 10°N and 75°N, as the mechanism in Kidston et al. (2010) would anticipate. (The rest of the shifts in convergence and divergence over the NH do not fit neatly with either of the other two mechanisms; there is a clear shift in the region of maximum convergence, but this is not accompanied by strong increase in the phase speed of the region of divergence.) Over the SH, there is, similarly, anomalous divergence at 20°S and 70°S, far from the jet core, as in Kidston et al. (2010). However, there is also an increase in zonal winds in the subtropics at about 30°S, as well as anomalous divergence there, similar to that in warm tropics experiments in Robinson (2002). Finally, both the climatological divergence maxima at 30°S and the climatological convergence are collocated with dipoles in the anomaly field, which clearly depict a shift towards higher phase speeds and latitudes as in Chen and Held (2007). The latter shifts appear responsible for the largest changes in net eddy momentum flux convergence by latitude at 250 hPa.

A crucial question to ask is to what degree the linear mechanisms described above are causative, rather than a response to already present circulation changes in the background wind field in which they develop. Two of the three mechanisms explicitly rely on changes in the zonal mean wind; Robinson (2002) on tropical westerlies aloft, and Chen and Held (2007) on winds in the UTLS region (they attribute the increased phase speeds to

accelerated winds in this region). Kidston et al. (2010) does not posit a cause for the lengthening of the eddy length scale (although they refute some which suggest it to be a reaction to the poleward shift of the jet, rather than a cause).

In order to more closely examine the sequence of events in the circulation response to SST warming, this section examines the eddy momentum flux convergence in latitude-phase speed space over 12-day periods for the SST_{2100} experiment. To compensate for the reduction in signal due to the shortness of this time period, an additional 1800 SST_{2100} spinup simulations are performed. The results for the first two consecutive 12-day periods are shown in Figure 32.

During the first 12 days, over the SH, the anomalous increases in convergence serve strengthen the already existing pattern present in climatology, although there is some additional divergence due to the zonally varying flow, coincident with increased zonal winds equatorward of 30°S; by the Robinson (2002) mechanism, one would expect to see convergence along these latitudes of accelerated westerlies, but they are not apparent here. It is possible that the contraction of the jet seen in Section 2.5 is too short lived to be resolved here. Some anomalous divergence also takes place poleward of the jet, and may be related to a change in the length scale of the flow. During days 13-24, however, the overall features seen in March (see Figure 32d) are all present. Zonal wind changes also increase substantially; a poleward shift and intensification of the jet can be seen both from the convergence patterns and in the zonal mean zonal wind plots. If the changes in the eddies described are indeed in response to, rather than the cause of a changing zonal mean

flow, then they are a fast response, occurring, as well as we can resolve, simultaneously with zonal wind shifts.

From Figure 32a, it is not clear whether the changing eddy length scale is playing a role or not. To better understand the changing eddy length scale during the first 24 days of the SST_{2100} experiment, we plot the control and spinup convergence and divergence in Figure 33. Here, we are careful to distinguish between changing convergence, and changing divergence. While the effects of increased convergence and decreased divergence are the

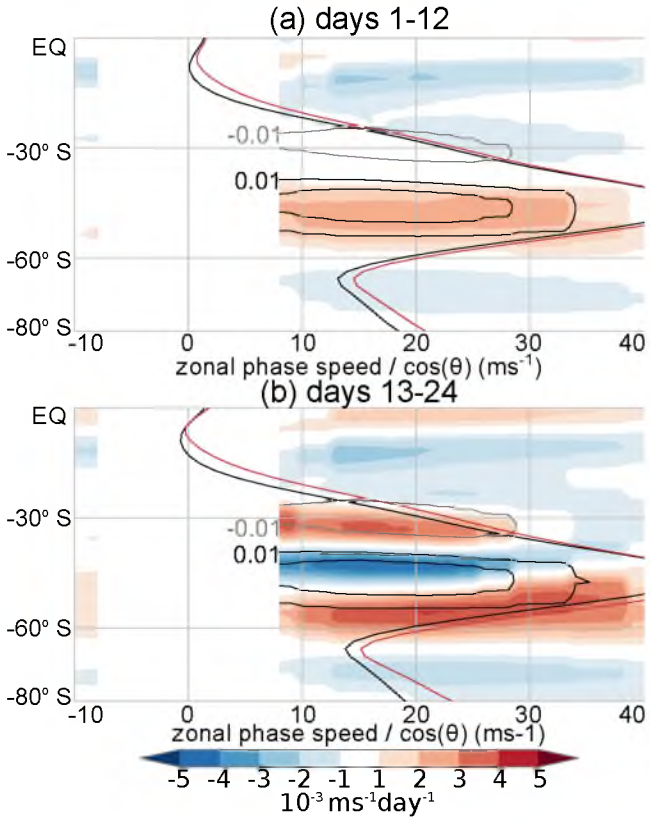

Fig. 32: Angular phase speed-latitude plots of ensemble mean, 12-day mean, control eddy momentum flux convergence (contoured every 1×10^{-2} $ms^{-1}day^{-1}$, divergence in gray) and spinup convergence anomalies (shaded every 1×10^{-3} $ms^{-1}day^{-1}$) at 250 hPa during March for the SST2100 experiment. Zonal mean angular wind speeds are also plotted for the control (black) and spinup (red) experiments.

same on the zonal mean flow, they are indicative of very different processes. For example, if eddy activity were to decrease broadly (if, for example, baroclinicity decreased), then one would see a decrease in both convergence and divergence; neither convergence or divergence would increase. In the case of eddies shifting to a longer length-scale, one would expect to see both decreasing convergence and decreasing divergence at higher wave numbers, and both increasing convergence and increasing divergence at lower wave numbers. Indeed, using warm colors to denote anomalies in convergence, cool colors to denote anomalies in divergence, and shading to denote an increase in either, it is apparent in Figure 33b that wave activity is shifting to lower wavenumbers. While the control maxima in both are at about wavenumber 6, the anomalous increases in convergence and divergence almost all occur at wavenumbers lower than this. The anomalous divergence at high latitudes is due largely to eddies at long length scales. Over the Northern hemisphere (not shown), the changes poleward of 60° mostly take place at or below wavenumber 2, adding some support to our suggestion that the high latitude divergence anomalies are in part due to changing planetary wave activity. During the first 12 days, however, there is no clear shift towards increased eddy length scales (smaller wave numbers). Rather, increases in convergence and divergence occur here almost strictly in line with their climatology, similar to Figure 32a.

It is also necessary to ask whether changes in the eddy momentum flux divergence seen affect the latitude of the eddy-driven jet. Kidston et al. (2010) argue that it matters particularly when regions of divergence and convergence overlap. Following Kidston et al.

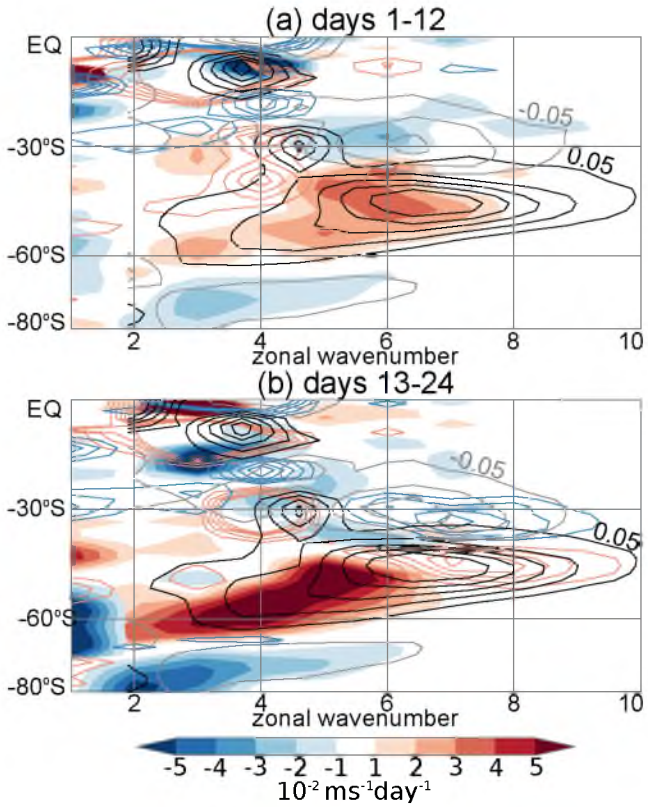

Fig. 33: Wavenumber-latitude plots of control eddy momentum flux convergence (black contours every 5×10^{-2} ms^{-1}day^{-1}) control eddy momentum flux divergence (gray contours), spinup convergence anomalies (warm colors and shading every 10^{-2} ms^{-1}day^{-1}) and spinup divergence anomalies (cool colors and shading) for (a) days 1–12 and (b) days 13–24 of the SST_{2100} experiment. Increases in convergence and divergence are shaded, while decreases in convergence and divergence are contoured. Convergence and divergence are totaled separately over frequency, so some overlap between the two often occurs (e.g., black and gray contours overlap in latitudes where convergence and divergence occur together, at different frequencies).

(2010), we examine the lower level winds to get an approximate measure of the latitude of the existing eddy-driven jet, and the vertically integrated meridional heat flux to highlight the source regions for midlatitude waves. As in their work, we find that the vertically integrated heat flux is still strongly positive, even on the poleward edge of the jet. In contrast, we find that it is also positive on the equatorward side of the jet, suggesting that changes in eddy momentum flux divergence on this side of the jet will also affect

the net convergence, and is thus important in our experiments for diagnosing latitudinal shifts in the eddy-driven jet. This also suggests that an increasing length-scale here should act to widen the jet, as well as shift it poleward. This may be ascribed to differences in seasonality and model framework between the two studies. Kidston et al. (2010) focuses on the average over November-February in idealized, dry simulations.

5.5 Summary and further questions

Key points in this section include:

- Our use of prescribed SSTs produces fast responses and clear signals.
- Our inclusion of the seasonal cycle helps to highlight different stratosphere-troposphere interactions.
- Suggestions for future research are provided.

This study documents the transient response of the atmospheric global circulation to instantaneously applied climate forcings in the context of a seasonally varying background climate. The framework is similar to Wu et al. (2011) and Wu et al. (2012) in this respect, although they perform coupled simulations spanning several years, with fewer ensemble members. The $4\times CO_2$ and SST_{2100} spinup experiments show substantial similarities with their coupled $2\times CO_2$ experiment. The author attributes differences between the two studies to our use of fixed SST, and the resulting reduction in spinup time.

This work contrasts with Simpson et al. (2012) and Chen et al. (2012), in that they maintain constant relaxation profiles or solstitial sea surface temperature conditions. Chen

et al. (2012) furthermore examine the effect of uniformly warming SSTs. Nevertheless the two-stage adjustment of the atmosphere to warming SSTs is quite similar to that seen in their study, even though our SST forcing pattern is far from uniform. This supports the use of idealized simulations.

It is significant that the NH polar night jet decelerates in the switch-on O_3 depletion experiment, comparably to the equilibrium O_3 experiment (see Figure 3a in Staten et al. (2011)). This suggests that, while the SH jet shift during December–February is largely a result of a strong polar vortex during the preceding months, the weakening of the NH polar night jet is a near-real-time response to the existing thermal structure of the stratosphere. This also highlights the fact that the impacts of ozone depletion and recovery are not just limited to summertime or to the SH, but that they also have the potential to impact tropospheric climate during the annular mode active season, when the polar stratosphere and the troposphere are strongly dynamically linked.

These results emphasize the importance of winds in the UTLS region in modulating wave activity. Except for the strong heat flux into the NH lower troposphere in the SST_{2100} spinup simulations, most of the temperature and wind anomalies in the extratropics propagate down from the UTLS region. The fact that greenhouse gas increases (given fixed SSTs) and ozone depletion impact the troposphere from above is not surprising. More interesting is the fact that SST warming impacts high latitudes by modulating eddies, likewise after the winds have changed in the UTLS region.

The similarity between the AM2.1 L24 and L48 models and the CAM4 model corroborates with Sigmond et al. (2008), which suggests that the link between the stratosphere and the troposphere may depend more on the simulation of wind strength in the lower stratosphere than on the stratospheric resolution. However, in the case of the weakening NH polar vortex during late winter and early spring, stratospheric winds may be especially sensitive to a model's formulation, including its vertical resolution.

The difference in the tropical response to modeled responses to greenhouse gas increases in the different models is surprising, as is the direction of the shift in the ITCZ during all but the last weeks of the spinup simulations, and the cause of each is certainly worth investigating.

It also may be worth examining the spinup response to decreasing SSTs, e.g., imposed year-1900 SSTs against a year-2000 control, in order to examine the degree to which the spinup simulation experimental framework is subject to hysteresis. Examining the response to ozone depletion during different times of the year may also be of interest. For example, beginning a simulation a couple of months earlier may yield better insight into the mechanisms by which ozone depletion affects the SH. Alternatively, stratospheric temperatures could be manually nudged more quickly to their equilibrium cold state, so that the transient effects of a cold stratosphere can be directly examined during January.

CHAPTER 6

CONCLUSION

This dissertation is a three-part work, with the overall goal of improving understanding of the mechanisms behind circulation widening in a changing climate. The first part, presented in Chapter 3 examines the equilibrium climate response to individual forcings. The second part, described in Chapter 4, attempts to understand the mechanisms behind the forced responses by examining internal atmospheric year to year variability. The third part, covered in Chapter 5, attempts to understand the transient forced climate response, with this internal variability removed.

In Chapter 3, we highlight the role of increasing eddy phase speeds on shifting the jet. However, while the increase in phase speeds may explain a large portion of the shifts due to ozone depletion and greenhouse gas increases, we suspect that some other mechanism is likely at play in the SST experiments. The SST experiment produces the strongest shifts; it is also the only experiment to strongly warm the troposphere, with warming being particularly strong in the tropics. The GFDL model appears less sensitive to ozone depletion than the NCAR models.

In Chapter 4, we confirm the importance of the tropical tropospheric temperature and wind structure in determining how susceptible the tropics are to the influence of eddies. We also demonstrate that tropical variability affects the Hadley cell edge latitude from year to year, even though it is usually difficult to discern because of the strong influence of internal variability.

In Chapter 5, we filter out this internal variability by examining large ensembles. We find that tropical SSTs do have an influence on the general circulation as a whole, and that a substantial portion of this influence propagates downward from the upper troposphere-lower stratosphere, as with ozone depletion and greenhouse gas increases. Ozone depletion weakens the arctic stratospheric polar vortex during the boreal winter, by weakening the north-to-south wintertime stratospheric temperature gradient. The transient responses to switch-on forcings are qualitatively consistent between models, and our response to forced SSTs agrees with the response in more idealized work. The NCAR model response to greenhouse gas increases, however, lacks strong tropical warming in the tropopause region, which is a major feature of the response in the GFDL model. We again highlight evidence that the phase speed mechanism, as early as two weeks into the simulated transient response. However, we cannot elimintate the possibility that other mechanisms, particularly those that focus on eddy lifecycles, are probably playing a role as well.

Some pressing questions include:

- Why do the GFDL and NCAR modeled responses to greenhouse gas increases differ so strongly in the deep tropics?

- How do the responses to SST warming compare in the GFDL and CAM4 models?
- How does the circulation change in the extreme members of our ensemble experiments?
- How well do changes in the potential vorticity gradient explain changing eddy momentum flux convergence, and the shifting mean flow?

With the substantial number of time-slice and transient simulations performed, we have enough data for several years of research. More simulations are currently being performed. Of particular interest is a switch-on SST warming experiment using CAM4, and additional ensemble members of the other experiments from CAM4; together, these will help us better diagnose changes from this model; presently, the number of ensemble members is too few to examine some aspects of the climate response with any degree of certainty.

We have demonstrated the ability to isolate the forced climate response to individual forcings, but more work is needed in order to disprove (if possible) hypothesized circulation mechanisms. Moist isentropic vorticity analysis may shed some light on mechanisms. The quasi-Lagrangian approach by Nakamura and Solomon (2010), Nakamura and Zhu (2010), and Chen et al. (2012) also seems promising.

APPENDIX

Ratios of Ferrel cell versus Hadley cell shifts for the datasets in Chapter 4. Tables 7–14 contain the time-mean HC, the time-mean FC, the median, 2.5, and 97.5 percentile values for the interannual FC:HC ratio, and the median, 2.5, and 97.5 percentile values for the decadal FC:HC ratio for nearly every experiment, hemisphere, and season in this chapter. Ratios were not archived for the slab ocean simulation, and decadal 2.5 and 97.5 percentile values are omitted for reanalyses, since they are too short for bootstrapping to produce meaningful results. Tables 15 and 16 contain the median, 2.5, and 97.5 percentile values for the daily FC:HC ratio for the AM2.1 (L24) and CM2.1 control simulations.

Table 7: NH DJF interannual and decadal ratios

Experiment	$\overline{HC}$	$\overline{FCC}$	interannual FCC:HC slope median	2.5%	97.5%	decadal FCC:HC slope median	2.5%	97.5%
L24 0.5×CO_2 SST_{1870}	29.6	42.9	81.6	80.7	82.6	78.2	75.1	81.1
L24 2×CO_2 SST_{2100}	30.9	45.5	78.9	77.4	80.5	84.2	80.8	87.3
L24 2×CO_2 SST_{1870}	29.6	43.5	83.9	82.9	84.9	85.4	82.2	88.1
L24 4×CO_2 SST_{1870}	29.6	43.9	85.2	84.4	85.9	84.4	81.7	87.3
L24 CO_2 O_3 SST_{2050}	30.5	44.4	81.4	80.3	82.6	78.4	75.1	81.5
L24 CO_2 O_3 SST_{1870}	29.6	43.1	82.4	81.6	83.3	84.3	81.4	87.3
L24 CO_2 O_3 SST_{2000}	29.8	43.2	82.9	82.0	83.6	82.0	79.5	84.9
L24 CO_2 SST_{1870}	29.6	43.2	82.5	81.8	83.2	79.7	76.4	82.8
L24 CO_2 SST_{2000}	29.8	43.3	83.4	82.5	84.3	83.9	81.3	87.1
L24 $CO_{2,2050}$ SST_{2050}	30.5	44.4	80.6	79.3	81.9	79.8	76.8	82.4
L24 2×O_3 SST_{1870}	29.6	43.1	83.5	82.5	84.5	83.8	81.5	86.3
L24 O_3 SST_{1870}	29.6	42.9	82.0	81.3	82.8	82.0	78.6	84.9
L24 O_3 SST_{2000}	29.8	42.9	82.2	81.2	83.1	79.2	76.2	82.1
L24 -0.4×O_3 SST_{1870}	29.6	43.2	82.3	81.4	83.1	83.2	80.1	85.8
L24 SST_{2050}	30.5	44.3	80.3	79.3	81.4	79.5	77.0	81.7
L24 SST_{2100}	30.9	44.9	75.7	74.1	77.3	81.6	76.7	84.1
L24 SST_{1870}	29.6	43.1	82.1	81.7	82.5	80.1	78.9	81.3
L24 SST_{2000}	29.8	43.1	81.7	80.9	82.6	82.3	79.3	85.3
CM2.1 control	29.3	41.5	78.4	78.0	78.9	80.7	79.3	82.0
CCSM4 control	30.7	45.2	69.8	68.1	71.4	73.1	68.0	77.8
CAM3 control	31.4	45.7	72.3	68.5	76.8	-89.8	-89.7	89.3
CCSM3 control	29.9	44.1	73.6	70.8	76.4	75.9	68.2	85.2
NNR	31.1	45.1	67.1	63.3	71.5	79.4	-	-
ERA40	30.4	44.9	63.6	58.4	68.9	50.5	-	-
ERA-Interim	30.3	45.2	70.2	64.8	73.5	81.0	-	-
C20R	28.7	42.8	71.1	68.3	74.1	42.0	-	-

Table 7 cont.

Experiment	$\overline{HC}$	$\overline{FCC}$	interannual FCC:HC slope median	2.5%	97.5%	decadal FCC:HC slope median	2.5%	97.5%
L48 0.5×CO_2 SST_{1870}	30.0	42.6	80.9	80.0	81.7	77.4	74.4	79.7
L48 2×CO_2 SST_{2100}	31.1	44.9	74.8	73.2	76.1	79.9	77.7	82.1
L48 2×CO_2 SST_{1870}	30.0	43.0	82.1	81.2	83.0	80.4	78.3	83.1
L48 4×CO_2 SST_{1870}	30.0	43.1	82.8	82.1	83.5	83.2	80.6	85.5
L48 CO_2 O_3 SST_{2050}	30.5	43.7	79.5	78.5	80.4	77.8	75.1	80.8
L48 CO_2 O_3 SST_{1870}	30.0	42.6	81.2	80.1	82.2	78.3	75.5	81.1
L48 CO_2 O_3 SST_{2000}	30.0	42.4	81.0	80.0	82.0	80.4	77.3	82.8
L48 CO_2 SST_{1870}	30.0	42.7	81.2	80.3	82.1	82.0	79.0	84.7
L48 CO_2 SST_{2000}	30.0	42.5	81.0	79.9	81.8	79.3	76.7	82.0
L48 $CO_{2,2050}$ SST_{2050}	30.6	43.9	79.0	77.9	80.1	81.2	79.0	83.2
L48 2×O_3 SST_{1870}	30.0	42.3	79.6	78.5	80.6	79.4	73.8	82.0
L48 O_3 SST_{1870}	29.9	42.4	80.4	79.1	81.5	79.5	77.0	81.9
L48 O_3 SST_{2000}	30.0	42.2	79.3	78.3	80.3	78.7	76.2	81.6
L48 -0.4×O_3 SST_{1870}	29.9	42.5	80.9	80.0	81.9	83.8	80.9	87.5
L48 SST_{2050}	30.6	43.7	78.8	77.7	79.8	80.7	77.8	84.5
L48 SST_{2100}	31.0	44.4	75.8	74.1	77.5	77.0	74.5	79.8
L48 SST_{1870}	30.0	42.6	80.6	80.0	81.1	81.6	80.2	83.0
L48 SST_{2000}	30.0	42.4	80.9	79.9	81.8	78.5	75.6	81.9

Table 8: NH MAM interannual and decadal ratios

Experiment	$\overline{HC}$	$\overline{FCC}$	interannual FCC:HC slope median	2.5%	97.5%	decadal FCC:HC slope median	2.5%	97.5%
L24 0.5×CO_2 SST_{1870}	27.1	39.1	78.1	76.6	79.4	80.7	78.4	83.4
L24 2×CO_2 SST_{2100}	27.9	41.5	76.5	74.9	77.9	70.7	63.6	76.7
L24 2×CO_2 SST_{1870}	27.2	39.8	77.8	75.9	79.7	75.4	72.5	79.2
L24 4×CO_2 SST_{1870}	27.2	40.2	76.4	74.7	78.2	80.4	74.5	84.6
L24 CO_2 O_3 SST_{2050}	27.9	40.8	75.1	73.8	76.5	70.9	64.8	76.8
L24 CO_2 O_3 SST_{1870}	27.1	39.6	76.9	75.4	78.3	77.7	75.1	80.5
L24 CO_2 O_3 SST_{2000}	27.7	40.3	74.8	72.8	76.6	67.7	61.4	74.1
L24 CO_2 SST_{1870}	27.2	39.5	75.9	74.5	77.2	80.8	77.5	83.8
L24 CO_2 SST_{2000}	27.7	40.3	74.6	72.8	76.4	67.8	61.9	74.1
L24 $CO_{2,2050}$ SST_{2050}	27.9	40.7	73.7	72.3	75.2	74.4	69.8	78.9
L24 2×O_3 SST_{1870}	27.2	39.4	76.4	75.0	77.6	77.3	74.0	80.5
L24 O_3 SST_{1870}	27.1	39.4	76.6	75.1	78.1	77.6	74.8	79.9
L24 O_3 SST_{2000}	27.7	40.3	76.1	74.2	77.7	62.7	57.2	66.8
L24 -0.4×O_3 SST_{1870}	27.0	39.3	80.0	78.5	81.3	80.6	77.9	83.0
L24 SST_{2050}	27.9	40.4	75.7	74.2	77.1	68.7	63.2	74.4
L24 SST_{2100}	27.9	41.0	77.2	75.4	78.8	75.0	70.5	78.2
L24 SST_{1870}	27.1	39.3	76.6	76.0	77.2	77.8	76.6	79.0
L24 SST_{2000}	27.7	40.2	73.7	71.8	75.3	71.3	65.3	78.0
CM2.1 control	27.0	39.1	68.1	67.6	68.6	76.9	75.9	78.0
CCSM4 control	26.9	43.5	70.9	69.2	72.5	80.8	77.5	83.9
CAM3 control	30.3	44.9	76.5	72.9	79.9	76.7	-85.5	87.2
CCSM3 control	28.8	43.7	77.4	74.7	79.9	79.7	72.1	86.7
NNR	28.5	42.8	71.7	65.9	75.7	59.1	-	-
ERA40	26.1	41.8	69.1	62.6	77.1	52.0	-	-
ERA-Interim	27.9	43.2	67.8	61.2	71.8	75.8	-	-
C20R	26.9	41.8	72.8	69.3	75.3	51.9	-	-

Table 8 cont.

Experiment	$\overline{HC}$	$\overline{FCC}$	interannual FCC:HC slope median	2.5%	97.5%	decadal FCC:HC slope median	2.5%	97.5%
L48 0.5×CO_2 SST_{1870}	27.5	38.6	77.2	76.1	78.5	71.8	67.4	76.1
L48 2×CO_2 SST_{2100}	28.5	41.5	77.8	76.6	79.0	75.6	72.3	79.1
L48 2×CO_2 SST_{1870}	27.5	39.2	77.1	75.4	78.6	73.0	69.0	77.2
L48 4×CO_2 SST_{1870}	27.5	39.6	76.8	75.1	78.1	70.1	66.2	74.1
L48 CO_2 O_3 SST_{2050}	28.4	40.8	74.9	73.3	76.3	72.9	66.7	77.2
L48 CO_2 O_3 SST_{1870}	27.4	38.8	76.9	75.7	77.9	76.5	71.7	81.1
L48 CO_2 O_3 SST_{2000}	27.9	39.9	73.8	72.3	75.2	70.1	65.8	74.7
L48 CO_2 SST_{1870}	27.4	38.9	77.0	75.5	78.4	74.5	71.4	77.3
L48 CO_2 SST_{2000}	27.9	39.8	74.2	72.7	75.6	68.2	60.0	74.7
L48 $CO_{2,2050}$ SST_{2050}	28.4	41.0	77.7	76.2	79.0	74.8	70.9	78.6
L48 2×O_3 SST_{1870}	27.5	38.8	77.0	75.7	78.2	78.2	73.3	82.4
L48 O_3 SST_{1870}	27.4	38.6	76.5	75.4	77.5	76.8	72.5	81.1
L48 O_3 SST_{2000}	27.9	39.6	73.8	71.9	75.4	64.8	60.0	69.2
L48 -0.4×O_3 SST_{1870}	27.4	38.7	77.7	76.1	79.0	76.5	74.1	78.5
L48 SST_{2050}	28.4	40.7	76.3	75.0	77.5	75.4	72.6	78.6
L48 SST_{2100}	28.5	41.0	77.4	76.1	78.6	76.6	73.6	80.4
L48 SST_{1870}	27.4	38.7	77.5	76.8	78.2	77.8	75.8	79.8
L48 SST_{2000}	27.9	39.7	75.4	73.8	76.9	65.2	61.0	69.7

Table 9: NH JJA interannual and decadal ratios

Experiment	$\overline{HC}$	$\overline{FCC}$	interannual FCC:HC slope median	2.5%	97.5%	decadal FCC:HC slope median	2.5%	97.5%
L24 0.5×CO_2 SST_{1870}	34.4	49.2	17.6	15.4	19.7	14.9	9.6	34.1
L24 2×CO_2 SST_{2100}	38.0	51.8	11.2	9.5	12.8	3.2	1.1	5.1
L24 2×CO_2 SST_{1870}	36.5	49.8	22.0	19.4	24.7	25.9	16.1	38.2
L24 4×CO_2 SST_{1870}	36.8	49.9	20.2	17.7	22.8	32.4	14.3	46.2
L24 CO_2 O_3 SST_{2050}	38.3	51.3	13.2	11.4	15.0	3.3	1.2	5.2
L24 CO_2 O_3 SST_{1870}	36.1	49.7	19.0	16.7	21.4	14.6	11.0	35.6
L24 CO_2 O_3 SST_{2000}	36.7	50.3	16.1	14.1	18.1	6.8	4.7	12.4
L24 CO_2 SST_{1870}	35.7	49.6	17.8	15.6	20.0	20.4	14.5	49.2
L24 CO_2 SST_{2000}	37.0	50.5	15.0	13.1	16.9	8.0	6.1	15.4
L24 $CO_{2,2050}$ SST_{2050}	38.0	51.2	13.5	11.5	15.3	4.0	2.1	5.9
L24 2×O_3 SST_{1870}	35.8	49.6	15.5	13.5	17.6	16.1	9.1	33.7
L24 O_3 SST_{1870}	35.6	49.5	16.6	14.9	18.3	15.8	11.8	27.3
L24 O_3 SST_{2000}	36.7	50.4	11.8	9.7	13.7	4.1	2.2	5.9
L24 -0.4×O_3 SST_{1870}	35.3	49.3	19.0	16.9	21.2	29.8	14.9	45.5
L24 SST_{2050}	38.0	51.0	11.4	9.4	13.3	2.6	0.6	4.7
L24 SST_{2100}	38.2	51.3	13.1	10.9	15.1	2.9	1.2	4.7
L24 SST_{1870}	35.4	49.5	18.2	17.1	19.2	27.7	21.8	36.2
L24 SST_{2000}	36.5	50.1	15.9	13.8	17.6	5.9	3.9	9.8
CM2.1 control	33.6	48.2	35.7	34.7	36.8	45.4	40.4	51.0
CCSM4 control	34.3	49.6	38.9	36.2	41.8	40.4	24.5	63.8
CAM3 control	39.3	52.1	16.0	9.7	22.4	33.7	-71.6	73.1
CCSM3 control	36.5	49.8	16.0	13.1	18.9	8.6	0.6	24.6
NNR	38.5	50.8	38.1	28.6	44.7	25.5	-	-
ERA40	31.8	48.5	25.1	19.7	33.8	50.9	-	-
ERA-Interim	37.3	51.3	31.5	9.3	45.5	5.2	-	-
C20R	42.3	54.0	48.9	40.3	60.6	14.3	-	-

Table 9 cont.

Experiment	$\overline{HC}$	$\overline{FCC}$	interannual FCC:HC slope median	2.5%	97.5%	decadal FCC:HC slope median	2.5%	97.5%
L48 0.5×CO_2 SST_{1870}	35.0	48.4	31.6	28.2	35.3	37.6	25.1	48.7
L48 2×CO_2 SST_{2100}	37.2	51.1	19.8	17.6	22.0	14.8	9.0	42.6
L48 2×CO_2 SST_{1870}	36.0	49.2	29.3	25.4	33.4	33.3	19.3	44.2
L48 4×CO_2 SST_{1870}	36.5	49.4	29.8	27.5	31.9	39.9	30.1	48.8
L48 CO_2 O_3 SST_{2050}	37.6	50.6	19.2	16.7	21.7	11.3	6.5	17.4
L48 CO_2 O_3 SST_{1870}	36.1	49.1	24.9	22.2	27.8	36.6	10.5	65.2
L48 CO_2 O_3 SST_{2000}	36.6	49.7	22.4	20.1	25.0	28.4	22.5	36.5
L48 CO_2 SST_{1870}	35.8	49.0	29.1	26.1	32.3	28.2	17.5	35.7
L48 CO_2 SST_{2000}	36.6	49.8	19.4	16.9	21.5	30.5	19.9	40.5
L48 $CO_{2,2050}$ SST_{2050}	37.4	50.7	18.1	15.6	20.6	10.2	6.1	42.5
L48 2×O_3 SST_{1870}	35.9	49.1	24.6	22.3	27.0	33.1	24.5	44.5
L48 O_3 SST_{1870}	35.9	49.1	21.3	19.0	23.7	35.0	22.2	46.1
L48 O_3 SST_{2000}	36.4	49.7	19.6	17.2	22.0	25.7	17.3	33.2
L48 -0.4×O_3 SST_{1870}	35.4	48.7	27.1	24.3	30.3	47.9	34.0	59.9
L48 SST_{2050}	37.2	50.4	21.1	18.2	23.8	22.3	11.8	47.8
L48 SST_{2100}	37.4	50.7	21.4	19.2	23.5	8.6	3.2	12.6
L48 SST_{1870}	35.5	48.8	27.1	25.7	28.6	34.6	30.9	38.3
L48 SST_{2000}	36.3	49.6	21.9	18.8	25.0	26.6	16.8	36.1

Table 10: NH SON interannual and decadal ratios

Experiment	$\overline{HC}$	$\overline{FCC}$	interannual FCC:HC slope median	2.5%	97.5%	decadal FCC:HC slope median	2.5%	97.5%
L24 0.5×CO_2 SST_{1870}	36.7	48.5	50.4	48.3	52.4	49.0	44.0	54.0
L24 2×CO_2 SST_{2100}	38.3	50.9	55.0	52.9	57.4	53.7	47.0	60.7
L24 2×CO_2 SST_{1870}	36.9	49.3	49.2	47.1	51.3	49.5	43.3	56.1
L24 4×CO_2 SST_{1870}	37.2	49.9	45.7	43.8	48.0	47.2	41.3	55.0
L24 CO_2 O_3 SST_{2050}	37.6	49.8	54.1	52.2	55.8	55.3	49.0	60.5
L24 CO_2 O_3 SST_{1870}	36.7	48.8	49.2	46.6	51.6	51.6	43.7	57.2
L24 CO_2 O_3 SST_{2000}	36.8	49.0	55.7	53.1	58.2	49.8	41.9	56.9
L24 CO_2 SST_{1870}	36.8	49.0	49.3	46.8	51.5	44.4	37.3	50.3
L24 CO_2 SST_{2000}	36.9	49.2	56.5	54.5	58.6	59.0	51.4	65.3
L24 $CO_{2,2050}$ SST_{2050}	37.7	50.0	51.8	50.0	53.6	55.5	49.8	62.4
L24 2×O_3 SST_{1870}	36.6	48.6	50.8	48.1	53.0	47.3	38.4	56.2
L24 O_3 SST_{1870}	36.6	48.6	51.5	49.4	53.7	45.9	41.5	50.7
L24 O_3 SST_{2000}	36.7	48.8	55.6	53.4	57.9	54.2	47.5	62.1
L24 -0.4×O_3 SST_{1870}	36.7	48.7	51.4	49.1	53.7	54.0	48.8	59.3
L24 SST_{2050}	37.5	49.6	56.6	54.6	58.6	51.8	47.6	56.9
L24 SST_{2100}	38.0	50.3	54.9	52.9	57.0	54.9	47.2	60.7
L24 SST_{1870}	36.7	48.7	50.8	49.8	51.8	52.1	49.1	55.1
L24 SST_{2000}	36.7	48.9	57.4	55.4	59.4	59.4	55.4	64.4
CM2.1 control	36.0	48.1	51.7	50.9	52.5	46.1	43.9	48.5
CCSM4 control	36.8	50.2	60.7	58.5	63.0	63.1	58.7	68.5
CAM3 control	37.0	49.9	39.2	35.1	42.8	46.8	36.8	54.8
CCSM3 control	35.5	48.6	35.7	32.8	38.2	32.8	21.0	44.4
NNR	38.6	50.6	42.7	35.9	49.6	24.1	-	-
ERA40	36.9	50.0	48.8	41.8	57.3	34.9	-	-
ERA-Interim	37.4	50.0	61.7	54.9	69.2	53.5	-	-
C20R	36.2	49.4	43.0	38.6	46.8	25.7	-	-

Table 10 cont.

Experiment	$\overline{HC}$	$\overline{FCC}$	interannual FCC:HC slope median	2.5%	97.5%	decadal FCC:HC slope median	2.5%	97.5%
L48 0.5×CO_2 SST_{1870}	36.4	48.1	49.2	46.8	51.9	43.3	36.9	50.4
L48 2×CO_2 SST_{2100}	38.5	50.9	54.2	52.5	56.1	46.5	41.1	51.9
L48 2×CO_2 SST_{1870}	36.5	48.7	56.0	53.4	58.8	60.3	55.9	66.0
L48 4×CO_2 SST_{1870}	36.6	49.0	53.4	51.5	55.2	54.8	50.0	60.1
L48 CO_2 O_3 SST_{2050}	37.7	49.8	51.9	50.0	53.7	46.1	33.6	55.5
L48 CO_2 O_3 SST_{1870}	36.5	48.5	52.3	50.2	54.3	56.2	46.5	62.8
L48 CO_2 O_3 SST_{2000}	36.2	48.3	59.7	57.9	61.5	56.3	48.6	64.0
L48 CO_2 SST_{1870}	36.6	48.5	51.2	49.0	53.4	53.2	45.8	60.4
L48 CO_2 SST_{2000}	36.2	48.3	59.3	57.3	61.5	56.3	50.4	62.2
L48 $CO_{2,2050}$ SST_{2050}	37.6	49.9	53.2	51.6	54.8	54.8	50.1	59.4
L48 2×O_3 SST_{1870}	36.5	48.3	53.4	51.2	55.6	50.8	44.2	60.9
L48 O_3 SST_{1870}	36.5	48.3	52.5	50.0	55.2	57.0	52.3	61.8
L48 O_3 SST_{2000}	36.0	48.1	61.7	59.8	63.6	52.9	44.5	61.0
L48 -0.4×O_3 SST_{1870}	36.5	48.4	53.8	51.1	56.1	52.2	46.0	58.8
L48 SST_{2050}	37.5	49.6	51.8	50.1	53.6	53.1	48.9	57.4
L48 SST_{2100}	38.3	50.5	49.9	47.8	51.9	42.6	30.8	53.1
L48 SST_{1870}	36.5	48.3	52.8	51.9	53.8	51.8	48.5	55.3
L48 SST_{2000}	36.1	48.1	61.0	58.9	62.8	65.6	60.0	73.3

Table 11: SH DJF interannual and decadal ratios

Experiment	$\overline{HC}$	$\overline{FCC}$	interannual FCC:HC slope median	2.5%	97.5%	decadal FCC:HC slope median	2.5%	97.5%
L24 0.5×CO_2 SST_{1870}	-34.7	-45.3	59.4	58.3	60.5	60.0	56.5	63.2
L24 2×CO_2 SST_{2100}	-36.4	-48.4	56.6	55.0	58.0	59.9	54.4	64.9
L24 2×CO_2 SST_{1870}	-35.7	-46.5	59.1	57.7	60.5	63.0	59.3	67.2
L24 4×CO_2 SST_{1870}	-36.0	-46.9	57.4	55.9	58.8	60.2	56.4	63.9
L24 CO_2 O_3 SST_{2050}	-36.0	-47.9	56.2	54.6	57.7	54.8	48.3	60.5
L24 CO_2 O_3 SST_{1870}	-35.5	-46.5	58.3	57.0	59.7	56.4	53.0	59.0
L24 CO_2 O_3 SST_{2000}	-36.1	-47.5	58.4	56.9	59.7	54.3	49.0	59.9
L24 CO_2 SST_{1870}	-35.4	-46.1	58.5	57.3	59.8	59.1	56.0	62.4
L24 CO_2 SST_{2000}	-36.0	-47.2	59.9	58.5	61.3	60.3	57.0	64.8
L24 $CO_{2,2050}$ SST_{2050}	-35.9	-47.5	56.5	55.0	58.0	56.9	52.4	61.3
L24 2×O_3 SST_{1870}	-35.4	-46.6	60.2	58.8	61.5	58.3	54.1	62.4
L24 O_3 SST_{1870}	-35.2	-46.2	60.0	58.8	61.3	60.9	57.9	64.2
L24 O_3 SST_{2000}	-35.8	-47.2	57.8	56.4	59.2	60.2	56.1	64.4
L24 -0.4×O_3 SST_{1870}	-35.0	-45.7	58.2	57.2	59.2	60.2	57.0	63.3
L24 SST_{2050}	-35.5	-47.1	57.7	56.4	59.1	55.0	51.5	59.5
L24 SST_{2100}	-35.9	-47.9	57.4	56.0	58.8	53.4	48.2	57.8
L24 SST_{1870}	-35.1	-45.8	58.9	58.2	59.4	61.0	59.8	62.3
L24 SST_{2000}	-35.6	-46.7	59.2	58.1	60.3	55.8	52.5	59.4
CM2.1 control	-35.1	-46.3	56.0	55.6	56.5	62.4	61.1	63.7
CCSM4 control	-37.0	-49.1	53.5	52.1	54.8	51.3	47.9	54.6
CAM3 control	-36.2	-47.9	58.8	57.2	60.5	57.8	52.2	70.0
CCSM3 control	-35.3	-47.2	58.9	57.6	60.3	61.9	58.9	65.7
NNR	-35.0	-47.5	51.6	46.4	57.6	54.9	-	-
ERA40	-34.7	-47.4	39.9	34.0	47.7	13.9	-	-
ERA-Interim	-36.4	-48.6	52.3	44.8	63.6	44.4	-	-
C20R	-34.9	-47.2	54.4	51.5	57.6	38.7	-	-

Table 11 cont.

Experiment	$\overline{HC}$	$\overline{FCC}$	interannual FCC:HC slope median	2.5%	97.5%	decadal FCC:HC slope median	2.5%	97.5%
L48 0.5×CO_2 SST_{1870}	-34.0	-44.4	58.6	57.3	59.9	61.4	58.3	65.0
L48 2×CO_2 SST_{2100}	-36.0	-47.9	57.6	56.1	58.9	52.6	49.1	55.8
L48 2×CO_2 SST_{1870}	-35.0	-45.7	60.3	59.1	61.4	64.1	61.5	66.3
L48 4×CO_2 SST_{1870}	-35.3	-46.0	59.7	58.9	60.6	60.1	58.0	62.3
L48 CO_2 O_3 SST_{2050}	-35.4	-47.2	58.5	57.2	59.7	55.3	49.4	60.7
L48 CO_2 O_3 SST_{1870}	-34.9	-45.8	61.6	60.3	62.8	64.6	62.0	67.3
L48 CO_2 O_3 SST_{2000}	-35.3	-46.6	60.4	59.1	61.7	60.5	56.3	64.2
L48 CO_2 SST_{1870}	-34.7	-45.2	59.4	58.2	60.6	59.8	56.7	62.7
L48 CO_2 SST_{2000}	-35.1	-46.1	60.3	59.1	61.5	62.7	58.6	67.3
L48 $CO_{2,2050}$ SST_{2050}	-35.3	-46.9	57.4	55.9	58.8	57.2	53.6	61.1
L48 2×O_3 SST_{1870}	-34.8	-45.9	60.6	59.4	61.9	60.3	57.2	62.7
L48 O_3 SST_{1870}	-34.6	-45.4	60.3	59.0	61.4	63.1	59.9	66.5
L48 O_3 SST_{2000}	-35.1	-46.3	61.0	59.8	62.1	64.8	62.1	67.4
L48 -0.4×O_3 SST_{1870}	-34.3	-44.7	58.8	57.6	60.1	57.3	54.6	60.1
L48 SST_{2050}	-35.0	-46.3	58.5	57.1	59.9	62.5	59.3	65.1
L48 SST_{2100}	-35.4	-47.1	59.9	58.3	61.2	60.5	56.5	63.7
L48 SST_{1870}	-34.4	-44.9	59.8	59.3	60.3	63.4	61.9	64.9
L48 SST_{2000}	-34.9	-45.7	59.4	58.3	60.5	63.8	60.7	67.2

Table 12: SH MAM interannual and decadal ratios

Experiment	$\overline{HC}$	$\overline{FCC}$	interannual FCC:HC slope median	2.5%	97.5%	decadal FCC:HC slope median	2.5%	97.5%
L24 0.5×CO_2 SST_{1870}	-32.7	-46.3	63.8	61.6	65.9	70.8	62.0	80.9
L24 2×CO_2 SST_{2100}	-34.2	-48.5	63.7	60.7	66.9	63.4	53.9	71.9
L24 2×CO_2 SST_{1870}	-33.2	-47.1	63.6	59.8	67.0	72.4	63.4	84.3
L24 4×CO_2 SST_{1870}	-33.3	-47.4	69.4	66.7	72.0	64.0	58.9	70.8
L24 CO_2 O_3 SST_{2050}	-33.6	-47.8	61.3	58.5	63.9	48.3	32.4	63.2
L24 CO_2 O_3 SST_{1870}	-33.0	-46.9	61.1	58.7	63.5	61.6	57.4	67.0
L24 CO_2 O_3 SST_{2000}	-33.7	-47.7	60.4	57.9	62.9	56.9	48.2	64.5
L24 CO_2 SST_{1870}	-33.0	-46.8	63.8	61.4	65.9	54.9	47.0	64.1
L24 CO_2 SST_{2000}	-33.7	-47.7	59.4	56.4	62.2	61.8	50.7	68.9
L24 $CO_{2,2050}$ SST_{2050}	-33.6	-47.9	63.9	61.5	66.5	61.0	52.7	71.0
L24 2×O_3 SST_{1870}	-32.9	-46.6	64.5	61.9	67.2	63.4	56.8	70.6
L24 O_3 SST_{1870}	-32.9	-46.7	63.6	61.3	65.9	63.8	58.2	69.1
L24 O_3 SST_{2000}	-33.6	-47.5	59.5	56.8	62.1	56.5	50.0	63.0
L24 -0.4×O_3 SST_{1870}	-32.8	-46.5	63.2	60.5	65.7	59.3	54.0	64.8
L24 SST_{2050}	-33.5	-47.6	61.7	59.2	64.0	53.0	43.7	64.1
L24 SST_{2100}	-34.0	-48.2	63.6	61.1	66.3	62.5	57.1	69.3
L24 SST_{1870}	-32.8	-46.6	64.6	63.6	65.7	65.7	63.2	68.4
L24 SST_{2000}	-33.6	-47.5	59.4	57.0	61.7	51.0	35.5	68.5
CM2.1 control	-33.0	-46.8	61.2	60.5	61.9	64.5	62.2	66.9
CCSM4 control	-35.4	-50.1	46.4	44.1	49.0	46.1	37.6	52.6
CAM3 control	-33.9	-47.7	60.3	55.7	64.9	53.4	36.7	63.9
CCSM3 control	-33.9	-47.9	60.3	57.6	63.1	66.2	57.5	74.8
NNR	-33.0	-47.7	51.4	44.3	58.4	52.8	-	-
ERA40	-33.0	-47.9	48.8	43.9	54.3	29.2	-	-
ERA-Interim	-33.8	-48.6	46.8	36.4	61.3	35.2	-	-
C20R	-33.2	-47.9	51.1	46.7	56.2	36.6	-	-

Table 12 cont.

Experiment	$\overline{HC}$	$\overline{FCC}$	interannual FCC:HC slope median	2.5%	97.5%	decadal FCC:HC slope median	2.5%	97.5%
L48 0.5×CO_2 SST_{1870}	-32.1	-45.3	64.3	62.0	66.5	65.4	58.6	73.0
L48 2×CO_2 SST_{2100}	-33.9	-48.1	59.2	57.1	61.3	50.4	43.6	59.0
L48 2×CO_2 SST_{1870}	-32.6	-46.2	64.3	62.3	66.3	61.1	55.8	67.8
L48 4×CO_2 SST_{1870}	-32.8	-46.5	61.2	59.6	63.1	62.5	57.9	67.0
L48 CO_2 O_3 SST_{2050}	-33.2	-47.3	63.4	61.3	65.5	59.4	51.0	64.1
L48 CO_2 O_3 SST_{1870}	-32.4	-45.9	63.6	61.5	65.7	67.7	61.7	73.4
L48 CO_2 O_3 SST_{2000}	-33.3	-47.0	61.5	59.3	63.4	57.1	50.5	64.1
L48 CO_2 SST_{1870}	-32.4	-46.0	62.4	60.5	64.1	62.2	56.0	68.4
L48 CO_2 SST_{2000}	-33.2	-46.8	60.9	58.9	63.2	64.2	57.6	69.7
L48 $CO_{2,2050}$ SST_{2050}	-33.2	-47.3	61.9	59.3	64.2	51.5	43.7	58.5
L48 2×O_3 SST_{1870}	-32.3	-45.8	66.8	64.3	69.3	68.3	61.1	77.5
L48 O_3 SST_{1870}	-32.3	-45.8	63.9	62.0	65.9	62.6	55.6	69.5
L48 O_3 SST_{2000}	-33.2	-46.7	59.8	57.5	62.2	57.3	50.2	65.0
L48 -0.4×O_3 SST_{1870}	-32.3	-45.7	64.9	62.9	66.9	66.4	59.9	72.0
L48 SST_{2050}	-33.0	-47.0	62.1	60.2	64.1	61.6	54.3	67.4
L48 SST_{2100}	-33.6	-47.7	61.7	59.3	64.0	53.8	45.7	62.7
L48 SST_{1870}	-32.3	-45.7	63.8	62.8	64.8	61.4	57.9	64.6
L48 SST_{2000}	-33.0	-46.7	61.5	59.3	63.5	65.5	59.3	71.7

Table 13: SH JJA interannual and decadal ratios

Experiment	$\overline{HC}$	$\overline{FCC}$	interannual FCC:HC slope median	2.5%	97.5%	decadal FCC:HC slope median	2.5%	97.5%
L24 0.5×CO_2 SST_{1870}	-28.4	-43.5	76.6	75.0	78.1	81.5	76.2	87.0
L24 2×CO_2 SST_{2100}	-30.0	-45.4	77.9	75.7	79.9	75.5	65.2	85.1
L24 2×CO_2 SST_{1870}	-28.8	-44.6	80.8	79.2	82.5	77.3	72.1	82.2
L24 4×CO_2 SST_{1870}	-29.0	-44.9	77.6	75.5	79.3	82.6	79.0	86.6
L24 CO_2 O_3 SST_{2050}	-29.3	-44.7	79.9	78.0	82.0	72.8	66.7	78.0
L24 CO_2 O_3 SST_{1870}	-28.6	-44.1	80.6	78.8	82.4	77.1	69.5	83.2
L24 CO_2 O_3 SST_{2000}	-29.0	-44.6	80.5	78.3	82.7	73.5	68.8	79.6
L24 CO_2 SST_{1870}	-28.6	-44.3	81.2	79.6	82.9	73.8	70.8	77.9
L24 CO_2 SST_{2000}	-29.0	-44.6	80.2	78.5	82.0	81.3	75.7	86.8
L24 $CO_{2,2050}$ SST_{2050}	-29.4	-44.9	80.0	78.0	82.1	70.6	64.5	76.7
L24 2×O_3 SST_{1870}	-28.5	-43.9	80.2	78.5	81.9	79.4	74.2	84.5
L24 O_3 SST_{1870}	-28.6	-43.9	80.3	78.9	81.7	76.8	72.6	82.1
L24 O_3 SST_{2000}	-29.0	-44.3	78.8	77.0	80.6	83.7	73.2	88.4
L24 -0.4×O_3 SST_{1870}	-28.5	-44.0	79.1	77.7	80.6	78.8	73.0	84.1
L24 SST_{2050}	-29.2	-44.5	82.0	80.2	83.9	80.0	75.3	85.1
L24 SST_{2100}	-29.7	-45.0	77.4	75.7	79.2	85.7	-88.7	88.9
L24 SST_{1870}	-28.5	-44.0	80.1	79.4	80.9	79.5	77.0	81.7
L24 SST_{2000}	-28.9	-44.4	77.9	76.2	79.7	74.6	68.8	80.1
CM2.1 control	-28.4	-43.3	79.2	78.6	79.8	79.4	77.6	81.3
CCSM4 control	-29.6	-45.8	75.0	73.3	76.6	71.4	63.9	78.8
CAM3 control	-29.0	-43.7	68.9	64.7	72.2	68.1	27.6	76.0
CCSM3 control	-29.1	-45.1	73.0	69.7	76.2	48.4	29.0	63.3
NNR	-28.2	-43.6	73.3	67.0	78.4	68.4	-	-
ERA40	-28.6	-44.3	64.9	49.6	78.2	41.9	-	-
ERA-Interim	-28.9	-44.8	75.4	66.6	84.7	25.3	-	-
C20R	-28.4	-43.9	68.9	64.6	73.1	50.3	-	-

Table 13 cont.

Experiment	$\overline{HC}$	$\overline{FCC}$	interannual FCC:HC slope median	2.5%	97.5%	decadal FCC:HC slope median	2.5%	97.5%
L48 0.5×CO_2 SST_{1870}	-28.8	-43.3	80.0	78.7	81.2	76.3	71.7	81.1
L48 2×CO_2 SST_{2100}	-30.5	-45.7	73.6	71.6	75.6	73.5	68.6	79.6
L48 2×CO_2 SST_{1870}	-29.1	-44.1	78.7	77.3	80.1	76.4	71.3	80.8
L48 4×CO_2 SST_{1870}	-29.2	-44.6	78.5	77.4	79.7	76.3	72.8	79.9
L48 CO_2 O_3 SST_{2050}	-29.6	-44.5	77.9	76.0	79.7	75.3	68.2	82.2
L48 CO_2 O_3 SST_{1870}	-28.9	-43.8	79.9	78.3	81.2	81.8	78.3	85.3
L48 CO_2 O_3 SST_{2000}	-29.2	-44.1	78.9	77.5	80.5	78.9	74.6	83.0
L48 CO_2 SST_{1870}	-28.9	-43.7	79.6	77.8	81.2	78.4	71.4	84.3
L48 CO_2 SST_{2000}	-29.2	-44.2	78.3	76.8	80.0	69.3	62.5	76.5
L48 $CO_{2,2050}$ SST_{2050}	-29.7	-44.6	77.7	75.8	79.7	72.7	63.9	80.8
L48 2×O_3 SST_{1870}	-28.9	-43.5	79.6	78.2	80.9	77.7	72.3	82.7
L48 O_3 SST_{1870}	-28.9	-43.6	80.3	78.7	81.8	78.0	73.7	82.3
L48 O_3 SST_{2000}	-29.1	-44.0	77.4	75.4	79.2	79.1	74.8	82.3
L48 -0.4×O_3 SST_{1870}	-28.9	-43.7	79.0	77.4	80.7	79.0	75.9	82.1
L48 SST_{2050}	-29.5	-44.3	77.5	75.4	79.5	73.5	68.2	79.9
L48 SST_{2100}	-30.0	-45.1	74.6	72.9	76.3	72.3	66.2	77.1
L48 SST_{1870}	-28.9	-43.6	80.0	79.4	80.7	79.2	76.9	81.1
L48 SST_{2000}	-29.1	-44.0	78.5	76.2	80.5	77.4	72.2	82.5

Table 14: SH SON interannual and decadal ratios

Experiment	$\overline{HC}$	$\overline{FCC}$	interannual FCC:HC slope median	2.5%	97.5%	decadal FCC:HC slope median	2.5%	97.5%
L24 0.5×CO_2 SST_{1870}	-30.4	-45.5	70.1	68.4	71.8	62.3	56.5	69.9
L24 2×CO_2 SST_{2100}	-32.0	-47.5	69.3	66.8	71.9	68.5	63.2	73.1
L24 2×CO_2 SST_{1870}	-31.1	-46.5	72.6	70.6	74.7	71.2	65.5	77.3
L24 4×CO_2 SST_{1870}	-31.3	-46.7	70.7	68.9	72.7	67.3	55.2	79.3
L24 CO_2 O_3 SST_{2050}	-31.6	-46.8	69.2	67.2	71.3	71.9	57.9	83.5
L24 CO_2 O_3 SST_{1870}	-30.9	-46.3	70.0	68.0	71.9	67.9	60.6	76.1
L24 CO_2 O_3 SST_{2000}	-31.2	-46.5	69.5	67.5	71.3	69.8	60.8	78.3
L24 CO_2 SST_{1870}	-30.9	-46.1	72.0	70.3	73.6	68.5	64.1	73.6
L24 CO_2 SST_{2000}	-31.3	-46.5	69.7	67.9	71.2	71.0	63.9	76.1
L24 $CO_{2,2050}$ SST_{2050}	-31.5	-46.7	69.8	67.8	71.8	68.4	54.7	77.5
L24 2×O_3 SST_{1870}	-30.8	-46.2	70.3	68.4	72.0	71.2	66.1	75.3
L24 O_3 SST_{1870}	-30.7	-46.0	72.0	70.5	73.5	71.4	67.0	76.4
L24 O_3 SST_{2000}	-31.1	-46.4	71.1	69.4	72.9	69.9	63.3	77.2
L24 -0.4×O_3 SST_{1870}	-30.7	-45.8	72.4	70.6	74.0	73.7	67.4	80.8
L24 SST_{2050}	-31.4	-46.5	68.3	66.5	70.1	68.1	61.5	75.5
L24 SST_{2100}	-31.8	-47.0	70.6	68.8	72.6	63.9	54.2	74.6
L24 SST_{1870}	-30.7	-45.9	70.9	70.1	71.7	71.4	68.9	73.7
L24 SST_{2000}	-31.1	-46.1	69.7	68.1	71.1	69.6	63.2	76.7
CM2.1 control	-30.8	-45.6	62.2	61.2	63.1	65.9	63.5	68.3
CCSM4 control	-31.9	-47.3	62.7	61.1	64.2	63.7	58.0	72.2
CAM3 control	-31.1	-46.2	63.7	59.8	67.1	72.6	-68.0	85.8
CCSM3 control	-30.7	-46.2	62.2	59.3	65.1	60.3	50.2	66.8
NNR	-29.7	-46.4	60.7	55.5	66.8	52.1	-	-
ERA40	-29.8	-46.6	43.6	27.7	66.5	29.3	-	-
ERA-Interim	-31.1	-47.3	61.7	44.5	75.6	71.4	-	-
C20R	-30.2	-46.1	56.6	51.7	60.6	52.2	-	-

Table 14 cont.

Experiment	$\overline{HC}$	$\overline{FCC}$	interannual FCC:HC slope median	2.5%	97.5%	decadal FCC:HC slope median	2.5%	97.5%
L48 0.5×CO_2 SST_{1870}	-30.5	-45.2	73.0	71.4	74.7	74.6	67.4	81.4
L48 2×CO_2 SST_{2100}	-32.0	-47.6	67.7	65.7	69.7	68.2	62.3	75.9
L48 2×CO_2 SST_{1870}	-31.0	-46.1	72.2	70.3	73.9	68.9	65.4	71.8
L48 4×CO_2 SST_{1870}	-31.1	-46.4	70.7	69.3	72.0	69.7	67.1	72.4
L48 CO_2 O_3 SST_{2050}	-31.3	-46.7	68.3	66.7	70.0	67.0	60.7	73.6
L48 CO_2 O_3 SST_{1870}	-30.8	-45.9	71.5	69.8	73.1	69.0	63.3	75.6
L48 CO_2 O_3 SST_{2000}	-31.1	-46.2	70.4	68.7	72.0	68.7	63.9	72.7
L48 CO_2 SST_{1870}	-30.8	-45.7	71.8	70.2	73.3	74.8	70.2	79.5
L48 CO_2 SST_{2000}	-31.0	-46.0	69.0	67.3	70.9	69.1	63.2	74.0
L48 $CO_{2,2050}$ SST_{2050}	-31.3	-46.7	70.8	68.8	72.6	61.0	52.3	68.0
L48 2×O_3 SST_{1870}	-30.8	-45.9	73.5	72.2	75.0	72.1	68.1	75.5
L48 O_3 SST_{1870}	-30.7	-45.7	70.8	69.0	72.5	70.6	65.9	75.8
L48 O_3 SST_{2000}	-31.0	-46.0	71.8	70.1	73.7	73.5	69.4	77.2
L48 -0.4×O_3 SST_{1870}	-30.7	-45.5	72.6	71.1	74.1	71.6	67.7	75.3
L48 SST_{2050}	-31.1	-46.4	72.5	70.5	74.3	74.6	71.4	78.2
L48 SST_{2100}	-31.6	-47.0	69.1	67.1	70.7	63.3	56.0	69.6
L48 SST_{1870}	-30.7	-45.6	71.7	71.0	72.4	71.8	69.7	74.0
L48 SST_{2000}	-30.9	-45.7	71.0	69.6	72.3	73.4	68.2	77.9

Table 15: CM2.1 daily FCC:HC ratios

Hemi	Season	Median	2.5%	97.5%
NH	DJF	63.834	60.818	67.003
	MAM	60.661	57.794	63.647
	JJA	41.488	37.468	45.467
	SON	43.502	40.056	46.667
SH	DJF	35.548	32.330	38.715
	MAM	42.683	39.599	45.913
	JJA	65.358	62.245	68.649
	SON	44.562	41.763	47.444

Table 16: AM2.1 daily FCC:HC ratios

Hemi	Season	Median	2.5%	97.5%
NH	DJF	70.0	65.9	74.1
	MAM	61.8	58.3	65.8
	JJA	42.3	39.8	44.7
	SON	44.0	41.2	46.9
SH	DJF	27.0	17.3	44.9
	MAM	54.3	50.8	58.0
	JJA	66.9	64.2	69.7
	SON	55.4	50.8	60.1

REFERENCES

Abatzoglou, J. T., and G. Magnusdottir, 2006: Planetary wave breaking and nonlinear reflection: Seasonal cycle and interannual variability. *J. Climate*, **19 (23)**, 6139–6152, URL http://dx.doi.org/10.1175/JCLI3968.1.

Alexander, M. J. et al., 2010: Recent developments in gravity-wave effects in climate models and the global distribution of gravity-wave momentum flux from observations and models. *Q.J.R. Meteorol. Soc.*, **136 (650)**, 1103–1124, URL http://dx.doi.org/10.1002/qj.637.

Allen, M. R., and W. J. Ingram, 2002: Constraints on future changes in climate and the hydrologic cycle. *Nature*, **419 (6903)**, 224–232, URL http://dx.doi.org/10.1038/nature01092.

Allen, R., and S. Sherwood, 2011: The impact of natural versus anthropogenic aerosols on atmospheric circulation in the Community Atmosphere Model. *Climate Dynamics*, **36 (9)**, 1959–1978, URL http://dx.doi.org/10.1007/s00382-010-0898-8.

Anderson, B. T. et al., 2004: The new GFDL global atmosphere and land model AM2-LM2: Evaluation with prescribed SST simulations. *J. Climate*, **17 (24)**, 4641–4673, doi: 10.1175/JCLI-3223.1, URL http://dx.doi.org/10.1175/JCLI-3223.1.

Arblaster, J. M., and G. A. Meehl, 2006: Contributions of external forcings to southern annular mode trends. *J. Climate*, **19 (12)**, 2896–2905, URL http://dx.doi.org/10.1175/JCLI3774.1.

Archer, C. L., and K. Caldeira, 2008: Historical trends in the jet streams. *Geophys. Res. Lett.*, **35 (8)**, L08 803, URL http://dx.doi.org/10.1029/2008GL033614.

Austin, J., J. Wilson, F. Li, and H. Vömel, 2007: Evolution of water vapor concentrations and stratospheric age of air in coupled chemistry-climate model simulations. *J. Atmos. Sci.*, **64 (3)**, 905–921, URL http://dx.doi.org/10.1175/JAS3866.1.

Baldwin, M. P., and D. W. Thompson, 2009: A critical comparison of stratosphere-troposphere coupling indices. *Q.J.R. Meteorol. Soc.*, **135 (644)**, 1661–1672, URL http://dx.doi.org/10.1002/qj.479.

Barnes, E. A., and D. L. Hartmann, 2011: Rossby wave scales, propagation, and the variability of eddy-driven jets. *J. Atmos. Sci.*, **68 (12)**, 2893–2908, URL http://dx.doi.org/10.1175/JAS-D-11-039.1.

Biasutti, M., and A. H. Sobel, 2009: Delayed sahel rainfall and global seasonal cycle in a warmer climate. *Geophys. Res. Lett.*, **36 (23)**, L23 707, URL http://dx.doi.org/10.1029/2009GL041303.

Bordoni, S., and T. Schneider, 2009: Regime transitions of steady and time-dependent Hadley circulations: Comparison of axisymmetric and eddy-permitting simulations. *J. Atmos. Sci.*, **67 (5)**, 1643–1654, URL http://dx.doi.org/10.1175/2009JAS3294.1.

Chang, E. K. M., 1995: The influence of hadley circulation intensity changes on extratropical climate in an idealized model. *J. Atmos. Sci.*, **52 (11)**, 2006–2024, URL http://dx.doi.org/10.1175/1520-0469(1995)052<2006:TIOHCI>2.0.CO;2.

Chang, E. K. M., 1998: Poleward-propagating angular momentum perturbations induced by zonally symmetric heat sources in the tropics. *J. Atmos. Sci.*, **55 (12)**, 2229–2248, URL http://dx.doi.org/10.1175/1520-0469(1998)055<2229:PPAMPI>2.0.CO;2.

Chen, G., and I. M. Held, 2007: Phase speed spectra and the recent poleward shift of Southern Hemisphere surface westerlies. *Geophys. Res. Lett.*, **34 (21)**, L21 805, URL http://dx.doi.org/10.1029/2007GL031200.

Chen, G., J. Lu, and D. M. W. Frierson, 2008: Phase speed spectra and the latitude of surface westerlies: Interannual variability and global warming trend. *J. Climate*, **21 (22)**, 5942–5959, URL http://dx.doi.org/10.1175/2008JCLI2306.1.

Chen, G., J. Lu, and L. Sun, 2012: Delineating the eddy-zonal flow interaction in the atmospheric circulation response to climate forcing: Uniform sst warming. *J. Atmos. Sci.*, **(accepted)**, URL wxmaps.org/jianlu/Chen_Lu_Sun.aqua_transient.2012.pdf.

Chiang, J., and C. Bitz, 2005: Influence of high latitude ice cover on the marine intertropical convergence zone. *Climate Dynamics*, **25 (5)**, 477–496, URL http://dx.doi.org/10.1007/s00382-005-0040-5.

Cionni, I. et al., 2011: Ozone database in support of cmip5 simulations: results and corresponding radiative forcing. *Atmos. Chem. Phys.*, **11 (21)**, 11 267–11 292, URL http://www.atmos-chem-phys.net/11/11267/2011/.

Clement, A., P. DiNezio, and C. Deser, 2011: Rethinking the oceans role in the southern oscillation. *J. Climate*, **24 (15)**, 4056–4072, URL http://dx.doi.org/10.1175/2011JCLI3973.1.

Collins, W. D. et al., 2006: The Community Climate System Model version 3 (ccsm3). *J. Climate*, **19 (11)**, 2122–2143, URL http://dx.doi.org/10.1175/JCLI3761.1.

Compo, G. P. et al., 2011: The Twentieth Century Reanalysis Project. *Q.J.R. Meteorol. Soc.*, **137 (654)**, 1–28, URL http://dx.doi.org/10.1002/qj.776.

Dee, D. P., and S. Uppala, 2009: Variational bias correction of satellite radiance data in the era-interim reanalysis. *Q.J.R. Meteorol. Soc.*, **135 (644)**, 1830–1841, URL http://dx.doi.org/10.1002/qj.493.

Delworth, T. L. et al., 2006: GFDL's CM2 global coupled climate models. Part I: Formulation and simulation characteristics. *J. Climate*, **19 (5)**, 643–674, URL http://dx.doi.org/10.1175/JCLI3629.1.

Deser, C., A. Phillips, V. Bourdette, and H. Teng, 2012: Uncertainty in climate change projections: the role of internal variability. *Clim. Dynam.*, **38 (3-4)**, 527–546, URL http://dx.doi.org/10.1007/s00382-010-0977-x.

Deser, C., and A. S. Phillips, 2009: Atmospheric circulation trends, 19502000: The relative roles of sea surface temperature forcing and direct atmospheric radiative forcing. *J. Climate*, **22 (2)**, 396–413, URL http://dx.doi.org/10.1175/2008JCLI2453.1.

Deser, C., R. Tomas, M. Alexander, and D. Lawrence, 2010: The seasonal atmospheric response to projected arctic sea ice loss in the late twenty-first century. *J. Climate*, **23 (2)**, 333–351, URL http://dx.doi.org/10.1175/2009JCLI3053.1.

Frierson, D. M. W., and Y.-T. Hwang, 2012: Extratropical influence on ITCZ shifts in slab ocean simulations of global warming. *J. Climate*, **25 (2)**, 720–733, URL http://dx.doi.org/10.1175/JCLI-D-11-00116.1.

Fu, Q., C. M. Johanson, J. M. Wallace, and T. Reichler, 2006: Enhanced mid-latitude tropospheric warming in satellite measurements. *Science*, **312 (5777)**, 1179–1179, URL http://www.sciencemag.org/content/312/5777/1179.abstract.

Fyfe, J. C., G. J. Boer, and G. M. Flato, 1999: The Arctic and Antarctic oscillations and their projected changes under global warming. *Geophys. Res. Lett.*, **26 (11)**, 1601–1604, URL http://dx.doi.org/10.1029/1999GL900317.

Gent, P. R. et al., 2011: The Community Climate System Model version 4. *J. Climate*, **24 (19)**, 4973–4991, URL http://dx.doi.org/10.1175/2011JCLI4083.1.

Geophysical Fluid Dynamics Laboratory, 2012: Flexible modeling system web site. National Oceanographic and Atmospheric Administration, URL http://www.gfdl.noaa.

gov/fms, retrieved on 2012.02.16, URL http://www.gfdl.noaa.gov/fms, retrieved on 2012.02.16.

Gerber, E. P., and L. M. Polvani, 2009: Stratospheretroposphere coupling in a relatively simple AGCM: The importance of stratospheric variability. *J. Climate*, **22 (8)**, 1920–1933, URL http://dx.doi.org/10.1175/2008JCLI2548.1.

Gerber, E. P., and G. K. Vallis, 2007: Eddyzonal flow interactions and the persistence of the zonal index. *J. Atmos. Sci.*, **64 (9)**, 3296–3311, URL http://dx.doi.org/10.1175/JAS4006.1.

Gillett, N. P., M. R. Allen, and K. D. Williams, 2002: The role of stratospheric resolution in simulating the Arctic Oscillation response to greenhouse gases. *Geophys. Res. Lett.*, **29 (10)**, 1500, URL http://dx.doi.org/10.1029/2001GL014444.

Gillett, N. P., J. F. Scinocca, D. A. Plummer, and M. C. Reader, 2009: Sensitivity of climate to dynamically-consistent zonal asymmetries in ozone. *Geophys. Res. Lett.*, **36 (10)**, L10 809, URL http://dx.doi.org/10.1029/2009GL037246.

Gillett, N. P., and D. W. J. Thompson, 2003: Simulation of recent southern hemisphere climate change. *Science*, **302 (5643)**, 273–275, URL http://www.sciencemag.org/content/302/5643/273.abstract.

Gnanadesikan, A. et al., 2006: GFDL's CM2 global coupled climate models. Part II: The baseline ocean simulation. *J. Climate*, **19 (5)**, 675–697, URL http://dx.doi.org/10.1175/JCLI3630.1.

Haynes, P. H., M. E. McIntyre, T. G. Shepherd, C. J. Marks, and K. P. Shine, 1991: On the downward control of extratropical diabatic circulations by eddy-induced mean zonal forces. *J. Atmos. Sci.*, **48 (4)**, 651–678, URL http://dx.doi.org/10.1175/1520-0469(1991)048<0651:OTCOED>2.0.CO;2.

Held, I. M., 2000: The general circulation of the atmosphere. *The General Circulation of the Atmosphere: 2000 Program in Geophysical Fluid Dynamics, Tech. Rep. WHOI-2001-03*, Woods Hole, Mass, Woods Hole Oceanogr. Inst., 1–54, URL http://hdl.handle.net/1912/15.

Held, I. M., 2005: The gap between simulation and understanding in climate modeling. *Bull. Amer. Meteor. Soc.*, **86 (11)**, 1609–1614, URL http://dx.doi.org/10.1175/BAMS-86-11-1609.

Held, I. M., and A. Y. Hou, 1980: Nonlinear axially symmetric circulations in a nearly inviscid atmosphere. *J. Atmos. Sci.*, **37 (3)**, 515–533, URL http://dx.doi.org/10.1175/1520-0469(1980)037<0515:NASCIA>2.0.CO;2.

Held, I. M., and B. J. Soden, 2000: Water vapor feedback and global warming. *Annu. Rev. Energy. Environ.*, **25 (1)**, 441–475, URL http://dx.doi.org/10.1146/annurev.energy.25.1.441.

Held, I. M., and B. J. Soden, 2006: Robust responses of the hydrological cycle to global warming. *J. Climate*, **19 (21)**, 5686–5699, URL http://dx.doi.org/10.1175/JCLI3990.1.

Horowitz, L. W. et al., 2003: A global simulation of tropospheric ozone and related tracers: Description and evaluation of mozart, version 2. *J. Geophys. Res.*, **108 (D24)**, 4784, URL http://dx.doi.org/10.1029/2002JD002853.

Hu, Y., and Q. Fu, 2007: Observed poleward expansion of the hadley circulation since 1979. *Atmos. Chem. Phys.*, **7 (19)**, 5229–5236, URL http://www.atmos-chem-phys.net/7/5229/2007/.

Hu, Y., C. Zhou, and J. Liu, 2011: Observational evidence for poleward expansion of the Hadley circulation. *Adv. Atmos. Sci.*, **28 (1)**, 33–44, URL http://dx.doi.org/10.1007/s00376-010-0032-1.

Hudson, R. D., M. F. Andrade, M. B. Follette, and A. D. Frolov, 2006: The total ozone field separated into meteorological regimes – part II: Northern hemisphere mid-latitude total ozone trends. *Atmos. Chem. Phys.*, **6 (12)**, 5183–5191, URL http://www.atmos-chem-phys.net/6/5183/2006/.

Jeffreys, H., 1926: On the dynamics of ceostrophic winds. *Q.J.R. Meteorol. Soc.*, **52 (217)**, 85–104, URL http://dx.doi.org/10.1002/qj.49705221708.

Johanson, C. M., and Q. Fu, 2009: Hadley cell widening: Model simulations versus observations. *J. Climate*, **22 (10)**, 2713–2725, URL http://dx.doi.org/10.1175/2008JCLI2620.1.

Kalnay, E. et al., 1996: The NCEP/NCAR 40-year Reanalysis Project. *Bull. Amer. Meteor. Soc.*, **77 (3)**, 437–471, URL http://dx.doi.org/10.1175/1520-0477(1996)077<0437:TNYRP>2.0.CO;2.

Kang, S. M., D. M. W. Frierson, and I. M. Held, 2009: The tropical response to extratropical thermal forcing in an idealized GCM: The importance of radiative feedbacks and convective parameterization. *J. Atmos. Sci.*, **66 (9)**, 2812–2827, URL http://dx.doi.org/10.1175/2009JAS2924.1.

Kang, S. M., I. M. Held, D. M. W. Frierson, and M. Zhao, 2008: The response of the ITCZ to extratropical thermal forcing: Idealized slab-ocean experiments with a GCM. *J. Climate*, **21 (14)**, 3521–3532, URL http://dx.doi.org/10.1175/2007JCLI2146.1.

Kang, S. M., and J. Lu, 2012: Expansion of the Hadley cell under global warming: winter versus summer. *J. Atmos. Sci.*, doi:10.1175/JCLI-D-12-00323.1, URL http://dx.doi.org/10.1175/JCLI-D-12-00323.1.

Kang, S. M., and L. M. Polvani, 2010: The interannual relationship between the latitude of the eddy-driven jet and the edge of the Hadley cell. *J. Climate*, **24 (2)**, 563–568, URL http://dx.doi.org/10.1175/2010JCLI4077.1.

Kang, S. M., L. M. Polvani, J. C. Fyfe, and M. Sigmond, 2011: Impact of polar ozone depletion on subtropical precipitation. *Science*, **332 (6032)**, 951–954, URL http://www.sciencemag.org/content/332/6032/951.abstract.

Karpechko, A. Y., N. P. Gillett, G. J. Marshall, and A. A. Scaife, 2008: Stratospheric influence on circulation changes in the Southern Hemisphere troposphere in coupled climate models. *Geophys. Res. Lett.*, **35 (20)**, L20 806, URL http://dx.doi.org/10.1029/2008GL035354.

Kidston, J., and E. P. Gerber, 2010: Intermodel variability of the poleward shift of the austral jet stream in the CMIP3 integrations linked to biases in 20th century climatology. *Geophys. Res. Lett.*, **37 (9)**, L09 708, URL http://dx.doi.org/10.1029/2010GL042873.

Kidston, J., and G. K. Vallis, 2010: Relationship between eddy-driven jet latitude and width. *Geophys. Res. Lett.*, **37 (21)**, L21 809, URL http://dx.doi.org/10.1029/2010GL044849.

Kidston, J., G. K. Vallis, S. M. Dean, and J. A. Renwick, 2010: Can the increase in the eddy length scale under global warming cause the poleward shift of the jet streams? *J. Climate*, **24 (14)**, 3764–3780, URL http://dx.doi.org/10.1175/2010JCLI3738.1.

Korty, R. L., and T. Schneider, 2008: Extent of Hadley circulations in dry atmospheres. *Geophys. Res. Lett.*, **35 (23)**, L23 803, URL http://dx.doi.org/10.1029/2008GL035847.

Kunz, T., K. Fraedrich, and F. Lunkeit, 2009: Response of idealized baroclinic wave life cycles to stratospheric flow conditions. *J. Atmos. Sci.*, **66 (8)**, 2288–2302, URL http://dx.doi.org/10.1175/2009JAS2827.1.

Kushner, P. J., I. M. Held, and T. L. Delworth, 2001: Southern hemisphere atmospheric circulation response to global warming. *J. Climate*, **14 (10)**, 2238–2249, URL http://dx.doi.org/10.1175/1520-0442(2001)014<0001:SHACRT>2.0.CO;2.

Kushner, P. J., and L. M. Polvani, 2004: Stratospheretroposphere coupling in a relatively simple agcm: The role of eddies. *J. Climate*, **17 (3)**, 629–639, URL http://dx.doi.org/10.1175/1520-0442(2004)017<0629:SCIARS>2.0.CO;2.

Levine, X. J., and T. Schneider, 2010: Response of the hadley circulation to climate change in an aquaplanet GCM coupled to a simple representation of ocean heat transport. *J. Atmos. Sci.*, **68 (4)**, 769–783, URL http://dx.doi.org/10.1175/2010JAS3553.1.

Liepert, B. G., and M. Previdi, 2009: Do models and observations disagree on the rainfall response to global warming? *J. Climate*, **22 (11)**, 3156–3166, URL http://dx.doi.org/10.1175/2008JCLI2472.1.

Lindzen, R. S., and B. Farrell, 1980: A simple approximate result for the maximum growth rate of baroclinic instabilities. *J. Atmos. Sci.*, **37 (7)**, 1648–1654, URL http://dx.doi.org/10.1175/1520-0469(1980)037<1648:ASARFT>2.0.CO;2.

Lindzen, R. S., and A. V. Hou, 1988: Hadley circulations for zonally averaged heating centered off the equator. *J. Atmos. Sci.*, **45 (17)**, 2416–2427, URL http://dx.doi.org/10.1175/1520-0469(1988)045<2416:HCFZAH>2.0.CO;2.

Lorenz, D. J., and E. T. DeWeaver, 2007: Tropopause height and zonal wind response to global warming in the IPCC scenario integrations. *J. Geophys. Res.*, **112 (D10)**, D10 119, URL http://dx.doi.org/10.1029/2006JD008087.

Lu, J., G. Chen, and D. M. W. Frierson, 2008: Response of the zonal mean atmospheric circulation to El Niño versus global warming. *J. Climate*, **21 (22)**, 5835–5851, URL http://dx.doi.org/10.1175/2008JCLI2200.1.

Lu, J., G. Chen, and D. M. W. Frierson, 2010: The position of the midlatitude storm track and eddy-driven westerlies in aquaplanet AGCMs. *J. Atmos. Sci.*, **67 (12)**, 3984–4000, URL http://dx.doi.org/10.1175/2010JAS3477.1.

Lu, J., G. A. Vecchi, and T. Reichler, 2007: Expansion of the Hadley cell under global warming. *Geophys. Res. Lett.*, **34 (6)**, L06 805, URL http://dx.doi.org/10.1029/2006GL028443.

Mantsis, D. F., and A. C. Clement, 2009: Simulated variability in the mean atmospheric meridional circulation over the 20th century. *Geophys. Res. Lett.*, **36 (6)**, L06 704, URL http://dx.doi.org/10.1029/2008GL036741.

McLandress, C., T. G. Shepherd, J. F. Scinocca, D. A. Plummer, M. Sigmond, A. I. Jonsson, and M. C. Reader, 2010: Separating the dynamical effects of climate change and ozone depletion. Part II: Southern Hemisphere troposphere. *J. Climate*, **24 (6)**, 1850–1868, URL http://dx.doi.org/10.1175/2010JCLI3958.1.

Medeiros, B., B. Stevens, I. M. Held, M. Zhao, D. L. Williamson, J. G. Olson, and C. S. Bretherton, 2008: Aquaplanets, climate sensitivity, and low clouds. *J. Climate*, **21 (19)**, 4974–4991, URL http://dx.doi.org/10.1175/2008JCLI1995.1.

Meehl, G. A., C. Covey, K. E. Taylor, T. Delworth, R. J. Stouffer, M. Latif, B. McAvaney, and J. F. B. Mitchell, 2007: The WCRP CMIP3 multimodel dataset: A new era in climate change research. *Bull. Amer. Meteor. Soc.*, **88 (9)**, 1383–1394, URL http://dx.doi.org/10.1175/BAMS-88-9-1383.

Miller, R. L., G. A. Schmidt, and D. T. Shindell, 2006: Forced annular variations in the 20th century Intergovernmental Panel on Climate Change Fourth Assessment Report models. *J. Geophys. Res.*, **111 (D18)**, D18 101, URL http://dx.doi.org/10.1029/2005JD006323.

Nakamura, N., and A. Solomon, 2010: Finite-amplitude wave activity and mean flow adjustments in the atmospheric general circulation. Part I: Quasigeostrophic theory and analysis. *J. Atmos. Sci.*, **67 (12)**, 3967–3983, URL http://dx.doi.org/10.1175/2010JAS3503.1.

Nakamura, N., and D. Zhu, 2010: Finite-amplitude wave activity and diffusive flux of potential vorticity in eddymean flow interaction. *J. Atmos. Sci.*, **67 (9)**, 2701–2716, URL http://dx.doi.org/10.1175/2010JAS3432.1.

Neale, R. B., J. Richter, S. Park, P. H. Lauritzen, S. J. Vavrus, P. J. Rasch, and M. Zhang, 2011: The mean climate of the Community Atmosphere Model (CAM4) in forced SST and fully coupled experiments. *J. Climate*, **(In preparation)**, URL http://www.cesm.ucar.edu/publications/jclim10/docs/neale.ccsm4.cam4overview.pdf.

Orlanski, I., 2003: Bifurcation in eddy life cycles: Implications for storm track variability. *J. Atmos. Sci.*, **60 (8)**, 993–1023, URL http://dx.doi.org/10.1175/1520-0469(2003)60<993:BIELCI>2.0.CO;2.

Orlanski, I., 2005: A new look at the pacific storm track variability: Sensitivity to tropical ssts and to upstream seeding. *J. Atmos. Sci.*, **62 (5)**, 1367–1390, URL http://dx.doi.org/10.1175/JAS3428.1.

Perlwitz, J., 2011: Atmospheric science: Tug of war on the jet stream. *Nature Clim. Change*, **1 (1)**, 29–31, URL http://dx.doi.org/10.1038/nclimate1065.

Perlwitz, J., S. Pawson, R. L. Fogt, J. E. Nielsen, and W. D. Neff, 2008: Impact of stratospheric ozone hole recovery on Antarctic climate. *Geophys. Res. Lett.*, **35 (8)**, L08 714, URL http://dx.doi.org/10.1029/2008GL033317.

Phillips, N. A., 1954: Energy transformations and meridional circulations associated with simple baroclinic waves in a two-level, quasi-geostrophic model1. *Tellus*, **6 (3)**, 273–286, URL http://dx.doi.org/10.1111/j.2153-3490.1954.tb01123.x.

Pierrehumbert, R. T., 1986: An essay on the parameterization of orographic gravity wave drag. *Proc. ECMWF 1986 Seminar, Vol. I*, Reading, United Kingdom, ECMWF, 251282.

Polvani, L. M., and P. J. Kushner, 2002: Tropospheric response to stratospheric perturbations in a relatively simple general circulation model. *Geophys. Res. Lett.*, **29 (7)**, 1114, URL http://dx.doi.org/10.1029/2001GL014284.

Polvani, L. M., M. Previdi, and C. Deser, 2011a: Large cancellation, due to ozone recovery, of future Southern Hemisphere atmospheric circulation trends. *Geophys. Res. Lett.*, **38 (4)**, L04 707, URL http://dx.doi.org/10.1029/2011GL046712.

Polvani, L. M., D. W. Waugh, G. J. P. Correa, and S.-W. Son, 2011b: Stratospheric ozone depletion: The main driver of twentieth-century atmospheric circulation changes in the Southern Hemisphere. *J. Climate*, **24 (3)**, 795–812, URL http://dx.doi.org/10.1175/2010JCLI3772.1.

Previdi, M., and B. G. Liepert, 2007: Annular modes and Hadley cell expansion under global warming. *Geophys. Res. Lett.*, **34 (22)**, L22 701, URL http://dx.doi.org/10.1029/2007GL031243.

Previdi, M., and B. G. Liepert, 2008: Interdecadal variability of rainfall on a warming planet. *Eos Trans. AGU*, **89 (21)**, URL http://dx.doi.org/10.1029/2008EO210002.

Randel, W. J., and I. M. Held, 1991: Phase speed spectra of transient eddy fluxes and critical layer absorption. *J. Atmos. Sci.*, **48 (5)**, 688–697, URL http://dx.doi.org/10.1175/1520-0469(1991)048<0688:PSSOTE>2.0.CO;2.

Randel, W. J., and F. Wu, 2007: A stratospheric ozone profile data set for 1979-2005: Variability, trends, and comparisons with column ozone data. *J. Geophys. Res.*, **112 (D6)**, D06 313, URL http://dx.doi.org/10.1029/2006JD007339.

Reichler, T., 2009: Chapter 7 - Changes in the Atmospheric Circulation as Indicator of Climate Change. *Climate Change*, T. M. Letcher, Ed., Elsevier, Amsterdam, 145 – 164, doi:10.1016/B978-0-444-53301-2.00007-5, URL http://dx.doi.org/10.1016/B978-0-444-53301-2.00007-5.

Reichler, T., M. Dameris, and R. Sausen, 2003: Determining the tropopause height from gridded data. *Geophys. Res. Lett.*, **30 (20)**, 2042, URL http://dx.doi.org/10.1029/2003GL018240.

Reichler, T., and I. Held, 2005: Widening trend of the hadley cell over the past 40 years. *AMS Conference on Climate Variability and Change*, Cambridge, MA, URL http://www.inscc.utah.edu/~reichler/talks/papers/AMS_0506.pdf.

Ring, M. J., and R. A. Plumb, 2008: The response of a simplified GCM to axisymmetric forcings: Applicability of the fluctuationdissipation theorem. *J. Atmos. Sci.*, **65 (12)**, 3880–3898, URL http://dx.doi.org/10.1175/2008JAS2773.1.

Rivire, G., 2009: Effect of latitudinal variations in low-level baroclinicity on eddy life cycles and upper-tropospheric wave-breaking processes. *J. Atmos. Sci.*, **66 (6)**, 1569–1592, URL http://dx.doi.org/10.1175/2008JAS2919.1.

Rivire, G., 2011: A dynamical interpretation of the poleward shift of the jet streams in global warming scenarios. *J. Atmos. Sci.*, **68 (6)**, 1253–1272, URL http://dx.doi.org/10.1175/2011JAS3641.1.

Robinson, W. A., 2002: On the midlatitude thermal response to tropical warmth. *Geophys. Res. Lett.*, **29 (8)**, 1190, URL http://dx.doi.org/10.1029/2001GL014158.

Rosenlof, K. H., 2002: Transport changes inferred from HALOE water and methane measurements. *J. Meteor. Soc. Japan*, **80 (4B)**, 831–848, URL http://dx.doi.org/10.2151/jmsj.80.831.

Rutz, J., 2010: Past shifts in the general circulation: Causation, structure, and effects on hydroclimate. M.S. thesis, Atmospheric Sciences, University of Utah.

Scheff, J., and D. Frierson, 2012: Twenty-first-century multimodel subtropical precipitation declines are mostly midlatitude shifts. *J. Climate*, **25 (12)**, 4330–4347, URL http://dx.doi.org/10.1175/JCLI-D-11-00393.1.

Schneider, T., 2012: Personal communication between p. w. staten and t. schneider.

Schneider, T., and S. Bordoni, 2008: Eddy-mediated regime transitions in the seasonal cycle of a Hadley circulation and implications for monsoon dynamics. *J. Atmos. Sci.*, **65 (3)**, 915–934, URL http://journals.ametsoc.org/doi/abs/10.1175/2007JAS2415.1.

Schneider, T., P. A. O'Gorman, and X. J. Levine, 2010: Water vapor and the dynamics of climate changes. *Rev. Geophys.*, **48 (3)**, RG3001, URL http://dx.doi.org/10.1029/2009RG000302.

Scinocca, J. F., N. A. McFarlane, M. Lazare, J. Li, and D. Plummer, 2008: Technical note: The CCCma third generation AGCM and its extension into the middle atmosphere. *Atmos. Chem. Phys.*, **8 (23)**, 7055–7074, URL http://www.atmos-chem-phys.net/8/7055/2008/.

Screen, J. A., I. Simmonds, C. Deser, and R. Tomas, 2012: The atmospheric response to three decades of observed Arctic sea ice loss. *J. Climate*, URL http://dx.doi.org/10.1175/JCLI-D-12-00063.1.

Seager, R., N. Harnik, Y. Kushnir, W. Robinson, and J. Miller, 2003: Mechanisms of hemispherically symmetric climate variability*. *J. Climate*, **16 (18)**, 2960–2978, URL http://dx.doi.org/10.1175/1520-0442(2003)016<2960:MOHSCV>2.0.CO;2.

Seidel, D. J., Q. Fu, W. J. Randel, and T. J. Reichler, 2008: Widening of the tropical belt in a changing climate. *Nature Geosci.*, **1 (1)**, 21–24, URL http://dx.doi.org/10.1038/ngeo.2007.38.

Seidel, D. J., and W. J. Randel, 2007: Recent widening of the tropical belt: Evidence from tropopause observations. *J. Geophys. Res.*, **112 (D20)**, D20 113, URL http://dx.doi.org/10.1029/2007JD008861.

Shindell, D. T., and G. A. Schmidt, 2004: Southern hemisphere climate response to ozone changes and greenhouse gas increases. *Geophys. Res. Lett.*, **31 (18)**, L18 209, URL http://dx.doi.org/10.1029/2004GL020724.

Sigmond, M., J. F. Scinocca, and P. J. Kushner, 2008: Impact of the stratosphere on tropospheric climate change. *Geophys. Res. Lett.*, **35 (12)**, L12 706, URL http://dx.doi.org/10.1029/2008GL033573.

Simpson, I. R., M. Blackburn, and J. D. Haigh, 2009: The role of eddies in driving the tropospheric response to stratospheric heating perturbations. *J. Atmos. Sci.*, **66 (5)**, 1347–1365, URL http://dx.doi.org/10.1175/2008JAS2758.1.

Simpson, I. R., M. Blackburn, and J. D. Haigh, 2012: A mechanism for the effect of tropospheric jet structure on the annular modelike response to stratospheric forcing. *J. Atmos. Sci.*, **69 (7)**, 2152–2170, URL http://dx.doi.org/10.1175/JAS-D-11-0188.1.

Simpson, I. R., M. Blackburn, J. D. Haigh, and S. N. Sparrow, 2010: The impact of the state of the troposphere on the response to stratospheric heating in a simplified gcm. *J. Climate*, **23 (23)**, 6166–6185, URL http://dx.doi.org/10.1175/2010JCLI3792.1.

Solomon, S., D. Qin, M. Manning, Z. Chen, M. Marquis, K. Averyt, M. Tignor, and H. Miller, 2007: *Climate Change 2007 - The Physical Science Basis: Working Group I Contribution to the Fourth Assessment Report of the IPCC*. Cambridge University Press, Cambridge, UK and New York, NY, USA, URL http://www.amazon.ca/exec/obidos/redirect?tag=citeulike09-20&path=ASIN/0521880092.

Son, S.-W., N. F. Tandon, L. M. Polvani, and D. W. Waugh, 2009a: Ozone hole and southern hemisphere climate change. *Geophys. Res. Lett.*, **36 (15)**, L15 705, URL http://dx.doi.org/10.1029/2009GL038671.

Son, S.-W. et al., 2008: The impact of stratospheric ozone recovery on the southern hemisphere westerly jet. *Science*, **320 (5882)**, 1486–1489, URL http://www.sciencemag.org/content/320/5882/1486.abstract.

Son, S.-W. et al., 2009b: The impact of stratospheric ozone recovery on tropopause height trends. *J. Climate*, **22 (2)**, 429–445, URL http://dx.doi.org/10.1175/2008JCLI2215.1.

Son, S.-W. et al., 2010: Impact of stratospheric ozone on southern hemisphere circulation change: A multimodel assessment. *J. Geophys. Res.*, **115**, D00M07, URL http://dx.doi.org/10.1029/2010JD014271.

Song, Y., and W. A. Robinson, 2004: Dynamical mechanisms for stratospheric influences on the troposphere. *J. Atmos. Sci.*, **61 (14)**, 1711–1725, URL http://dx.doi.org/10.1175/1520-0469(2004)061<1711:DMFSIO>2.0.CO;2.

Stachnik, J. P., and C. Schumacher, 2011: A comparison of the Hadley circulation in modern reanalyses. *J. Geophys. Res.*, **116 (D22)**, D22 102, URL http://dx.doi.org/10.1029/2011JD016677.

Staten, P. W., and T. Reichler, 2013: On the ratio between shifts in the eddy-driven jet and the hadley cell edge. *Clim. Dynam.*, **(submitted)**, –, URL http://www.inscc.utah.edu/~pstaten/publications/staten_reichler_ratio_2013_author_created.pdf.

Staten, P. W., J. J. Rutz, T. Reichler, and J. Lu, 2011: Breaking down the tropospheric circulation response by forcing. *Clim. Dynam.*, **39**, 2361–2375, doi:10.1007/s00382-011-1267-y, URL http://dx.doi.org/10.1007/s00382-011-1267-y.

Stern, W. F., and R. T. Pierrehumbert, 1988: The impact of an orographic gravity wave drag parameterization on extended range predictions with a GCM. *Preprints, Eighth Conf. on Numerical Weather Prediction*, Baltimore, MD, Amer. Meteor. Soc., 745 750.

Stouffer, R. J. et al., 2006: GFDL's CM2 global coupled climate models. Part IV: Idealized climate response. *J. Climate*, **19 (5)**, 723–740, URL http://dx.doi.org/10.1175/JCLI3632.1.

Strong, C., and R. E. Davis, 2007: Winter jet stream trends over the northern hemisphere. *Q.J.R. Meteorol. Soc.*, **133 (629)**, 2109–2115, URL http://dx.doi.org/10.1002/qj.171.

Thompson, D. W. J., and S. Solomon, 2002: Interpretation of recent southern hemisphere climate change. *Science*, **296 (5569)**, 895–899, URL http://www.sciencemag.org/content/296/5569/895.abstract.

Thompson, D. W. J., and J. M. Wallace, 2000: Annular modes in the extratropical circulation. Part I: Month-to-month variability. *J. Climate*, **13 (5)**, 1000–1016, URL http://dx.doi.org/10.1175/1520-0442(2000)013<1000:AMITEC>2.0.CO;2.

Thompson, D. W. J., J. M. Wallace, and G. C. Hegerl, 2000: Annular modes in the extratropical circulation. Part II: Trends. *J. Climate*, **13 (5)**, 1018–1036, URL http://dx.doi.org/10.1175/1520-0442(2000)013<1018:AMITEC>2.0.CO;2.

Uppala, S. M. et al., 2005: The ERA-40 re-analysis. *Q.J.R. Meteorol. Soc.*, **131 (612)**, 2961–3012, URL http://dx.doi.org/10.1256/qj.04.176.

Walker, C. C., and T. Schneider, 2006: Eddy influences on Hadley circulations: Simulations with an idealized GCM. *J. Atmos. Sci.*, **63 (12)**, 3333–3350, URL http://dx.doi.org/10.1175/JAS3821.1.

Waugh, D. W., L. Oman, P. A. Newman, R. S. Stolarski, S. Pawson, J. E. Nielsen, and J. Perlwitz, 2009: Effect of zonal asymmetries in stratospheric ozone on simulated southern hemisphere climate trends. *Geophys. Res. Lett.*, **36 (18)**, L18 701, URL http://dx.doi.org/10.1029/2009GL040419.

Wilcox, L. J., A. J. Charlton-Perez, and L. J. Gray, 2012: Trends in austral jet position in ensembles of high- and low-top CMIP5 models. *J. Geophys. Res.*, **117 (D13)**, D13 115, URL http://dx.doi.org/10.1029/2012JD017597.

Williams, G. P., 2006: Circulation sensitivity to tropopause height. *J. Atmos. Sci.*, **63 (7)**, 1954–1961, URL http://dx.doi.org/10.1175/JAS3762.1.

Wittenberg, A. T., A. Rosati, N.-C. Lau, and J. J. Ploshay, 2006: GFDL's CM2 global coupled climate models. Part III: Tropical pacific climate and ENSO. *J. Climate*, **19 (5)**, 698–722, URL http://dx.doi.org/10.1175/JCLI3631.1.

Wittman, M. A. H., A. J. Charlton, and L. M. Polvani, 2007: The effect of lower stratospheric shear on baroclinic instability. *J. Atmos. Sci.*, **64 (2)**, 479–496, URL http://dx.doi.org/10.1175/JAS3828.1.

Wittman, M. A. H., L. M. Polvani, R. K. Scott, and A. J. Charlton, 2004: Stratospheric influence on baroclinic lifecycles and its connection to the arctic oscillation. *Geophys. Res. Lett.*, **31 (16)**, L16 113, URL http://dx.doi.org/10.1029/2004GL020503.

Wu, Y., R. Seager, T. A. Shaw, M. Ting, and N. Naik, 2012: Atmospheric circulation response to an instantaneous doubling of carbon dioxide. Part II: Atmospheric transient adjustment and its dynamics. *J. Climate*, **(submitted)**, –, URL www.columbia.edu/~tas2163/Wu_etal_2012b.pdf.

Wu, Y., R. Seager, M. Ting, N. Naik, and T. A. Shaw, 2011: Atmospheric circulation response to an instantaneous doubling of carbon dioxide. Part I: Model experiments and transient thermal response in the troposphere. *J. Climate*, **25 (8)**, 2862–2879, URL http://dx.doi.org/10.1175/JCLI-D-11-00284.1.

Yang, X.-Y., R. X. Huang, and D. X. Wang, 2007: Decadal changes of wind stress over the southern ocean associated with antarctic ozone depletion. *J. Climate*, **20 (14)**, 3395–3410, URL http://dx.doi.org/10.1175/JCLI4195.1.

Zhou, Y. P., K.-M. Xu, Y. C. Sud, and A. K. Betts, 2011: Recent trends of the tropical hydrological cycle inferred from Global Precipitation Climatology Project and International Satellite Cloud Climatology Project data. *J. Geophys. Res.*, **116 (D9)**, D09 101, URL http://dx.doi.org/10.1029/2010JD015197.

VITA

Paul W. Staten

Department of Atmospheric Sciences
University of Utah
135 South 1460 East Room 819
Salt Lake City, UT 84112-0110

Phone: (801) 581-6136
Fax: (801) 581-4362
Office: WBB Rm. 801
Email: paul.staten@utah.edu
Homepage: http://inscc.utah.edu/~pstaten/

Employment

Postdoctoral Research Fellow, NASA Jet Propulsion Laboratory (JPL), California Institute of Technology, beginning 2013.

Research Assistant, Department of Atmospheric Sciences, University of Utah, 2006–Present.

Intern, NASA Jet Propulsion Laboratory (JPL), 2005.

Education

Pursuing a Ph.D. in Atmospheric Sciences, University of Utah, 2008–Present.

Dissertation: Understanding causes and mechanisms of atmospheric circulation change.

Committee: Thomas Reichler (chair), Jian Lu, Courtenay Strong, James Steenburgh, John Horel.

M. S. Meteorology, University of Utah, 2008.

Thesis: An evaluation of radio occultation measurements for long-term tropopause monitoring.

Committee: Thomas Reichler (chair), Gerald Mace, Chuntao Liu.

Attended C-SPARC Summer School on Dynamics, long-term memory, and trends in the climate system. 2008.

B. S. Mathematics, Weber State University, 2006.

Fields of Research Interest

Atmospheric Dynamics and Climate Change

Research

Refereed Articles

Staten, P. W., T. Reichler, J. Lu (2013): The instantaneous atmospheric response to imposed climate forcings, *Clim. Dynam.*, (in preparation).

Staten, P. W., and T. Reichler (2013): On the ratio between shifts in the eddy-driven jet and the Hadley cell edge, *Clim. Dynam.*, (submitted).

Staten, P. W., J. Rutz, T. Reichler, and J. Lu (2011): Breaking down the tropospheric circulation response by forcing, *Clim. Dynam.*, 39, 2361-2375, doi:10.1007/s00382-011-1267-y.

Staten, P. W., and T. Reichler (2009): Apparent precision of GPS Radio Occultation Temperatures, *Geophys. Res. Let.*, 36, L24806, doi:10.1029/2009GL041046.

Staten, P. W., and T. Reichler (2008): Use of radio occultation for long-term tropopause studies: uncertainties, biases, and instabilities, *J. Geophys. Res.*, 113, D00B05, doi:10.1029/2008JD009886.

Conference Presentations

Staten, P. and T. Reichler (2012): The relationship between latitudinal shifts in the eddy-driven jet and the Hadley cell, *AGU Fall Meeting*, San Francisco (CA), 3-7 December, (poster).

Reichler, T., P. Staten, and J. Lu (2012): Latitudinal shifts in precipitation: the role of anthropogenic forcings, *AGU Fall Meeting*, San Francisco (CA), 3-7 December, (talk).

Staten, P.W., T. Reichler, and J. Lu (2011): Southern hemisphere circulation shifts in a warming climate, *WCRP Open Science Conference*, Denver (CO), 24–28 October, (poster).

Staten, P.W., T. Reichler, and J. Lu (2010): Understanding the Direct and Indirect Circulation Response to Radiative Forcings, *AGU Fall Meeting*, San Francisco (CA), 13–17 December, (poster).

Staten, P.W., T. Reichler, J. Rutz, and J. Kim (2010): How Ozone Depletion Causes Southern Hemispheric Climate Change, *AGU 2010 Meeting of the Americas*, Foz do Iguassu, Brazil, 8–12 August, (talk).

Staten, P.W. and T. Reichler (2008): Practical GPS RO Temperature Precision, *AGU Fall Meeting*, San Francisco (CA), 15–19 December, (poster).

Staten, P.W. and T. Reichler (2008): Space-Born Detection of Long-Term Tropopause Trends, *SPARC General Assembly*, Bologna, Italy, 31 August–5 September, (poster).

Staten, P.W. and T. Reichler (2008): Space-Born Detection of Long-Term Tropopause Trends, *C-SPARC Summer School on dynamics, long-term memory, and trends in the climate system*, Banff, Canada, 17–23 May, (poster).

Staten, P.W. and T. Reichler (2007): Can radio occultation be used to discern long-term tropopause trends? EMS7/ECAM8 Abstracts, Vol. 4, EMS2007-A-00531, *7th EMS Annual Meeting / 8th ECAM*, El Escorial, Spain, 1–5 October, (talk).

Sellar, R. G., J. D. Farmer, P. Gardner, P. Staten, A. Kieta, J. Huang (2007): Improved spectrometric capabilities for in-situ microscopic imagers, *Seventh International Conference on Mars*, Pasadena (CA), 9–13 July (poster).

Teaching

University of Utah

Classroom Scientist, Think Globally Learn Locally, 2010–2012.

Group Discussion Leader, IDL Discussion Group, 2010.

Teaching Assistant, Atmospheric Dynamics (METEO 6010), 2007–2008.

Weber State University

Mathematics Tutor, 2004–2006.

Supplemental Instructor, Elementary Linear Algebra (MATH 2270), 2005.

Professional Activities

Reviewer for *Atmospheric Chemistry and Physics* and *JGR Atmospheres*.

Treasurer, American Meteorological Society, University of Utah Chapter, 2008–2009.

Member, American Geophysical Union, 2006–Present.

Member, American Meteorological Society, 2006–Present.

Honors, Awards, & Fellowships

Caltech Postdoctoral Fellowship, beginning 2013.

NSF GK-12 Fellowship, 2010–2012.

Zipser Award for Excellence in Graduate Research, 2008.

NASA Earth and Space Science Fellowship, 2007–2010.

Graduate Fellowship, University of Utah, 2006.

Outstanding Math Graduate, Weber State University, Ogden, UT, 2006.

Summer Undergraduate Research Fellowship, California Technical Institute, CA, 2005

Presidential Scholarship, Weber State University, Ogden, UT, 2001.